STABILITY ANALYSIS OF A H.V.D.C. TRANSMISSION LINK

A Thesis

Submitted to the Faculty of Graduate Studies

in Partial Fulfilment of the Requirements

for the Degree of

Master of Science

in the Department of Electrical Engineering

University of Saskatchewan

by

JAGDISH CHAND

Saskatoon, Saskatchewan

August, 1971

ACKNOWLEDGEMENTS

The author wishes to express his sincere thanks to Dr. M. S. Sachdev and Dr. R. J. Fleming for their advice and assistance in the preparation of this thesis. Appreciation is also extended to various members of the faculty of the Electrical Engineering Department for their helpful comments at various times during the course of this work. Gratitude is also expressed to the Bihar Institute of Technology, Sindri (India) for granting permission to do postgraduate work at the University of Saskatchewan.

Financial assistance for this work was provided by the National Research Council of Canada operating grant Numbers A-2765 and A-7249 and major equipment grant Number E-1407.

UNIVERSITY OF SASKATCHEWAN

Electrical Engineering Abstract 71A139

"STABILITY ANALYSIS OF A H.V.D.C. TRANSMISSION LINK"

Student: Jagdish Chand

Supervisors: Dr. M. S. Sachdev
Dr. R. J. Fleming

M.Sc. Thesis Presented to the College of Graduate Studies
August 1971.

ABSTRACT

This thesis presents a brief description of the steady state and dynamic operation of a high voltage d.c. transmission link. A block diagram model and the state space equations are developed from the small signal equations. The system stability regions and the current controller parameters for near-critical damping of the integral controller with and without phase lead compensation are determined from root locus plots. The time domain response of the system using these controllers was calculated by digital computer solution of the state space equations. These studies were repeated on a small scale model and the digital solutions were found to be similar to the simulator performance.

The state regulator technique was applied for optimal and suboptimal control of a h.v.d.c. link. The dynamic performance of the optimally and suboptimally controlled system were digitally calculated. The suboptimal controller was also designed and used for constant current control of the simulator. The calculated system performance compares favourably with the simulator response. The tracking technique is also used for constant current controller optimization and is found to increase the system response speed considerably.

This research was supported by the National Research Council under Grant Nos. A-2765 and A-7249.

TABLE OF CONTENTS

TABLE OF CONTENTS (cont'd)

LIST OF FIGURES

LIST OF FIGURES (cont'd)

LIST OF FIGURES (cont'd)

LIST OF FIGURES (cont'd)

LIST OF FIGURES (cont'd)

LIST OF FIGURES (cont'd)

LIST OF TABLES

1. INTRODUCTION

The economic and technical advantages of high voltage direct current transmission has been known for many decades. The present development phase of h.v.d.c. transmission started in 1952 with the development of multi-electrode grid-controlled mercury arc valve.[6] Since then the d.c. technology has sufficiently advanced and this transmission mode must be considered in the appraisal of long distance transmission, marine or underground cable installations and inter-connections between systems operating at different frequencies.[26]

The steady state performance of d.c. lines and convertor stations is described in the literature.[6] The system dynamic performance depends on the controller characteristics. Constant current or constant power control at the rectifier station and constant extinction angle control at the inverter has been developed and used for many d.c. transmission lines.[22-25] Automatic frequency ratio control has been applied for the maintenance of system frequency by controlling the transmitted power.[4,26] The d.c. transmission control schemes are briefly described in Chapter 2. Small signal equations for the d.c. line, convertor station and the controllers are derived from the steady state equations. The transfer function and a mathematical model of the d.c. transmission system have been developed from the small signal equations and this model has been used for dynamic stability studies. A high voltage d.c. simulator described in Chapter 3 has been used to verify the mathematical studies.

The composite a.c./d.c. system performance following a.c. and d.c. faults has been examined[5,16-21] The d.c. system dynamic

performance for small deviations has also been analyzed using Bode's and Nyquist plots.[7-13] These methods indicate the system stability regions and do not provide a time domain solution. The small signal equations have been used to formulate the state space mathematical model. The eigenvalues of the characteristic matrix are calculated for increasing current controller amplifier gain and the root locus plots are used to synthesize the controller. The system time domain performance is obtained by integrating the state space equations for a current order and for an inverter commutation voltage step change using the fourth order Runge-Kutta method and an IBM 360/50 digital computer. The mathematical studies were repeated on the simulator and performance similarity confirms the mathematical model validity.

The state regulator optimization technique is applied to improve the system performance. All the system states are used in the optimal controller. The inverter and the transmission line midpoint state signals are not readily available in a high voltage d.c. scheme. A suboptimal controller using the rectifier station state signals only is developed. The performance of the system equipped with optimal and suboptimal controller was studied from the mathematical model. The suboptimal controller developed has also been used in the simulator studies.

The system performance can also be improved by proper selection of the current controller feedback loop parameters. Two methods of modifying the current controller feedback loop for near critical system damping have been used. The system performance improves by providing phase lead compensation in many cases. The parameters of the integral current controller with phase lead compensation are calculated from the root locus plots for near critical damping. The digital computer and

the simulator studies using this controller are included. The tracking technique has also been examined for improving system response. The system dynamic studies using this optimization technique are given in Chapter 6.

2. HIGH VOLTAGE DIRECT CURRENT TRANSMISSION

The first high voltage direct current scheme using mercury arc valves was commissioned in 1954 following the development of high voltage grid controlled mercury arc valves by ASEA, Sweden.[6] High voltage d.c. is preferred for (i) long distance transmission of large blocks of power, (ii) transmission of power using underground and submarine cables and (iii) interconnecting power systems operating at different frequencies.[26] The economic and technical advantages of high voltage direct current transmission led to the development of other schemes which are also operating at present.[1-4] A few high voltage direct current schemes are at different stages of planning and construction. The theory of high voltage d.c. transmission and different types of controllers is reviewed. The small signal convertor and line performance equations are derived and subsequently used for system dynamic performance studies.

2.1 General

A typical high voltage direct current scheme consists of two converting stations and a transmission line as shown in Figure 2.1. Each converting station includes bridge connected mercury arc valves, bypass valve, convertor transformers, d.c. reactors, a.c. and d.c. filters, valve damping circuits and surge diverters as shown in Figure 2.2.[45] High voltage solid state valves have been developed and are being used in the Eel River h.v.d.c. convertor station.[44] A six valve full wave bridge converts a.c. voltage to d.c. at the rectifier

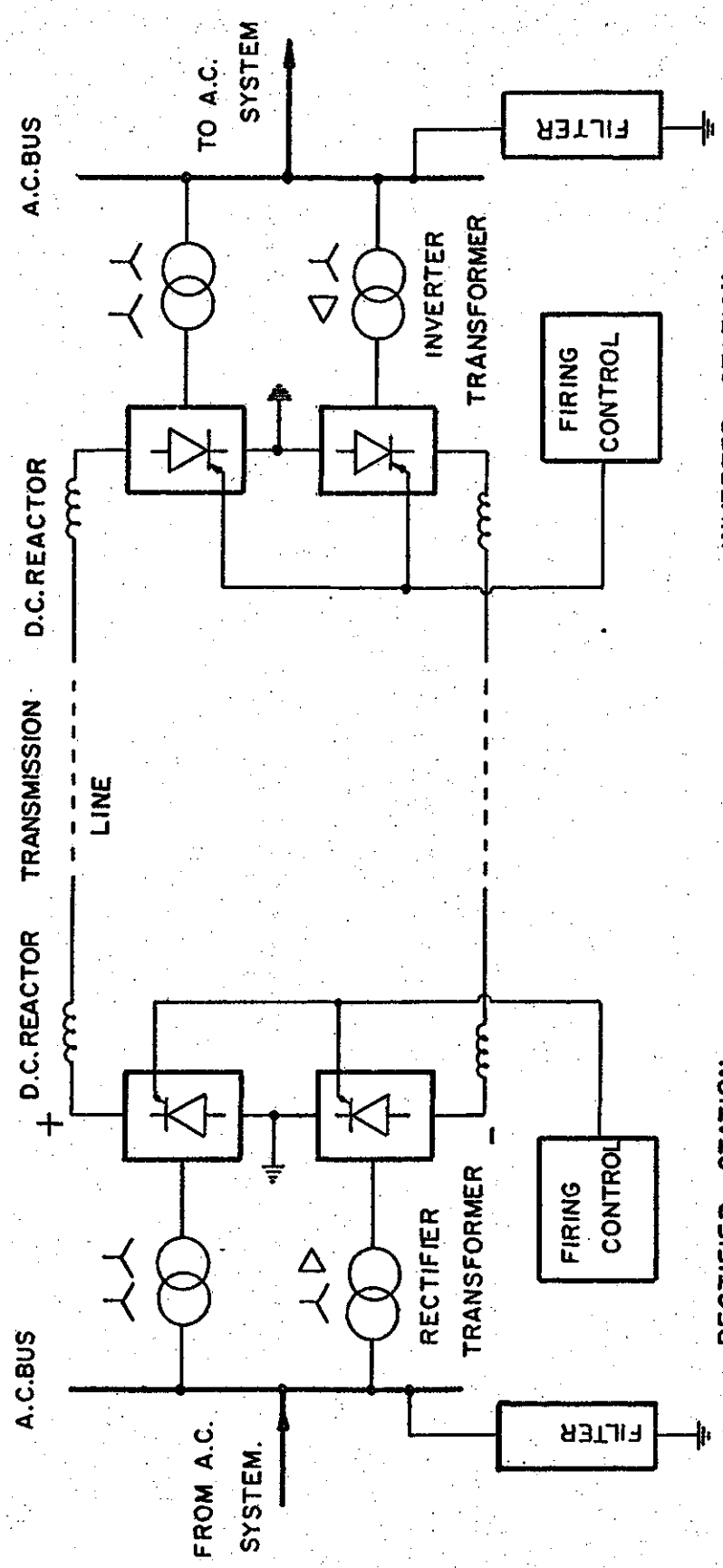

Figure 2.1 General layout of a h.v.d.c. scheme interconnecting two a.c. systems.

station. A similar arrangement converts d.c. to a.c. at the inverter station. Bridges are connected in series to increase the d.c. voltage level. Wye-wye and wye-delta convertor transformer connections are used to reduce voltage and current harmonics in d.c. and a.c. systems respectively. Filters are provided to eliminate the harmonics from the a.c. and d.c. systems. D.C. reactors keep the direct current almost invariant during normal operation and limit the rate of rise of current during convertor and d.c. line faults. The damping circuits provided across the valves suppress the high frequency oscillations and the surge diverters protect the valves from overvoltages in the a.c. and d.c. systems. The firing of rectifier valves is usually delayed by a small angle of five to fifteen degrees. Firing delays of greater than ninety degrees are required at an inverter station. A convertor station can operate as a rectifier or an inverter depending on the valve firing delay used.

2.2 Convertor Analysis -- Steady-State Operation

A functional representation of a bridge connected convertor station is shown in Figure 2.3. The inductance L_c represents the commutation reactance and the equivalent a.c. system reactance if no a.c. filters are provided. To facilitate convertor performance analysis the following assumptions are made.[6]

(i) The transformer and a.c. system resistances are negligible.

(ii) The voltage drop in a conducting valve and reverse current through a nonconducting valve are negligible.

(iii) The d.c. voltage and a.c. currents at the convertor station are constant and free from harmonics.

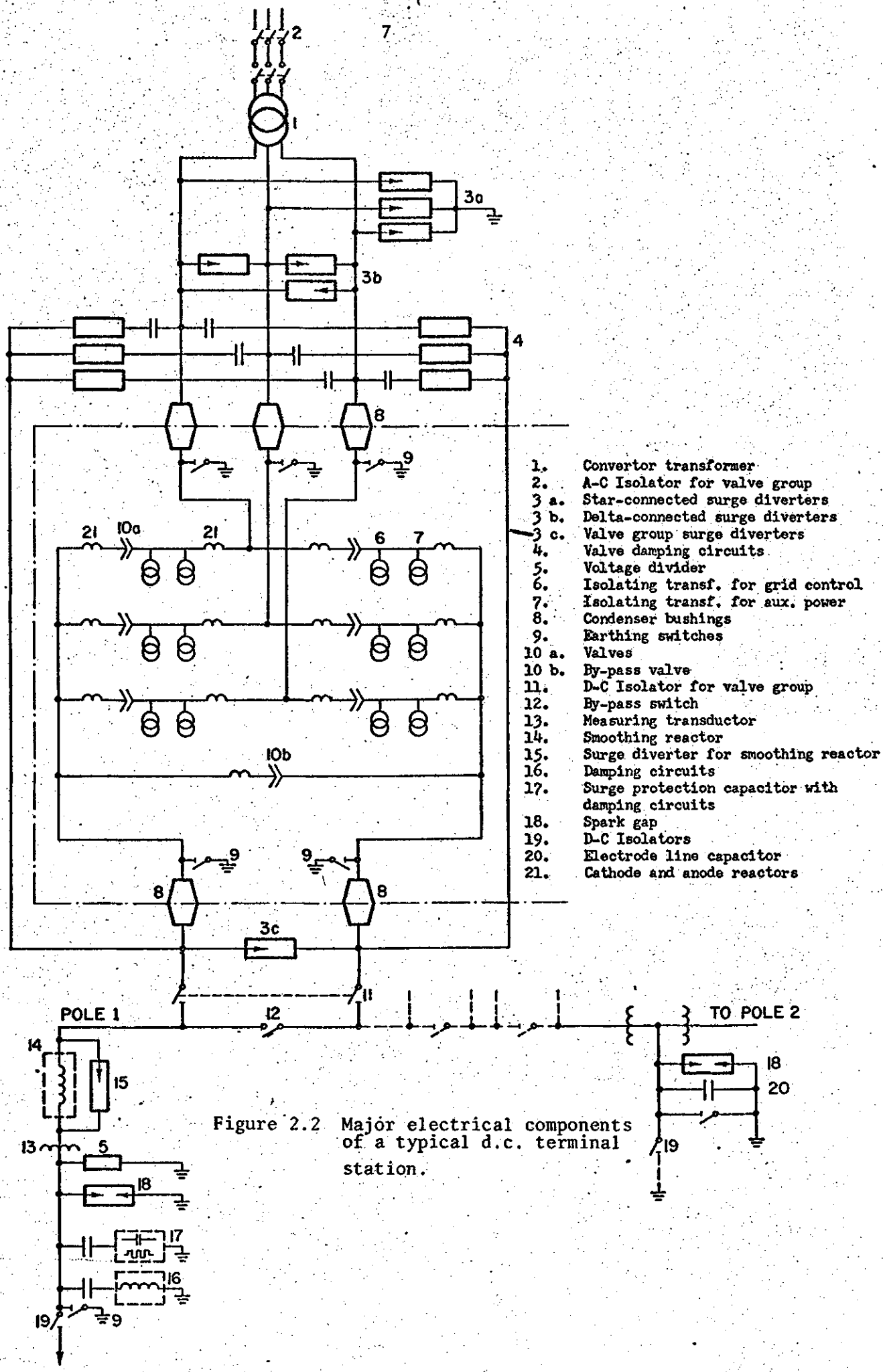

Figure 2.2 Major electrical components of a typical d.c. terminal station.

(iv) The a.c. system voltages e_r, e_y and e_b are balanced.

The voltage and current wave forms of a bridge connected rectifier including firing delays and finite commutation intervals are shown in Figure 2.4(a). The d.c. voltage wave form of an inverter is shown in Figure 2.4(b).

The average d.c. voltage, V_{dr} and d.c. current, I_{dr} at the rectifier are given by[6]

$$V_{dr} = \frac{3\sqrt{2}}{\pi} E_r \cos\alpha - \frac{3}{\pi}\omega L_r I_{dr} \qquad 2.1$$

$$I_{dr} = \frac{\sqrt{2}\, E_r}{2\omega L_r} \{\cos\alpha - \cos(\alpha+\gamma)\} \qquad 2.2$$

Where E_r is the line to line r.m.s. voltage of the rectifier transformer secondary at no load.

L_r is the commutation inductance for the rectifier circuit.

α is the rectifier firing delay angle.

γ is the commutation angle for the rectifier current.

The power factor at a rectifier transformer primary is given by by[6]

$$\cos\phi_r = \frac{3}{2\pi} \frac{\cos\alpha + \cos(\alpha+\gamma)}{\sqrt{1 - 3\Psi(\alpha,\gamma)}} \qquad 2.3$$

Where

$$\Psi(\alpha,\gamma) = \frac{1}{2\pi} \frac{\sin\gamma \{2 + \cos(2\alpha+\gamma)\} - \gamma\{1 + 2\cos\alpha \cos(\alpha+\gamma)\}}{\{\cos\alpha - \cos(\alpha+\gamma)\}^2}$$

The average d.c. voltage, V_{di} and d.c. current, I_{di} at the inverter are given by[6]

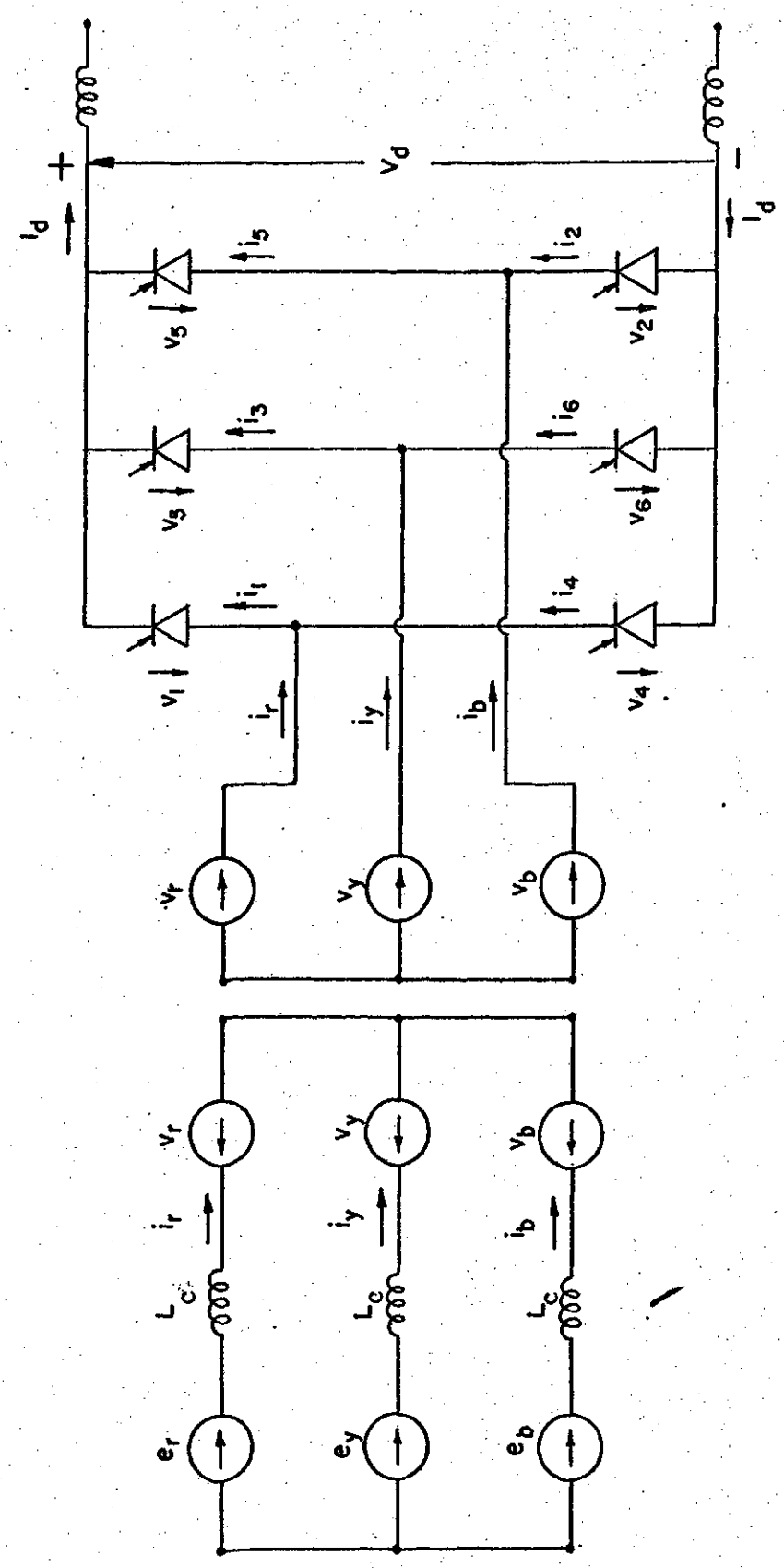

Figure 2.3 A functional representation of a bridge connected convertor.

$$V_{di} = \frac{3\sqrt{2}}{\pi} E_i \cos\beta + \frac{3}{\pi}\omega L_i I_{di} \qquad 2.4a$$

$$V_{di} = \frac{3\sqrt{2}}{\pi} E_i \cos\delta - \frac{3}{\pi}\omega L_i I_{di} \qquad 2.4b$$

$$I_{di} = \frac{\sqrt{2}\, E_i}{2\omega L_i} (\cos\delta - \cos\beta) \qquad 2.5$$

Where E_i is the line to line r.m.s. voltage of the inverter transformer secondary at no load.

L_i is the commutation inductance for the inverter circuit.

β is the inverter firing advance angle.

δ is the deionization margin angle at the inverter.

The power factor at an inverter transformer primary is given by[6]

$$\cos\phi_i = \frac{3}{2\pi} \frac{\cos\delta + \cos(\delta+\gamma)}{\sqrt{\{1 - 3\Psi(\delta,\gamma)\}}} \qquad 2.6$$

Where

$$\Psi(\delta,\gamma) = \frac{1}{2\pi} \frac{\sin\gamma\{2 + \cos(2\delta+\gamma)\} - \gamma\{1 + 2\cos\delta\cos(\delta+\gamma)\}}{\{\cos\delta - \cos(\delta+\gamma)\}^2}$$

The fundamental frequency currents at a convertor a.c. bus lag the fundamental frequency voltages due to valve firing delays and finite commutation times. A convertor, therefore, absorbs reactive power. An increase in the firing delay at the rectifier or deionization margin at the inverter increases the reactive power requirements.

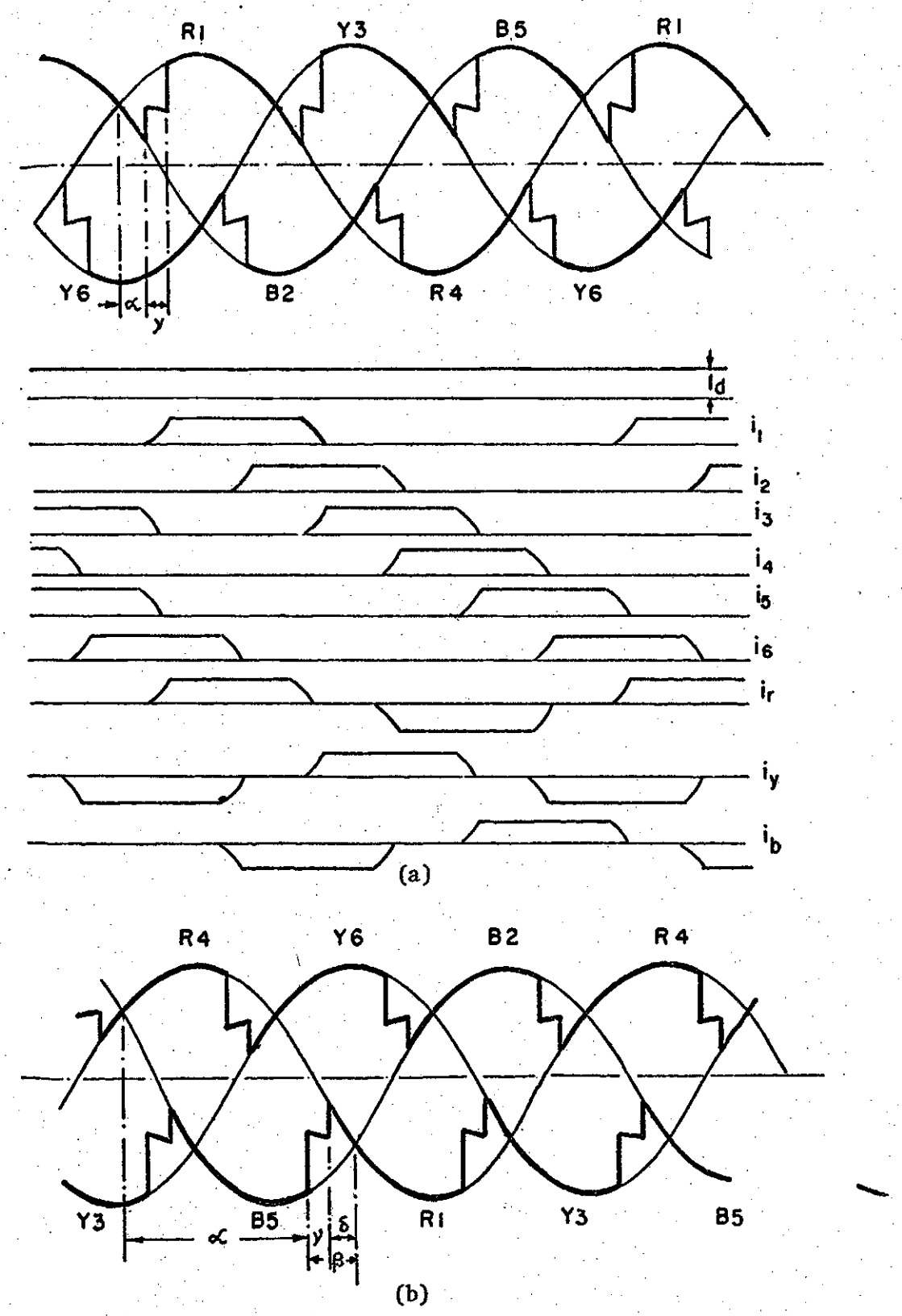

Figure 2.4 Three phase bridge connected convertor output waveforms (a) Rectifier d.c. voltage V_{dr}; direct, valve and phase currents. (b) Inverter d.c. voltage V_{di}.

2.2.1 Equivalent circuit representation

The equivalent circuits for convertor operating characteristics derived from equations 2.1 and 2.4 are shown in Figure 2.6. The terms $\frac{3\sqrt{2}}{\pi} E_r \cos\alpha$ and $\frac{3\sqrt{2}}{\pi} E_i \cos\beta$ represent source voltages in the equivalent circuits. The series resistances of $\frac{3}{\pi}\omega L_r$ and $\frac{3}{\pi}\omega L_i$ ohmic values produce voltage drops representing the finite commutation effects. The voltage sources of Figure 2.6 can be regulated either by controlling the a.c. supply voltages E_r and E_i or by controlling the firing delay angle α at the rectifier and the firing advance angle β at the inverter.

A d.c. system is operated at minimum deionization margin at the inverter and small firing delay at the rectifier to keep the line losses and reactive power requirements to a minimum. The convertor a.c. voltages are controlled by automatic tap changing devices such that the d.c. line operates at near nominal voltage and the rectifier operates with five to fifteen degrees valve firing delay. The mercury arc valves are sensitive to overcurrents. The line current is maintained at a desired value by controlling the rectifier d.c. voltage. The characteristics of a convertor provided with a constant current controller is shown in Figure 2.5.

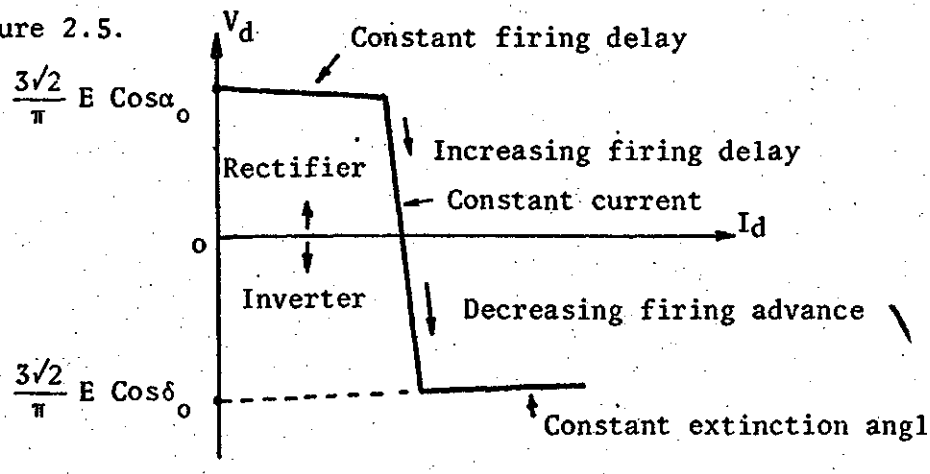

Figure 2.5 The characteristics of a convertor equipped with a constant current controller.

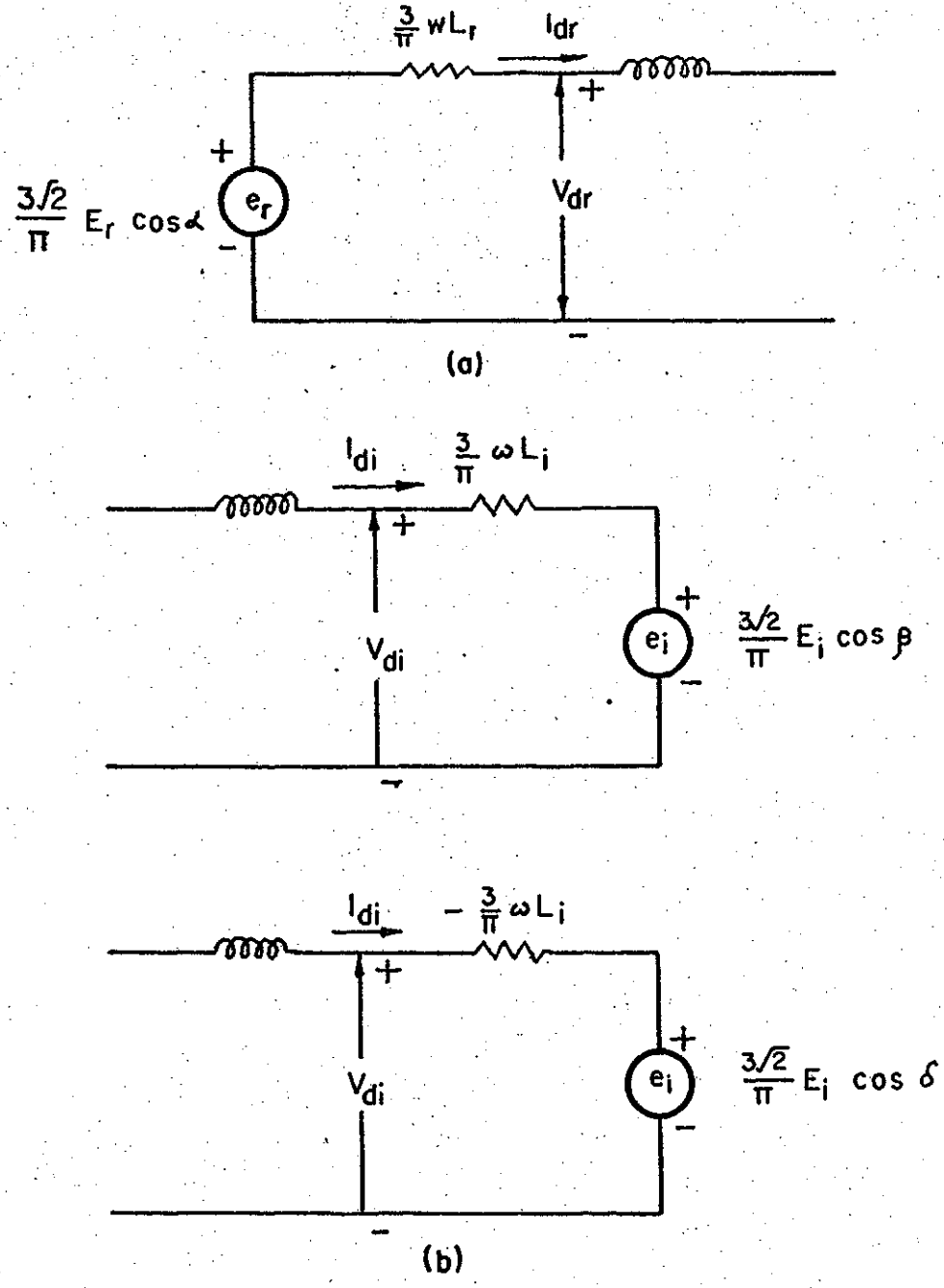

Figure 2.6 Equivalent circuits representing (a) rectifier and (b) inverter performances.

The rectifier normally operates in the constant current region and the inverter in the constant extinction angle region as shown in Figure 2.7.

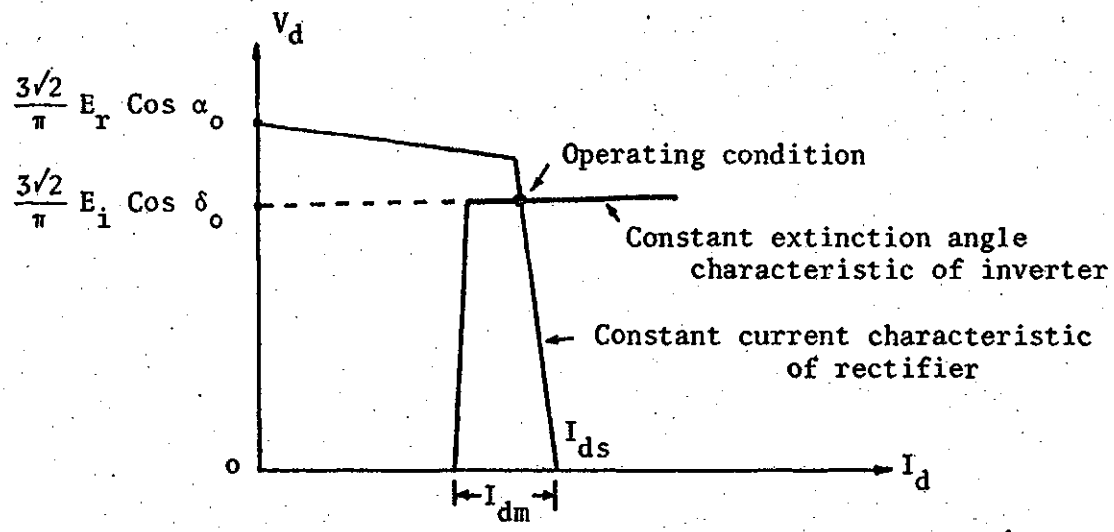

Figure 2.7 Operating characteristics of a d.c. interconnection.

A constant current controller is also provided at the inverter to avoid running down of the d.c. link in case of (i) low a.c. system voltage at the rectifier and (ii) high a.c. system voltage at the inverter.

2.3 Convertor Analysis — Dynamic Operation

The characteristics of controllers, protective devices and system parameters determine the dynamic behaviour of a d.c. link. AC-DC composite system performance during a disturbance produced by a.c. system faults has been reported earlier.[5,16,17,18-21] These studies are based on major changes in the system operating conditions and parameters. The performance of d.c. systems following small disturbances has also received attention.[7-15] Even

small fluctuations of load or a.c. supply voltages cause variations in the firing delay angles of the valves, d.c. voltages and d.c. line currents. The small signal equations for rectifier and inverter voltages derived from equations 2.1 and 2.4 are given by:

$$\Delta V_{dr} = \{\frac{3\sqrt{2}}{\pi} \text{Cos } \alpha_o\}\Delta E_r - \{\frac{3\sqrt{2}}{\pi} E_r \text{Sin}\alpha_o\} \Delta\alpha - \frac{3}{\pi}\omega L_r \Delta I_{dr} \qquad 2.7$$

$$\Delta V_{di} = \{\frac{3\sqrt{2}}{\pi} \text{Cos}\beta_o\} \Delta E_i - \{\frac{3\sqrt{2}}{\pi} E_i \text{Sin}\beta_o\}\Delta\beta + \frac{3}{\pi}\omega L_i \Delta I_{di} \qquad 2.8$$

Where Δ represents the small deviation and the subscript o denotes the initial value of the associated variable.

The d.c. current changes depend on the d.c. line parameters and changes of the rectifier and inverter d.c. voltages.

2.4 H.V.D.C. Convertor Controllers

A high voltage d.c. system can be controlled to deliver constant current or constant power to the receiving end a.c. system. A higher order control based on frequency ratio can also be used to maintain a.c. system frequencies. The constant current and constant power controllers are used when the receiving end system base load is allocated to the d.c. line. The frequency ratio controller allocates the receiving end system peak load to the d.c. interconnection.

2.4.1. Constant current control

Constant current controllers are provided at the rectifier and inverter stations for reasons already discussed in section 2.2.1. A rectifier normally operates on constant current control and an inverter on constant extinction angle control. Two basic methods are used to

achieve this control characteristic:

(i) Individual phase or consecutive grid control.

(ii) Equidistant firing control.

Individual phase control

The operation of this controller is based on equation 2.5 which is of the form

$$\sqrt{2}\ E\ \cos\beta = \sqrt{2}E\cos\delta\ - 2\omega L I_d \qquad 2.9$$

A time varying voltage is obtained by substituting $(180^\circ - \omega t)$ for β in this equation.

$$e = -\sqrt{2}\ E\ \cos\omega t - \sqrt{2}\ E\ \cos\delta\ + 2\omega L I_d \qquad 2.10$$

This voltage is zero when $(180-\omega t)$ equals the firing advance angle β for a specified deionization margin angle δ_c and d.c. line current I_d. Six control circuits, one for each valve, based on this concept are used to achieve constant extinction angle control of the inverter. An additional signal V_{cc}, the amplified difference of the desired current and the line current, is used to achieve the rectifier constant current characteristic based on the following equations:

$$V_{cc} = G\ (I_{ds} - I_d) \qquad 2.11$$

$$e = -\sqrt{2}\ E\ \cos\omega t - \sqrt{2}\ E\ \cos\delta_c + 2\omega L I_d + V_{cc} \qquad 2.12$$

Where G is the transfer function of the current error amplifier. Equations 2.10 and 2.12 are similar. The d.c. current settings at the rectifier and inverter are the same. A margin current signal is provided

at the inverter in addition to the desired current setting.[22-25] The net current setting at the inverter is thus smaller than the line current. The following operating requirements for the constant current controller are thus established:

(i) $I_{ds} < I_d$; $V_{cc} = o$; convertor should operate in constant extinction angle control mode.

(ii) $I_{ds} \geq I_d$; V_{cc} is finite; convertor should operate in constant current control mode.

A schematic block diagram to achieve this control mode is shown in Figure 2.8

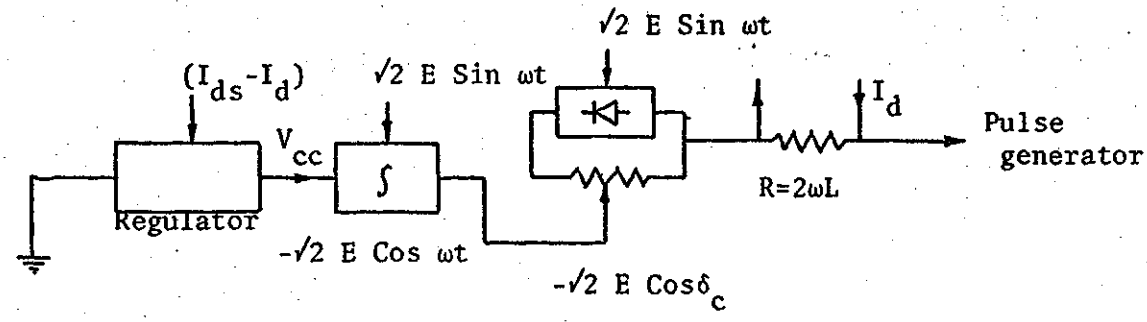

Figure 2.8 A schematic block diagram of an individual phase control.

Equidistant firing control

The individual phase control uses the amplified current error feedback signal and a.c. supply voltages. This method is adversely affected by the presence of even small harmonic contents in the a.c. voltages.[28-31] In addition to the normal (6k ± 1)th current harmonics in the a.c. system, abnormal harmonics of other orders may also be experienced due to unbalanced a.c. line voltages and convertor firing angle asymmetries. The abnormal harmonics are further amplified due to controller feedback action.

Equidistant firing control provides symmetrical firing of the valves and therefore, practically no abnormal harmonics are experienced.[28] The pulse repetition frequencies are directly proportional to the control signals derived from the rectifier constant current controller and the inverter minimum deionization margin angle controller. Under normal operation, pulse repetition frequency is six times the a.c. system frequency. A block diagram of this controller is shown in Figure 2.9. A further improvement consists of linearizing the current control signal at the rectifier for faster controller response.[29] A predictive type controller is used to provide enough deionization margin for inverter operation along with the modified equidistant firing controller for rectifier operation.

2.4.2 Constant power control

The constant current control does not maintain transmitted power during a.c. system voltage fluctuations. A constant power controller determines the desired current setting which is continuously updated.[18] The mercury arc valves are sensitive to overcurrent. The desired current is inversely proportional to the d.c. voltage for any power setting and therefore an upper limit on the current setting is included. Constant extinction angle and constant current controls described in section 2.3.1 are included to maintain the desired d.c. voltage and current levels in the system.

2.4.3 Automatic frequency ratio control

The automatic frequency ratio control device provided in conjunction with automatic frequency controllers of the interconnected a.c. systems reduces the frequency deviations and the response

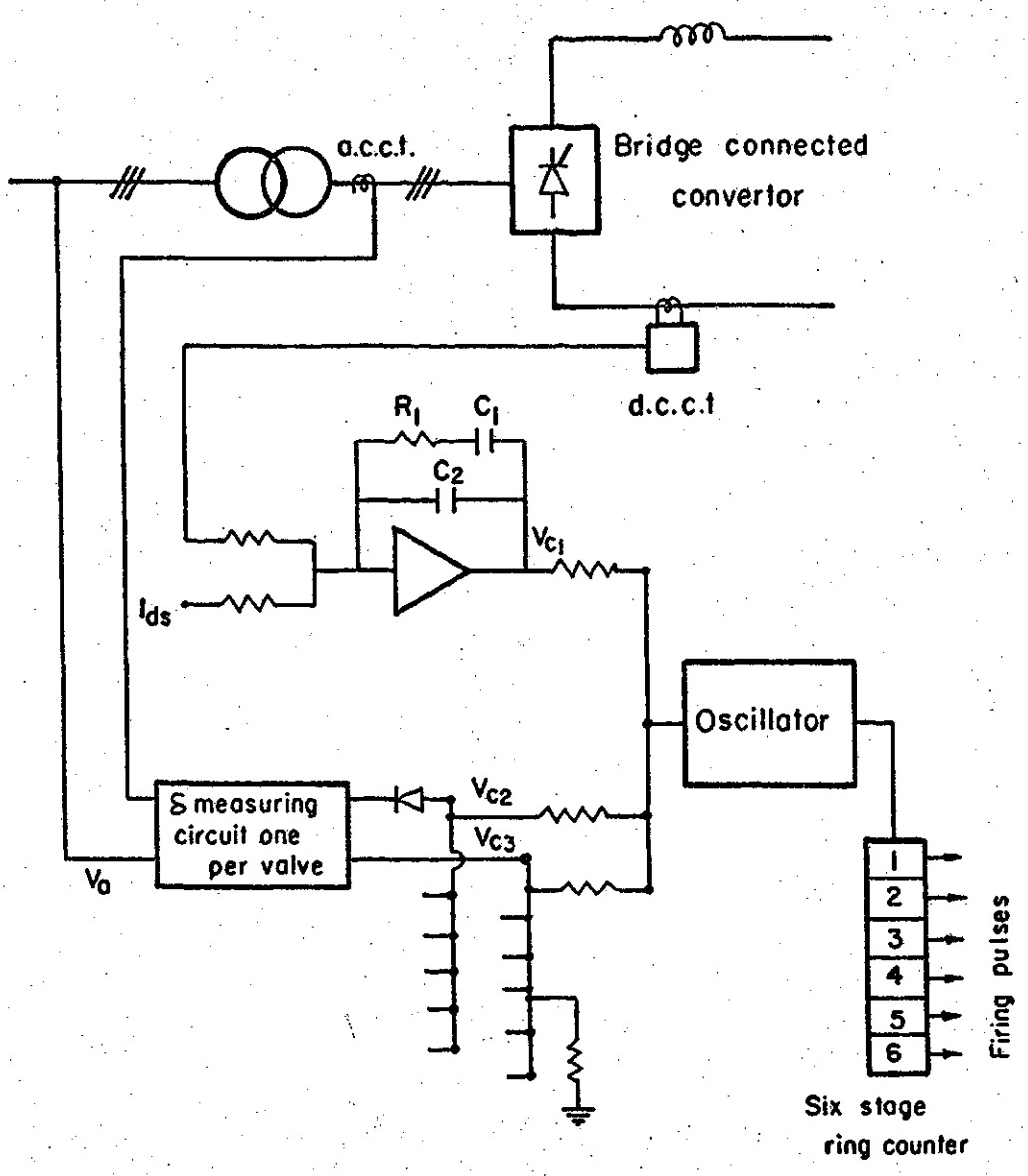

Figure 2.9 A schematic diagram of an equidistant firing control

time.[26, 27] A simplified block diagram of an automatic frequency ratio controller is shown in Figure 2.10. The frequency ratio deviation ΔF of two a.c. systems computed by the frequency detectors is given by

$$\Delta F = k_r \frac{\Delta f_r}{f_{ro}} - k_i \frac{\Delta f_i}{f_{io}} \qquad 2.13$$

Where k is the sensitivity of the frequency detector

r and i denote quantities associated with the rectifier and inverter a.c. systems respectively.

If the frequency ratio deviation is larger than the deadband, the d.c. line power setting is changed by ΔP_d which is given by

$$\Delta P_d = \lambda(k_r \frac{\Delta f_r}{f_{ro}} - k_i \frac{\Delta f_i}{f_{io}}) \qquad 2.14$$

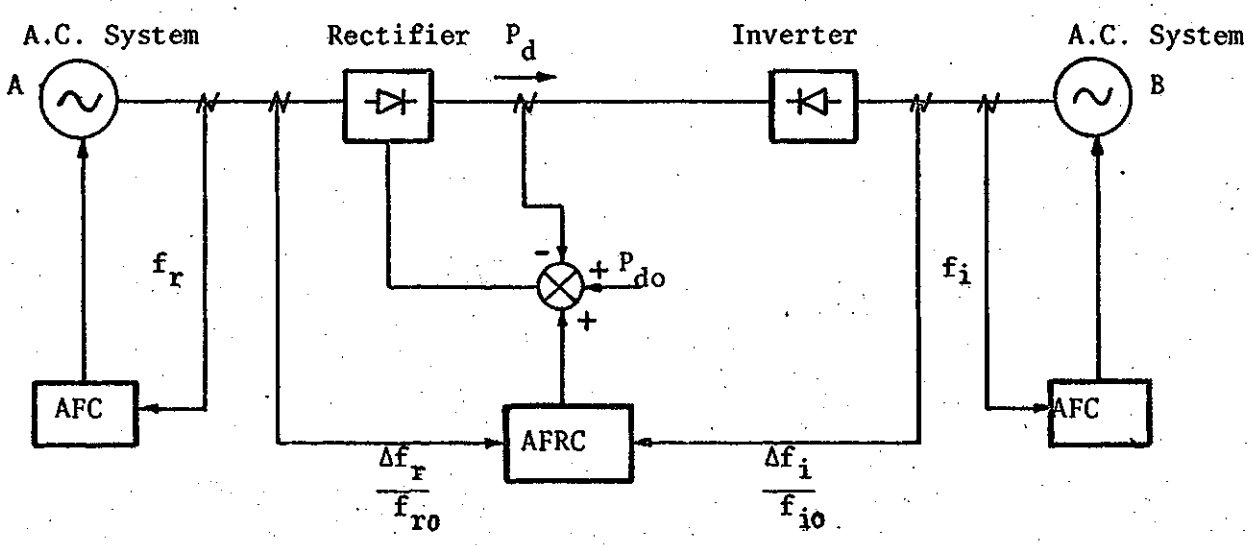

Figure 2.10 A simplified block diagram of an automatic frequency ratio controller.

This power flow change improves the a.c. system frequency damping characteristics.

2.5 D.C. Transmission Line

A transmission line is a distributed parameter system and its performance is usually examined in the form of voltage and current travelling waves.[32] The representation of a transmission line by a number of equivalent tee or pi sections leads to reasonably accurate solutions. In d.c. transmission studies, a line is quite frequently represented by a single equivalent tee network as shown in Figure 2.11. The parameters of this equivalent network are given as follows.[32]

$$Y_e = (G_e + j\omega C_e) = \frac{1}{Z_o} \text{Sinh } (r\sqrt{c/\ell} + j\omega\sqrt{\ell c})d \qquad 2.15a$$

$$Z_e = (R_e + j\omega L_e) = \frac{Z_o\{\text{Cosh}(r\sqrt{c/\ell} + j\omega\sqrt{\ell c})d - 1\}}{\text{Sinh}(r\sqrt{c/\ell} + j\omega\sqrt{\ell c})d}$$

Where Z_o is the characteristic impedance, $\sqrt{\ell/c}$.

d is the transmission line length in miles.

r, ℓ and c are resistance, inductance and capacitance per mile length of the transmission line.

G_e, C_e, R_e and L_e are conductance, capacitance, resistance and inductance of the equivalent tee network elements.

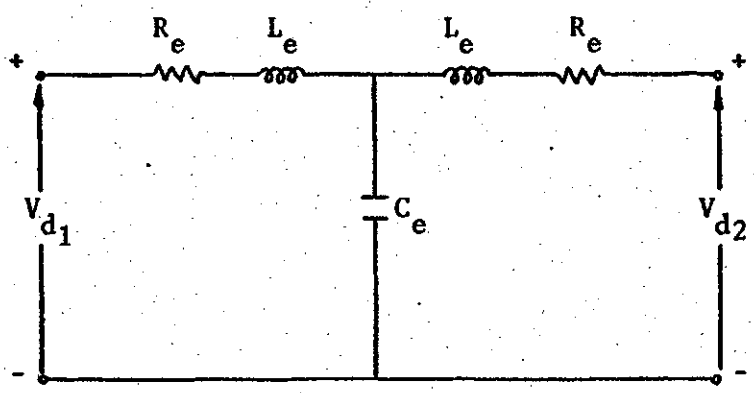

Figure 2.11 Equivalent tee network foran.v.d.c. transmission line.

The rectifier and inverter outputs are applied to the transmission line through d.c. reactors. The small signal rectifier and inverter voltages given by equations 2.7 and 2.8 and the tee network representation are combined to obtain the dynamic representation of a d.c. transmission system shown in Figure 2.12.

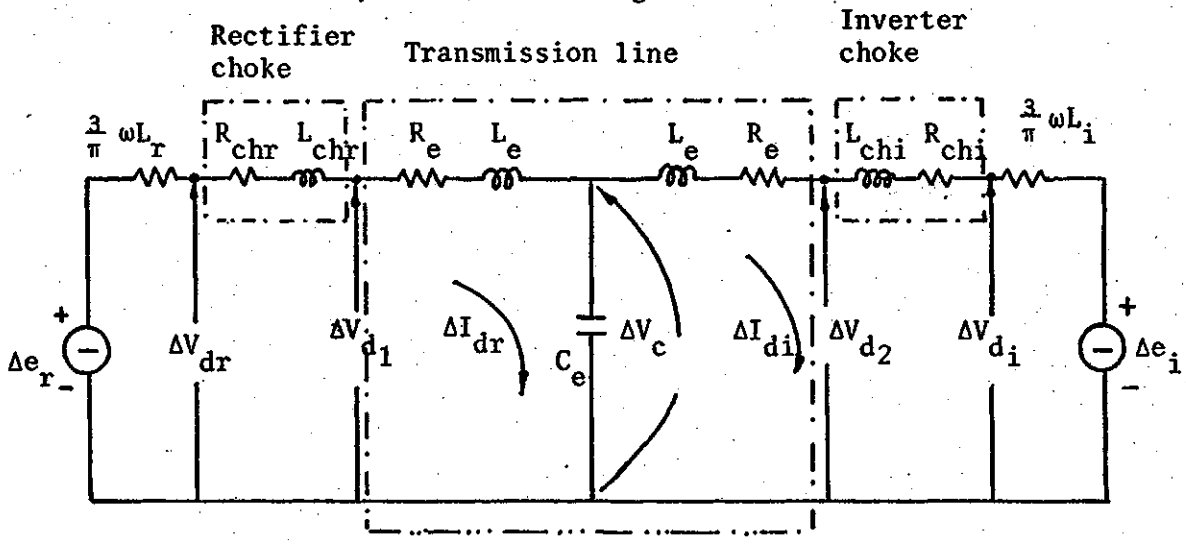

Figure 2.12 Dynamic representation of H.V.D.C. transmission system.

The small signal voltage-current equations representing the system are given by

$$\Delta e_r = R_1 \Delta I_{dr} + L_1 \frac{d\Delta I_{dr}}{dt} + \Delta V_c \qquad 2.16$$

$$-\Delta e_i = R_2 \Delta I_{di} + L_2 \frac{d\Delta I_{di}}{dt} - \Delta V_c \qquad 2.17$$

$$\Delta V_c = \frac{1}{C_e} \int (\Delta I_{dr} - \Delta I_{di}) dt \qquad 2.18$$

$$\Delta e_r = \left(\frac{3\sqrt{2}}{\pi} \cos\alpha_o\right) \Delta E_r - \left(\frac{3\sqrt{2}}{\pi} E_r \sin\alpha_o\right) \Delta\alpha \qquad 2.19$$

$$\Delta e_i = \left(\frac{3\sqrt{2}}{\pi} \cos\beta_o\right) \Delta E_i - \left(\frac{3\sqrt{2}}{\pi} E_i \sin\beta_o\right) \Delta\beta \qquad 2.20$$

Where R_1 is the series combination of the rectifier choke resistance, $\frac{3}{\pi}$ times the commutation reactance and the equivalent line resistance.

R_2 is the series combination of the inverter choke resistance, $\frac{3}{\pi}$ times the commutation reactance and the equivalent line resistance.

L_1 is the series combination of the rectifier d.c. reactor inductance and the equivalent inductance of the line.

L_2 is the series combination of the inverter d.c. reactor inductance and the equivalent inductance of the line.

The rectifier and inverter voltages depend on the a.c. system voltages and valve firing angles. The firing angles in turn depend on the dynamic behaviour of the controllers. The rectifier and inverter voltage changes given by equations 2.19 and 2.20 were modified to include the effect of controllers for the system studies reported in this thesis.

A general historical background of the development of h.v.d.c. systems has been described. The steady-state and dynamic operation of convertors has been discussed. The small signal deviations approach introduced in this chapter will be subsequently used in the stability studies of the d.c. systems.

3. H.V.D.C. SIMULATOR - COMMISSIONING AND TRANSFER FUNCTION IDENTIFICATION

The performance of a system can be predicted from digital or analog studies. Most digital studies consist of obtaining a solution of system performance equations by direct and/or iterative techniques. Analog studies may use a mathematical model or an actual system model comprised of small size system equipment and scaled system parameters. A h.v.d.c. simulator and an I.B.M. 360/50 digital computer have been used for the d.c. transmission system studies included in this thesis. The working of the h.v.d.c. simulator components is briefly described. The simulator transfer function was developed and is reported in this chapter.

3.1 H.V.D.C. Simulator

The h.v.d.c. simulator used for this work was purchased from M/S Robinson and Partner, London, England by means of a N.R.C. grant. The simulator has all the essential features of an actual h.v.d.c. transmission scheme and has a d.c. nominal rating of 100 volts and 1 ampere. It consists of back-to-back connected 3-phase bridge convertors, a transmission line, two smoothing reactors, protective and control circuits and a d.c. supply unit. The transistorised control circuits provide the individual phase control described in section 2.3.1. The major components of this simulator as listed in Table 3.1 are briefly described in this chapter.

Table 3.1 Major components of the h.v.d.c. simulator

Name of the component	Quantity - sets
Convertor units	2
Transmission line units	2
Manual control units	2
Protection units	2
Fault simulator unit	1
D.C. power supply unit	1

3.1.1 Convertor units

Each convertor unit consists of seven thyristors forming a three phase bridge convertor with a bypass valve. The necessary R-C damping circuits are provided across each thyristor to suppress high frequency oscillations. Three,single phase, three winding, 230/130/85 volts transformers provide a.c. supply to the convertors. The transformer primary and tertiary windings are wye and delta connected respectively. The transformer secondary windings have six taps and can be wye or delta connected for 85 volts nominal output. A d.c. current transformer is provided in each convertor anode terminal. Three single phase transformers provide six phase output for manual and automatic control circuits.

3.1.2 Transmission line

Each transmission line unit consists of twenty pi sections. Each pi section can be used to simulate an overhead or a cable transmission line by suitable element combinations. The rating of the pi sections elements provided are listed in Table 3.2. The voltages and currents can be monitored at the pi section terminals.

Table 3.2 Ratings of each pi section elements.

Elements	Overhead line	Cable
Series branch	R = 0.5 ohm	R = 0.25 ohm
	L = 5 mH	L = 2.5 mH
Each shunt branch	C = 0.022 μF	C = 1.022 μF

3.1.3 Manual control unit

The manual control unit of each convertor includes a phase shifting device and six firing pulse circuits which are used for manual as well as automatic control. A reduced three phase voltage is applied to the phase shifting device which provides a phase controlled output. A phase angle controlled six phase supply is obtained from three single phase transformers excited by the synchro output. The convertor bridge valves are fired at the synchro output voltage positive going zero crossing detected by a Schmitt level detector. The firing delays are controlled by adjusting the synchro output phase angles with respect to the a.c. system voltages.

A schematic diagram of the manual control arrangement is shown in Figure 3.1.

3.1.4 Automatic control unit

The simulator uses individual phase control discussed in section 2.4.1 for operation in the automatic mode. The system consists of six constant extinction angle (c.e.a.) control circuits and a constant current controller for each convertor. Each valve is independently controlled and its firing instant is computed every cycle. The c.e.a. control uses the integration of commutation voltage to determine the required firing instant. A block diagram of the arrangement is shown in Figure 3.2. The control circuit voltage $-\sqrt{2}\ E \sin \omega t$ proportional to one of the six commutation voltages is integrated by an operational amplifier integrator. A Schmitt level detector 'A' detects the zeros of control circuit voltage. A pulse operates a clamping circuit at the positive going zero of the control circuit voltage for the minimum dionization time δ_c. The circuit discharges the integrator and clamps the output to ground for the minimum deionization time. The integrator output is, therefore, given by

$$-\int_{-\pi+\delta_c}^{\omega t} -\sqrt{2}\ E \sin \omega t\, d\omega t = -\sqrt{2}\ E \cos \omega t - \sqrt{2}\ E \cos\delta_c .$$

A signal proportional to $2\omega L I_d$ is obtained from a potentiometer connected to the d.c. current transformer output. This signal and the integrator output are added at a summing junction to obtain the time varying voltage e of equation 2.10 reproduced here

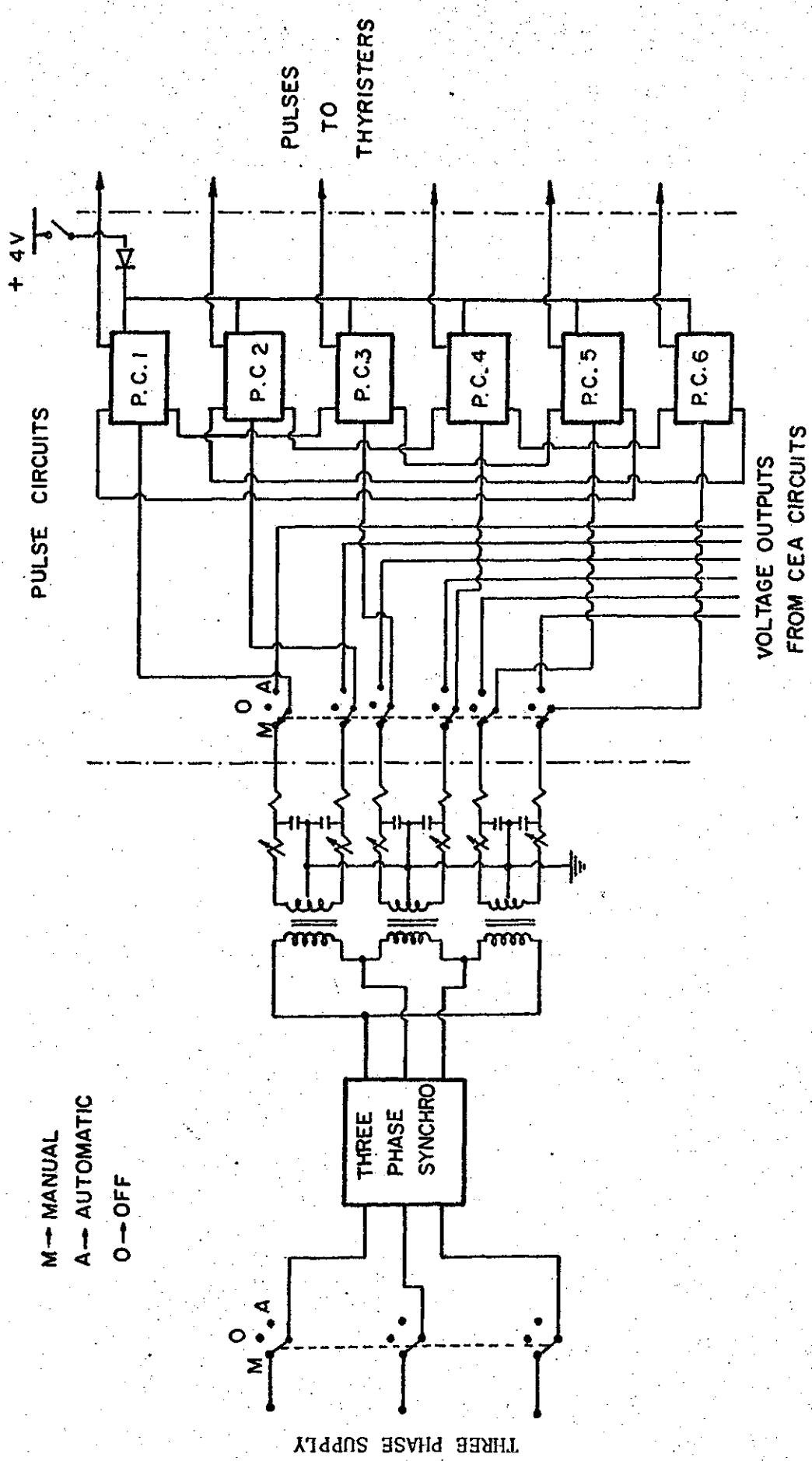

Figure 3.1 A schematic block diagram of simulator manual control mechanism.

$$e = -\sqrt{2}\ E\ \text{Cos}\ \omega t - \sqrt{2}\ E\ \text{Cos}\ \delta_c + 2\omega L I_d \qquad 3.1$$

The convertor valve is fired when the time varying voltage e passes through a positive going zero. An individual control for each of the six bridge thyristors is provided for inverter constant extinction angle control. The difference between the d.c. current transformer output proportional to I_{ds} is amplified by the constant current control operational amplifier circuit to obtain the voltage signal V_{cc}. This output is provided for $I_{ds} \geq I_d$ and is also applied to the summing junction described above to reduce the firing delay for the rectifier operation. The diode D1 as shown in Figure 3.3 clamps the amplifier output if I_{ds} is less than I_d and the convertor operates in the constant extinction angle mode. The time varying voltage e can be positive at all times if V_{cc} is too large. No firing pulses will be provided under these circumstances. To avoid this form of convertor failure, a negative pulse of width 5 electrical degrees is added to the c.e.a. output at the negative peak as shown in Figure 3.4. This negative pulse is provided by the clamping circuit of the c.e.a. control circuit of the other thyristor in the same arm of the bridge as shown in Figure 3.5.

3.1.5 Protection unit

Abnormal operating conditions such as overcurrent, commutation failure and back-fire can damage the convertor valves. The protection unit detects these faults and initiates the convertor blocking circuit which switches off the valve firing pulses and provides a deblocking pulse to the bypass valve. The d.c. system can be manually reset following the blocking of a bridge.

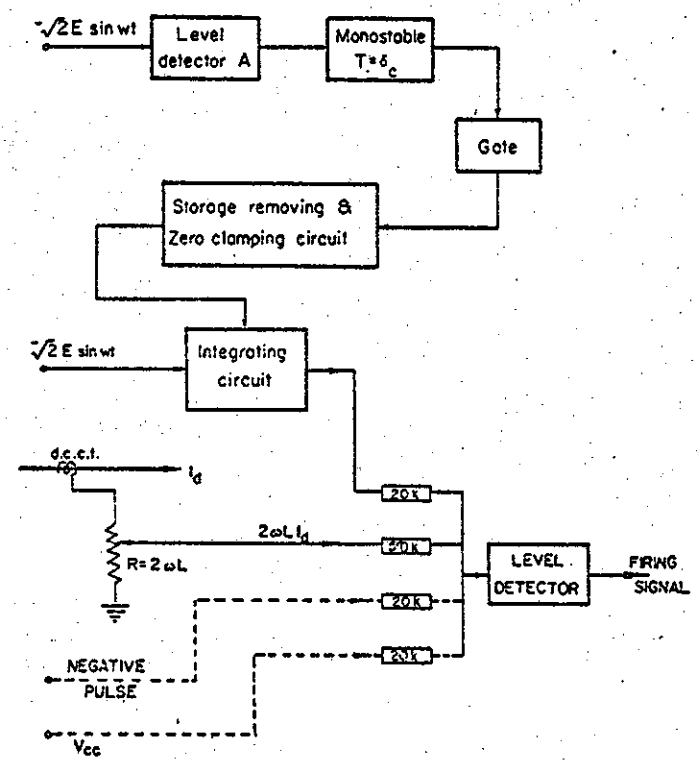

Figure 3.2 A schematic block diagram of constant extinction angle control.

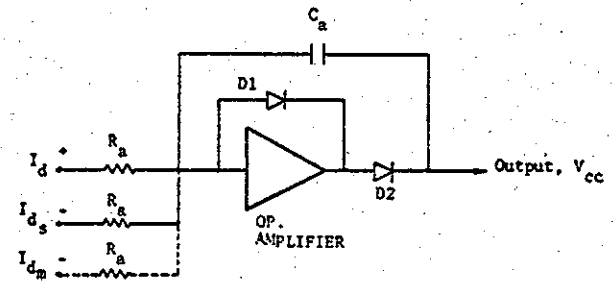

Figure 3.3 Simplified diagram of an operational amplifier for constant current control.

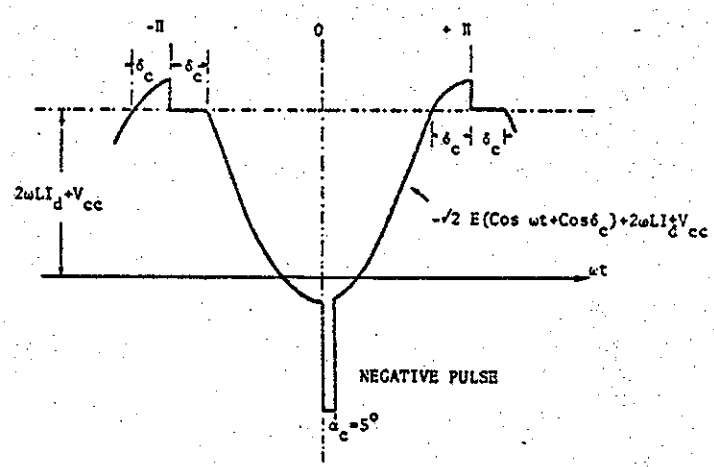

Figure 3.4 Firing signal waveform for automatic control.

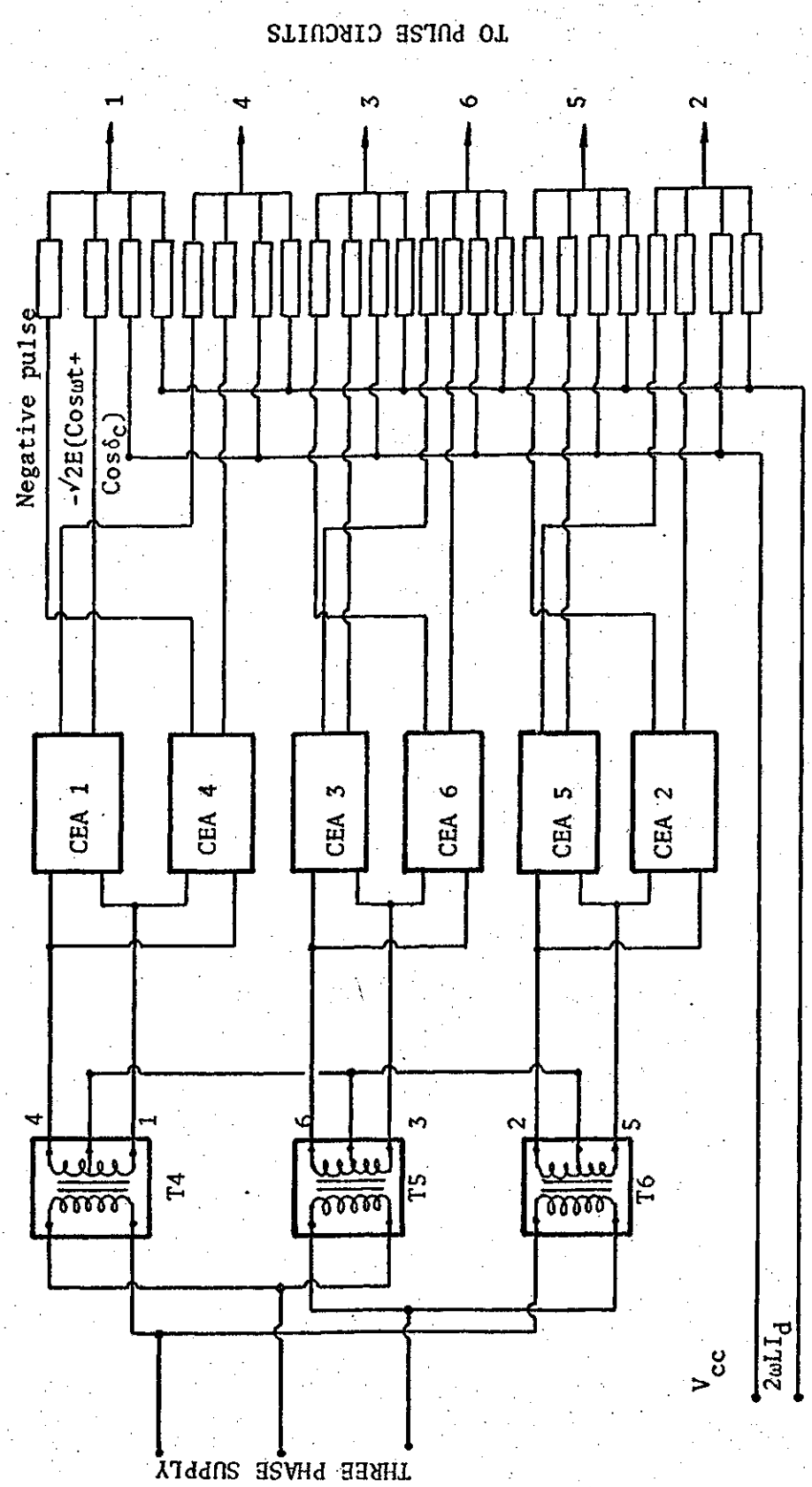

Figure 3.5 A schematic block diagram of simulator automatic control mechanism.

3.1.6 Fault simulator unit

The failure to fire, fire through or back fire single contingency fault can be simulated on either of the convertor units. The initiation, fault delay and duration of these faults can be controlled. The failure to fire, fire through or back fire faults are simulated by valve selection, initiation and biasing circuits.

The simulator was found inoperative when initially started. The causes of improper functioning and the remedial measures adopted are reported in Appendix IV. The parameters of the convertor transformers, d.c. current transformers and control circuit input/output were established as reported in Appendix IV. These settings were used to determine the operating point in the system identification.

3.2 The Simulator Transfer Function Identification

The transfer function of a system can be evaluated using a direct or an indirect approach. The direct approach computes the transfer function from the known dynamics and parameters of the system elements. If the dynamics and parameters of the system components are not known completely from design information or cannot be separately evaluated, indirect methods are used to obtain the transfer function. Bode's decomposition or Levy's curve fitting techniques can be used if the frequency response can be determined[34] and the Simoiu technique if the transient response is known.[33]

The main components of the h.v.d.c. simulator and its controllers are shown in Figure 3.6. The dynamics and parameters of the simulator elements are either known or can be measured. The transfer function of the simulator is, therefore, obtained by direct evaluation.

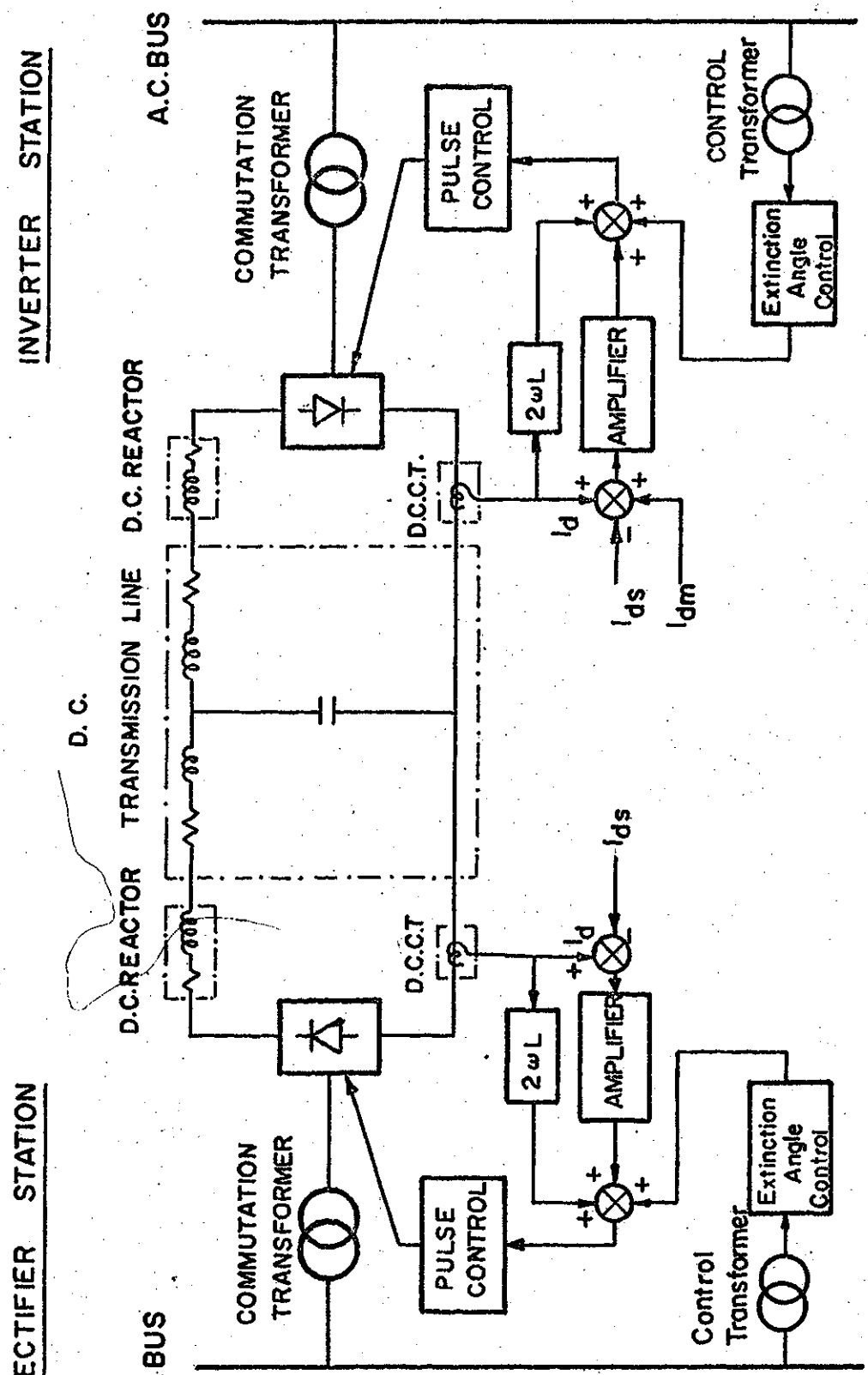

Figure 3.6: Main components of the h.v.d.c. simulator and its controllers.

3.2.1 Convertor bridge transfer function

A convertor bridge is a nonlinear switching device and requires different describing functions for different operating conditions. In high voltage d.c. transmission system studies it is reasonable to assume that the convertor output is equal to its average voltage output.[7] The rectifier and inverter performance can, therefore, be represented by equations 2.7 and 2.8 which are reproduced here.

$$\Delta V_{dr} = \Delta e_r - \frac{3}{\pi}\omega L_r \Delta I_{dr} \qquad 3.2$$

$$\Delta e_r = \left(\frac{3\sqrt{2}}{\pi} \cos\alpha_o\right) \Delta E_r - \left(\frac{3\sqrt{2}}{\pi} E_r \sin\alpha_o\right) \Delta\alpha \qquad 3.3$$

$$\Delta V_{di} = \Delta e_i + \frac{3}{\pi}\omega L_i \Delta I_{di} \qquad 3.4$$

$$\Delta e_i = \left(\frac{3\sqrt{2}}{\pi} \cos\beta_o\right) \Delta E_i - \left(\frac{3\sqrt{2}}{\pi} E_i \sin\beta_o\right) \Delta\beta \qquad 3.5$$

The block diagrams and transfer functions representing the small signal equations 3.3 and 3.5 are shown in Figure 3.7

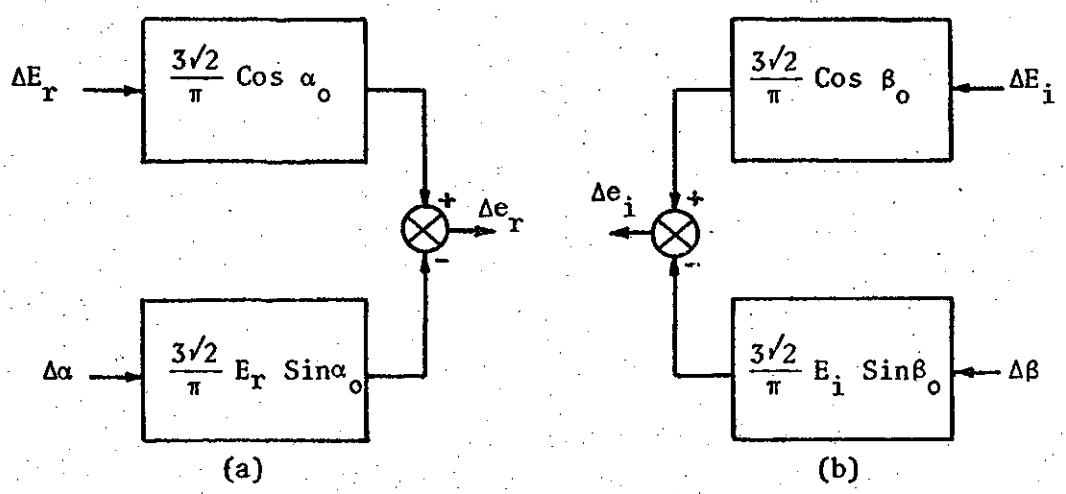

Figure 3.7 Transfer functions of (a) rectifier and (b) inverter bridges for zero commutation reactance.

The commutation reactance drop is simulated as a resistance in series with the transmission line.

3.2.2 Inverter firing control

The inverter firing advance angle β for a valve is determined by the c.e.a. control circuit simulating the equation

$$\frac{1}{K_2}\left(\sqrt{2}\,E_i\,\cos\beta - \sqrt{2}\,E_i\,\cos\delta_c + 2\omega L I_{di}\right) = 0 \qquad 3.6$$

The small signal equation at an operating point is given by

$$\sqrt{2}\,(\cos\beta_o - \cos\delta_c)\,\Delta E_i - (\sqrt{2}E_i\sin\beta_o)\,\Delta\beta + 2\omega L_i \Delta I_{di} = 0 \qquad 3.7$$

Where the subscript o denotes the values at the operating point. The firing advance angle change Δβ due to d.c. current and a.c. voltage changes is given by

$$\Delta\beta = \frac{1}{\sqrt{2}E_i\sin\beta_o}\left\{\sqrt{2}(\cos\beta_o - \cos\delta_c)\,\Delta E_i + (2\omega L_i)\Delta I_{di}\right\} \qquad 3.8$$

The block diagram and transfer functions for inverter firing control are shown in Figure 3.8.

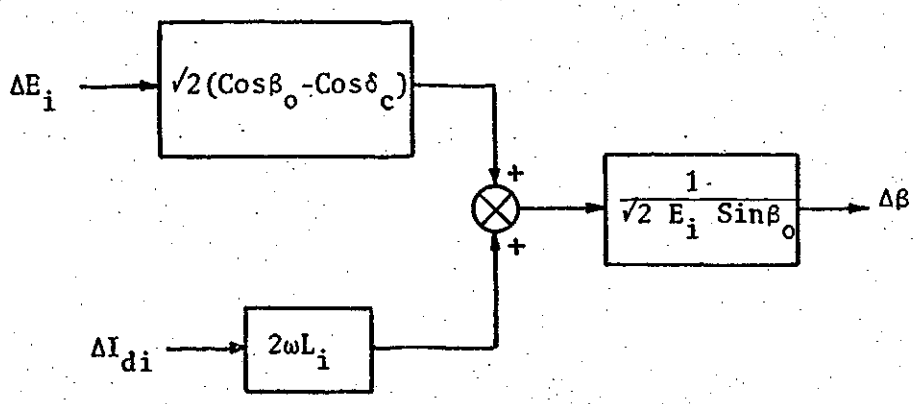

Figure 3.8 Transfer functions of inverter firing control.

3.2.3 Rectifier firing control

The rectifier firing is controlled by c.e.a., commutation reactance drop compensation and constant current controller circuits. A rectifier valve is fired when the voltage at the summation junction of Figure 3.2 is zero and is increasing. At this instant the following equation is satisfied

$$\frac{1}{K_2}(-\sqrt{2}E_r\cos\alpha - \sqrt{2}E_r\cos\delta_c + 2\omega L_r I_{dr}) + \frac{1}{K_p}V_{cc} = 0 \qquad 3.9$$

The small signal equation at the operating point is given by

$$\frac{-\sqrt{2}}{K_2}(\cos\alpha_o+\cos\delta_c)\ \Delta E_r+(\frac{\sqrt{2}}{K_2}E_r\sin\alpha_o)\ \Delta\alpha+(\frac{2\omega L_r}{K_2})\ \Delta I_{dr}+\frac{1}{K_p}\Delta V_{cc}=0 \qquad 3.10$$

The constant current controller output V_{cc} is given by

$$V_{cc} = \frac{1}{R_a C_a}\int(I_{ds}\ \text{signal} - \text{d.c.c.t. output})\ dt \qquad 3.11$$

In Laplace domain

$$V_{cc} = \frac{1}{R_a C_a S}(K_c I_{ds} - K_c I_{dr}) \qquad 3.12$$

Where K_c=4.4, R_a=15k , C_a=6.7 μF.

The small signal equation at the operating point is given by

$$\Delta V_{cc} = \frac{K_c}{R_a C_a S}(\Delta I_{ds} - \Delta I_{dr}) \qquad 3.13$$

The rectifier firing delay angle change $\Delta\alpha$ due to small changes in the set d.c. current and a.c. voltage obtained from equation 3.10 is given by

$$\Delta\alpha = \frac{1}{\sqrt{2}E_r \sin\alpha_o}\{-\sqrt{2}(\cos\alpha_o+\cos\delta_c)\ \Delta E_r + (2\omega L_r)\Delta I_{dr} + (\frac{K_2}{K_p})\Delta V_{cc}\} \quad 3.14$$

The block diagram and transfer functions for rectifier firing control obtained from equations 3.13 and 3.14 are shown in Figure 3.9 .

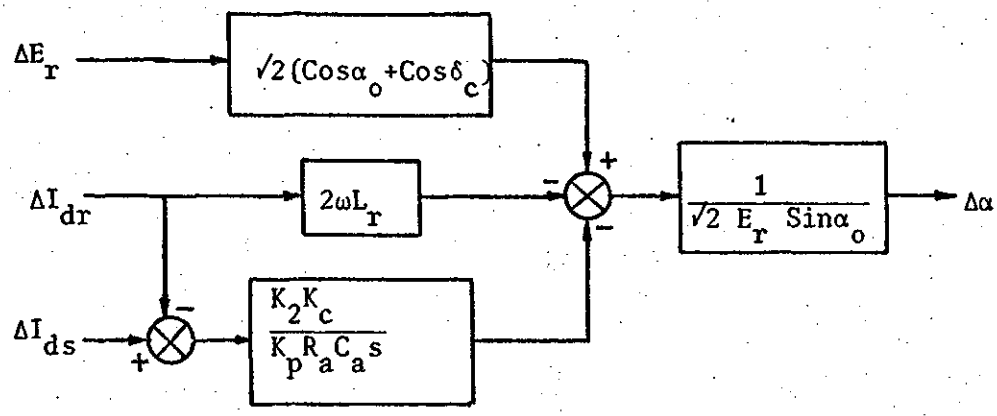

Figure 3.9 Transfer functions of rectifier firing control.

3.2.4 Transmission line

An equivalent tee representation of the transmission line, d.c. reactors and equivalent resistance representing the commutation voltage drop is shown in Figure 2.12. The small signal equations for this element are given by

$$\Delta e_r = (R_1 + sL_1 + \frac{1}{Cs})\ \Delta I_{dr} - (\frac{1}{Cs})\ \Delta I_{di} \quad 3.15$$

$$\Delta e_i = (\frac{1}{Cs})\ \Delta I_{dr} - (R_2 + sL_2 + \frac{1}{Cs})\ \Delta I_{di} \quad 3.16$$

The d.c. current changes obtained from equations 3.15 and 3.16 can be expressed in matrix form as follows:

$$\begin{bmatrix} \Delta I_{dr} \\ \Delta I_{di} \end{bmatrix} = \begin{bmatrix} G_{11}(s) & G_{12}(s) \\ G_{21}(s) & G_{22}(s) \end{bmatrix} \begin{bmatrix} \Delta e_r \\ \Delta e_i \end{bmatrix} \qquad 3.17$$

Where $$G_{11}(s) = \frac{\frac{1}{L_1}(s^2 + \frac{R_2 s}{L_2} + \frac{1}{L_2 C})}{D(s)}$$

$$D(s) = s^3 + s^2(\frac{R_1}{L_1} + \frac{R_2}{L_2}) + s(\frac{R_1}{L_1} \cdot \frac{R_2}{L_2} + \frac{1}{L_1 C} + \frac{1}{L_2 C}) + (\frac{R_1}{L_1}\frac{1}{L_2 C} + \frac{R_2}{L_2}\frac{1}{L_1 C})$$

$$G_{12}(s) = \frac{-(\frac{1}{L_1 L_2 C})}{D(s)}$$

$$G_{21}(s) = \frac{\frac{1}{L_1 L_2 C}}{D(s)}$$

$$G_{22}(s) = \frac{-\frac{1}{L_2}(s^2 + \frac{R_1 s}{L_1} + \frac{1}{L_1 C})}{D(s)}$$

The block diagram and transfer functions for the transmission line and the commutation reactance drop obtained from equation 3.17 is shown in Figure 3.10.

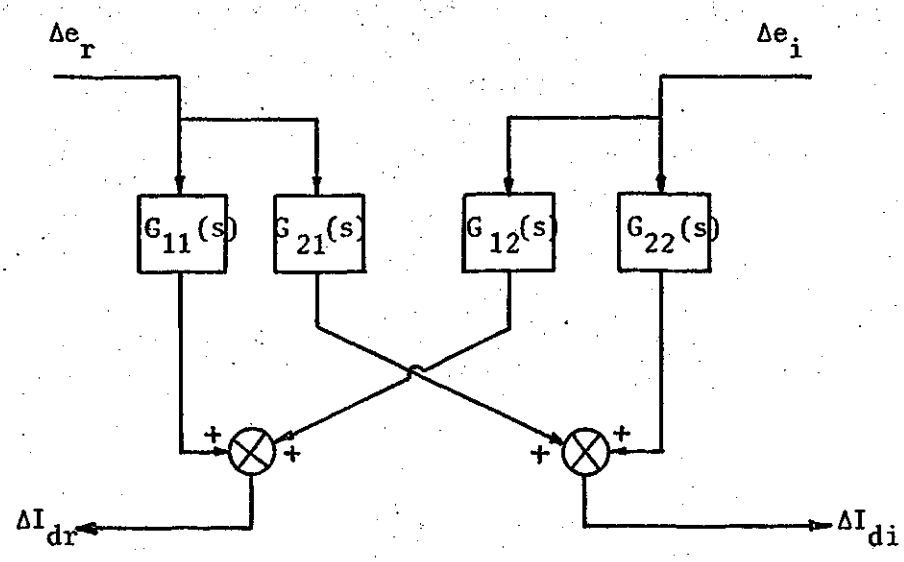

Figure 3.10 Transfer functions of the transmission line.

A complete block diagram and the transfer functions of the simulator and its controllers are shown in Figure 3.11. This model forms the basis of the state space analysis in Chapter 4.

The simulator components and their functions, circuit faults noticed and the changes made have been briefly described in this chapter. The simulator transfer functions and block diagram model representing small perturbations about an operating point established in this chapter can be used for system analysis and controller synthesis.

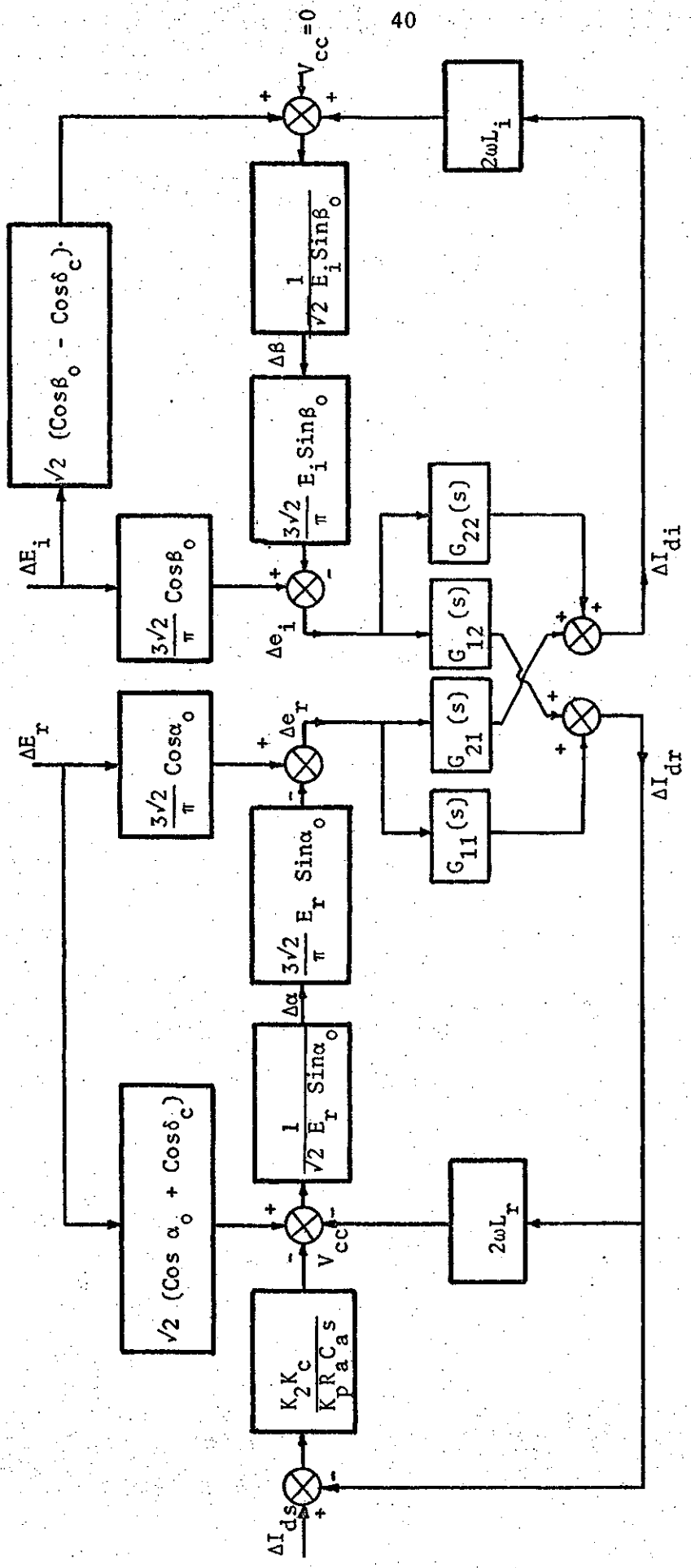

Figure 3.11 The simulator transfer function and block diagram model.

4. SYSTEM ANALYSIS

Two basic system analysis techniques viz classical and modern are used in Control Engineering.[34] Second and higher order differential equation representations, poles and zeros and frequency response constitute the classical approach. In this technique the controller design and optimization is based on Bode's, Nyquist or Root Locus plots. It does not provide a time domain solution but only indicates whether the system is stable or unstable. Moreover it is not convenient for fifth or higher order system studies. The first order differential equation representation called the state space technique and Hamilton's principle are used for system studies, controller design and optimization in the modern approach. This technique provides a time domain solution of the system dynamic equations. H.V.D.C. system stability studies using Nyquist plots have been reported in the past.[7-13] The performance of a hypothetical high voltage d.c. system interconnecting an isolated generator to an infinite bus has been investigated using the state space technique.[14,15] The state equations describing the h.v.d.c. simulator dynamics are formulated from the transfer functions developed in Chapter 3. A digital computer program including the controller non-linearities was developed and used for system stability studies. Simulator tests are included to confirm the digital model and stability studies.

4.1 State Space Theory

A set of first order differential equations are obtained by a transformation of the system dynamic equations.[34-37] If a system

is described by an nth order differential equation

$$x^{(n)} = f(x, \dot{x}, \ddot{x}, \ldots\ldots, x^{(n-1)} ; u ; t) \qquad 4.1$$

Where u is the forcing function

x is the system variable

t denotes time

and $\dot{}$ denotes the first derivative

then new variables $x_1, x_2, \ldots\ldots, x_n$ are described such that

$$x_1 = x^{(0)} = x$$

$$x_2 = x^{(1)} = \dot{x} = \dot{x}_1$$

$$x_3 = x^{(2)} = \ddot{x} = \dot{x}_2$$

.....

.....

$$x_n = x^{(n-1)} = \dot{x}_{n-1} \qquad 4.2$$

Using equation 4.2 $x^{(n)}$ is expressed as

$$x^{(n)} = f(x_1, x_2, x_3, \ldots\ldots, x_n ; u ; t) \qquad 4.3$$

Equations 4.2 and 4.3 provide n first order differential equations. Usually a system has more than one input and output . The state space

equations of an nth order system with r inputs and m outputs are given by

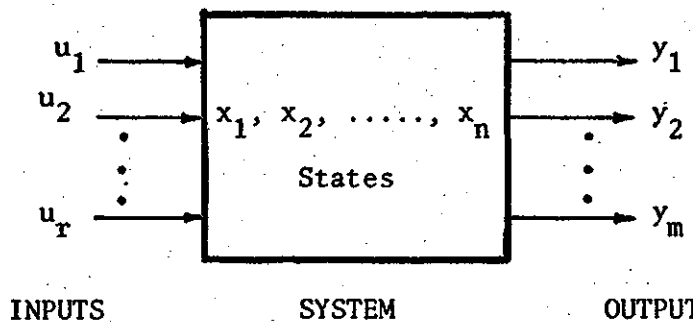

Figure 4.1 A linear system with r inputs, m outputs and n states.

$$\dot{x}_i = f_i(x_1, x_2, \ldots, x_n; u_1, u_2, \ldots, u_r; t) \qquad 4.4$$

Where $i = 1, 2, \ldots, n$.

$x_1, x_2, \ldots, x_n$ are state variables.

$u_1, u_2, \ldots, u_r$ are the forcing functions.

The output variables $y_1, y_2, \ldots, y_m$ are expressed by

$$y_j = g_j(x_1, x_2, \ldots, x_n; u_1, u_2, \ldots, u_r ; t) \qquad 4.5$$

Where $j = 1, 2, \ldots, m$; $m \leq n$.

The state space equations 4.4 and 4.5 are expressed in matrix form as follows

$$[\dot{x}] = [A][x] + [B][u] \qquad 4.6$$

$$[y] = [C][x] + [D][u] \qquad 4.7$$

Where $[x]$ - nx1 state vector

$[A]$ - nxn state coefficient matrix

$[B]$ - nxr forcing function coefficient matrix

$[u]$ - rx1 forcing function vector

$[y]$ - mx1 output vector

$[C]$ - mxn state-output coefficient matrix

$[D]$ - mxr forcing function output coefficient matrix.

This method is used to formulate the state space equations from a second or higher order differential equation.

A system may be described by a transfer function with m poles and n zeros instead of high order differential equations.

$$G(s) = \frac{V(s)}{U(s)} = \frac{K(a_m s^m + a_{m-1} s^{m-1} + \ldots + a_1 s+1)}{(b_n s^n + b_{n-1} s^{n-1} + \ldots + b_1 s+1)} \qquad 4.8$$

Where K is the system gain

V(s) and U(s) represent system output and input

s is the Laplace operator.

Rearranging equation 4.8 and dividing by s^n, the following equation is obtained

$$b_n V(s) + \frac{1}{s}(b_{n-1} V(s) + \ldots + \frac{1}{s}((b_m V(s) - Ka_m U(s)) + \frac{1}{s}((b_{m-1} V(s) - Ka_{m-1} U(s))$$

$$+\frac{1}{s}(\ldots + \frac{1}{s}((b_1 V(s) - Ka_1 U(s)) + \frac{1}{s}(V(s) - KU(s))) \ldots) = 0 \qquad 4.9$$

If x_1, x_2, x_3, ... , x_n new variables are defined such that

$$s\,x_1(s) = V(s) - K\,U(s)$$

$$s\,x_2(s) = b_1\,V(s) - K\,a_1\,U(s) + x_1(s)$$

.....

.....

$$s\,x_n(s) = b_{n-1}\,V(s) + x_{n-1}(s) \quad , \qquad 4.10$$

equation 4.9 reduces to the form

$$b_n V(s) = -x_n(s)$$

$$V(s) = -\frac{1}{b_n}\,x_n(s) \qquad 4.11$$

The time domain equations are obtained from equation 4.10 by substituting for V(s) from equation 4.11.

$$\dot{x}_1(t) = -\frac{1}{b_n}x_n(t) - K\,U(t)$$

$$\dot{x}_2(t) = x_1(t) - \frac{b_1}{b_n}\,x_n(t) - K\,a_1\,U(t)$$

$$\dot{x}_3(t) = x_2(t) - \frac{b_2}{b_n}\,x_n(t) - K\,a_2\,U(t)$$

.....

.....

$$\dot{x}_n(t) = x_{n-1}(t) - \frac{b_{n-1}}{b_n}\,x_n(t) \qquad 4.12$$

Equation 4.12 is conveniently expressed in the matrix form

$$[\dot{x}] = [A][x] + [B][u] \qquad 4.13$$

Where $[x] = [x_1 \quad x_2 \quad x_3 \quad \ldots\ldots \quad x_n]^T$

$$[A] = \begin{bmatrix} 0 & 0 & 0 \ldots\ldots 0 & -\frac{1}{b_n} \\ 1 & 0 & 0 \ldots\ldots 0 & -\frac{b_1}{b_n} \\ 0 & 1 & 0 \ldots\ldots 0 & -\frac{b_2}{b_n} \\ \ldots\ldots\ldots\ldots\ldots\ldots & & & \\ \ldots\ldots\ldots\ldots\ldots\ldots & & & \\ 0 & 0 & 0 \ldots\ldots 1 & -\frac{b_{n-1}}{b_n} \end{bmatrix} ; \quad [B] = -K \begin{bmatrix} 1 \\ a_1 \\ a_2 \\ \vdots \\ a_m \\ 0 \\ \vdots \\ 0 \end{bmatrix}$$

These equations can be used for single input and single output system dynamic studies. The h.v.d.c. transmission schemes and the simulator are multi-input, multi-output systems and therefore multivariable state space representation of equations 4.6 and 4.7 has been used in this thesis.

In the classical approach, roots of the $|A - \lambda I| = 0$ characteristic equation called eigenvalues determine the stability of a system. The system is stable if the real parts of all eigenvalues are negative. The damping ratio and the damping factor also known as the figures of merit indicate the relative stability. Percentage overshoot, rise time and settling time indicate the stability criteria in time domain.

4.2 Mathematical Model of the H.V.D.C. Simulator

The d.c. simulator model is described by equations 3.2 to 3.16 and by the block diagram of Figure 3.16. The small signal equations 4.14 to 4.17 describing the simulator dynamic performance are obtained from this model.

$$\frac{d\Delta I_{dr}}{dt} = \frac{-(R_1 - \frac{6}{\pi}\omega L_r)}{L_1}\ \Delta I_{dr} - \frac{1}{L_1}\Delta V_c + (\frac{3}{\pi}\frac{K_2}{K_p}\frac{1}{L_1})\Delta V_{cc} - (\frac{3\sqrt{2}}{\pi L_1}\cos\delta_c)\ \Delta E_r \qquad 4.14$$

$$\frac{d\Delta I_{di}}{dt} = \frac{-(R_2 - \frac{6}{\pi}\omega L_i)}{L_2}\ \Delta I_{di} + \frac{1}{L_2}\Delta V_c - (\frac{3\sqrt{2}}{\pi L_2}\cos\delta_c)\ \Delta E_i \qquad 4.15$$

$$\frac{d\Delta V_c}{dt} = \frac{1}{C}\ \Delta I_{dr} - \frac{1}{C}\ \Delta I_{di} \qquad 4.16$$

$$\frac{d\Delta V_{cc}}{dt} = -K_c K_a \Delta I_{dr} + K_c K_a\ \Delta I_{ds} \qquad 4.17$$

Where K_a is the gain of the amplifier = $1/R_aC_a$.
Δ denotes a small change in the associated quantity.

Defining ΔI_{dr}, ΔI_{di}, ΔV_c and ΔV_{cc} as the four system state variables x_1, x_2, x_3 and x_4 respectively equations 4.14 through 4.17 are expressed as

$$\begin{bmatrix} \dot{x}_1 \\ \dot{x}_2 \\ \dot{x}_3 \\ \dot{x}_4 \end{bmatrix} = \begin{bmatrix} \frac{-(R_1 - \frac{6}{\pi}\omega L_r)}{L_1} & 0 & \frac{-1}{L_1} & \frac{3}{\pi}\frac{K_2}{K_p}\frac{1}{L_1} \\ 0 & \frac{-(R_2 - \frac{6}{\pi}\omega L_i)}{L_2} & \frac{1}{L_2} & 0 \\ \frac{1}{C} & \frac{-1}{C} & 0 & 0 \\ -K_c K_a & 0 & 0 & 0 \end{bmatrix} \begin{bmatrix} x_1 \\ x_2 \\ x_3 \\ x_4 \end{bmatrix}$$

$$+ \begin{bmatrix} -(\frac{3\sqrt{2}}{\pi}\frac{1}{L_1}\cos\delta_c) & 0 & 0 \\ 0 & -(\frac{3\sqrt{2}}{\pi}\frac{\cos\delta_c}{L_2}) & 0 \\ 0 & 0 & 0 \\ 0 & 0 & K_c K_a \end{bmatrix} \begin{bmatrix} \Delta E_r \\ \Delta E_i \\ \Delta I_{ds} \end{bmatrix} \qquad 4.18$$

Equation 4.18 describes the d.c. simulator state space model used for stability analysis reported in this chapter.

4.3 Stability Analysis I - Root Locus Technique

The stability of a system depends on the equipment parameters and the controller settings. The equipment parameters of a d.c. transmission system are chosen considering transmission capability requirements in addition to its dynamic stability. In the h.v.d.c. simulator, the constant current controller gain can be conveniently varied. The eigenvalues of the simulator characteristic equation for different values of the

amplifier gain were calculated using the I.B.M. Scientific Subroutine Programs HSBG and ATEIG. Subroutine HSBG transforms the state coefficient matrix A to an almost trianglular matrix A_1 using the Hessenberg similarity transformation method. The modified characteristic equation $|A_1-\lambda I|=0$ is then solved for the eigenvalues by the ATEIG subroutine. The root locus plot for increasing amplifier gain is shown in Figure 4.2. It is noticed that roots 1 and 2 are complex conjugates and move slowly as the amplifier gain K_a increases. These roots correspond to 1212 rad/sec frequency which is close to the transmission line natural frequency. Roots 3 and 4 are real and negative for $K_a \leq 3.2$ and complex conjugates for higher gains. These roots show a marked change with increased gain for $K_a > 3.2$ move almost vertically at a rate faster than that of roots 1 and 2. Therefore the system response largely depends on these dominant roots. The amplifier gain for a 0.707 damping ratio as calculated from the root locus plot is 7.5. The current amplifier saturates if 7.5 gain is used as its output overshoots the permissible limit before the d.c. line current increases to the set value. The amplifier feedback gain is adjusted to provide a gain of 10 which corresponds to a 0.495 damping ratio and allows successful simulator starting.

4.4 Stability Analysis II - State Space Technique

The simulator dynamic performance equations are obtained by substituting the system parameters in equation 4.18 and are as follows:

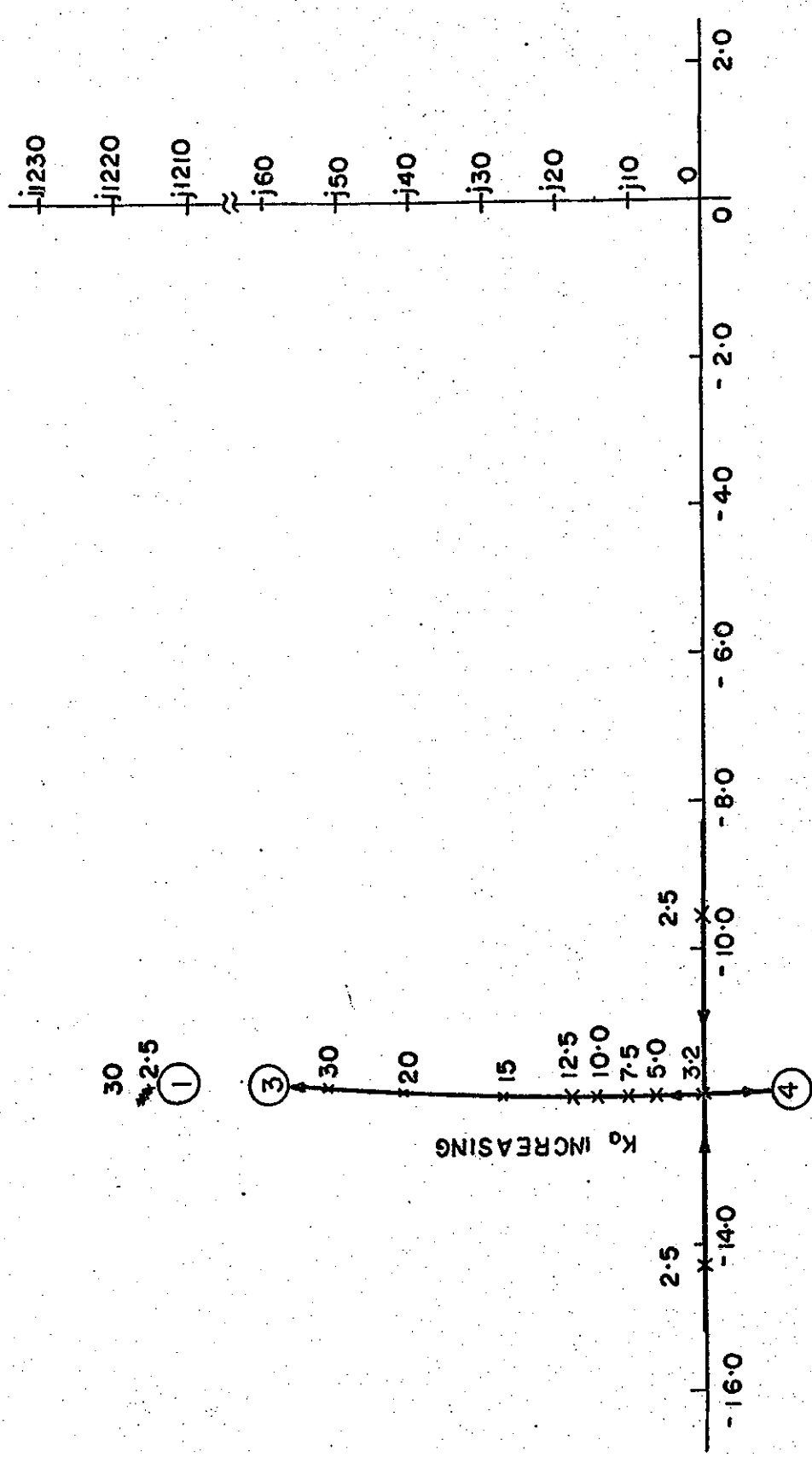

Figure 4.2 Root locus plot for increasing amplifier gain.

$$\begin{bmatrix} \dot{x}_1 \\ \dot{x}_2 \\ \dot{x}_3 \\ \dot{x}_4 \end{bmatrix} = \begin{bmatrix} -23.98975 & 0 & -1.29870 & 103.20797 \\ 0 & -23.98975 & 1.29870 & 0 \\ 5.68181 \times 10^5 & -5.68181 \times 10^5 & 0 & 0 \\ -17.86400 & 0 & 0 & 0 \end{bmatrix} \begin{bmatrix} x_1 \\ x_2 \\ x_3 \\ x_4 \end{bmatrix} +$$

$$\begin{bmatrix} -1.72750 & 0 & 0 \\ 0 & -1.72750 & 0 \\ 0 & 0 & 0 \\ 0 & 0 & -17.8640 \end{bmatrix} \begin{bmatrix} \Delta E_r \\ \Delta E_i \\ \Delta I_{ds} \end{bmatrix} \qquad 4.19$$

The simulator d.c. line current is 0.924 amps if the inverter and rectifier commutation voltages, inverter deionization margin angle and the rectifier delay angle are 76.5 volts, 76.5 volts, 10 and 15 electrical degrees respectively. The constant current controller output and midpoint d.c. transmission line voltages are 2.5 and 80 volts respectively. These operating values are selected as the initial conditions of the four system states for the digital and simulator studies. The commutation voltages have been assumed to remain constant. The fourth-order Runge-Kutta method and a time interval of 0.001 sec were used to calculate the system responses by the state space technique.

A step change of +0.04 amps current order was applied. The digitally calculated d.c. line current due to the current order change is shown in Figure 4.3. The line current settles at the new set value of 0.964 amps after a transient period of 0.27 secs. The rise time is

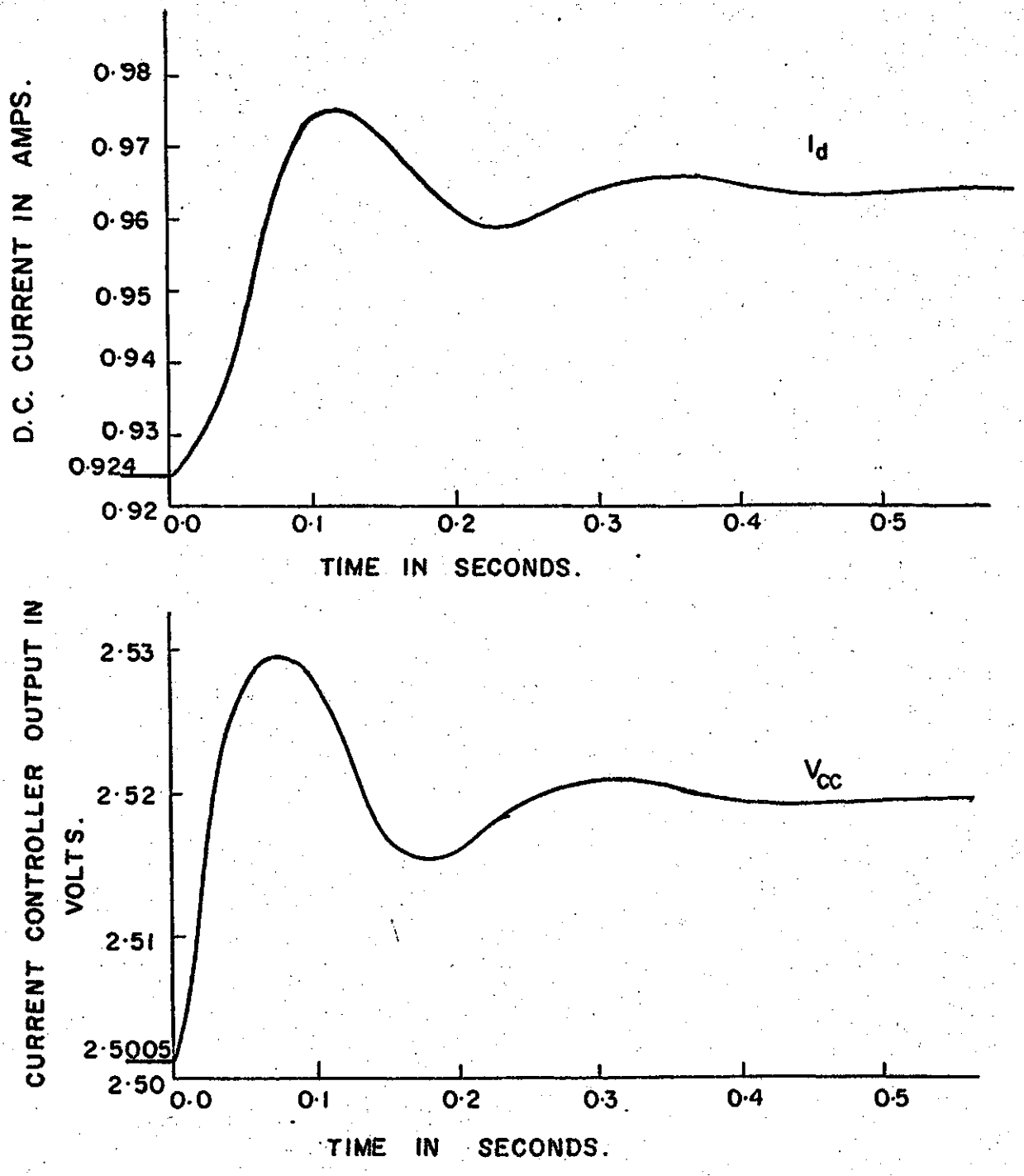

Figure 4.3 The digitally calculated d.c. line current and current controller output response for a+0.04 amp. current order step change.

0.05 secs and approximately 25 percent overshoot occurs 0.11 secs after the step change is applied. The constant current controller output is also plotted in Figure 4.3. The changes in rectifier and inverter d.c. voltages and firing angles during the transient are shown in Figure 4.4 and 4.5 respectively. These responses are similar to that of the d.c. line current. The commutation reactance drop compensation signal is small and therefore the inverter firing advance angle and the inverter d.c. voltage changes are relatively small. The inverter response time delay is due to the transmission line time constant. The line current and rectifier and inverter d.c.voltages recorded at the simulator for the same current order step change are shown in Figure 4.6. The current order change increases the constant current controller output voltage which decreases the rectifier firing delay. This in turn increases the rectifier d.c. voltage and hence the d.c. current. The increased d.c. current modifies the commutation reactance drop compensation and this increases the firing advance angle. The inverter d.c. voltage decreases and further increases the d.c. line current. When the d.c. line current overshoots the set value the above process repeats with converse changes. The settling time, rise time and percentage overshoot from digital and analog studies are shown in Table 4.1. The system responses obtained from digital and analog studies are comparable in form and magnitude.

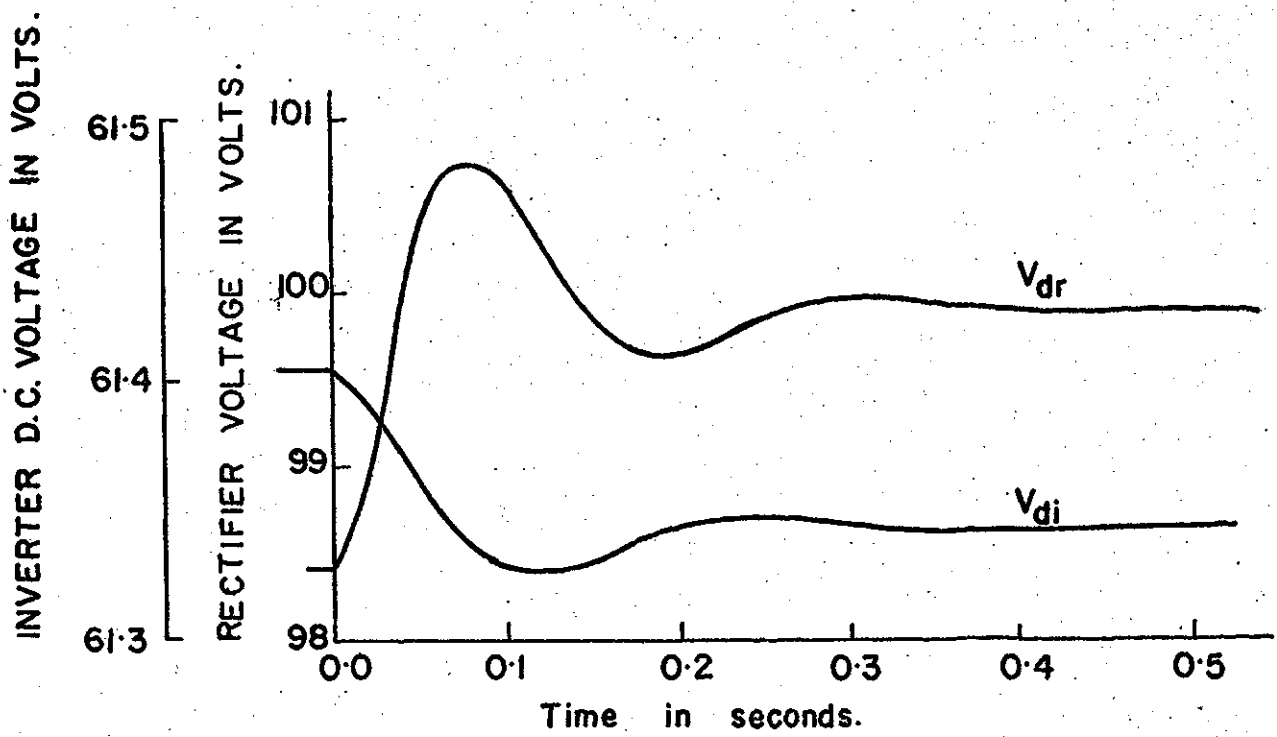

Figure 4.4 The digitally calculated convertor d.c. voltage changes for α+0.04 amp. current order step change.

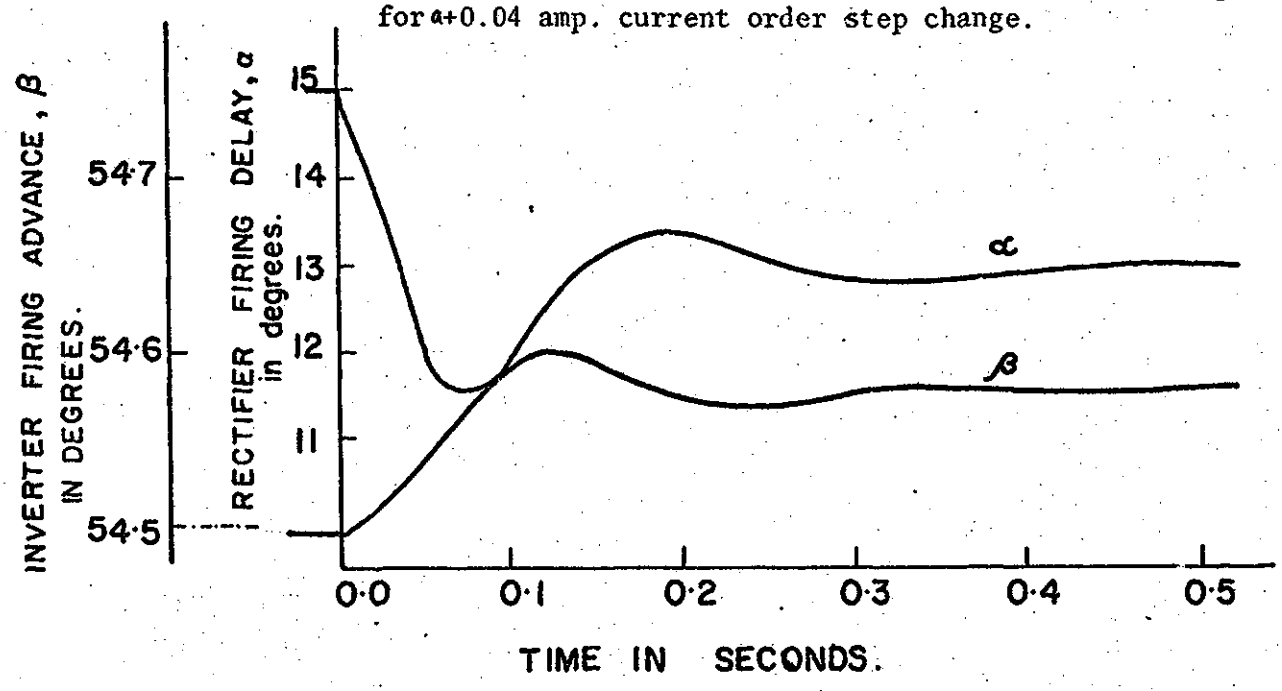

Figure 4.5 The digitally calculated convertor firing angle changes for α+0.04 amp. current order step change.

Table 4.1 Time domain performance of the simulator from digital and analog studies.

	Digital	Analog
Settling time	0.27 sec	0.29 sec
Rise time	0.05 sec	0.055 sec
Overshoot	25%	24%
Time to overshoot	0.11 sec	0.13 sec

A sudden decrease of load in the inverter a.c. system will increase its commutation voltage. A two percent step increase of the inverter commutation voltage was considered to assess the stability of the system. The rectifier commutation voltage and the d.c. line current order were 76.5 volts and 0.924 amps respectively and did not change during the disturbance. The digitally calculated d.c. line current during the disturbance is shown in Figure 4.7. The line current settles within +0.05% of the set value after a transient period of 0.27 secs. A minimum line current of approximately 2.8 percent less than the current order was experienced 0.06 secs after the step change was applied. The constant current controller output is shown in Figure 4.8. The changes in the rectifier and inverter d.c. voltages and firing angles during the transient are shown in Figures 4.9 and 4.10 respectively. The rectifier voltage settles at the new value of 100.4 volts after a transient period of 0.30 secs. The rise time is 0.07 secs and approximately 25% overshoot occurs 0.15 secs

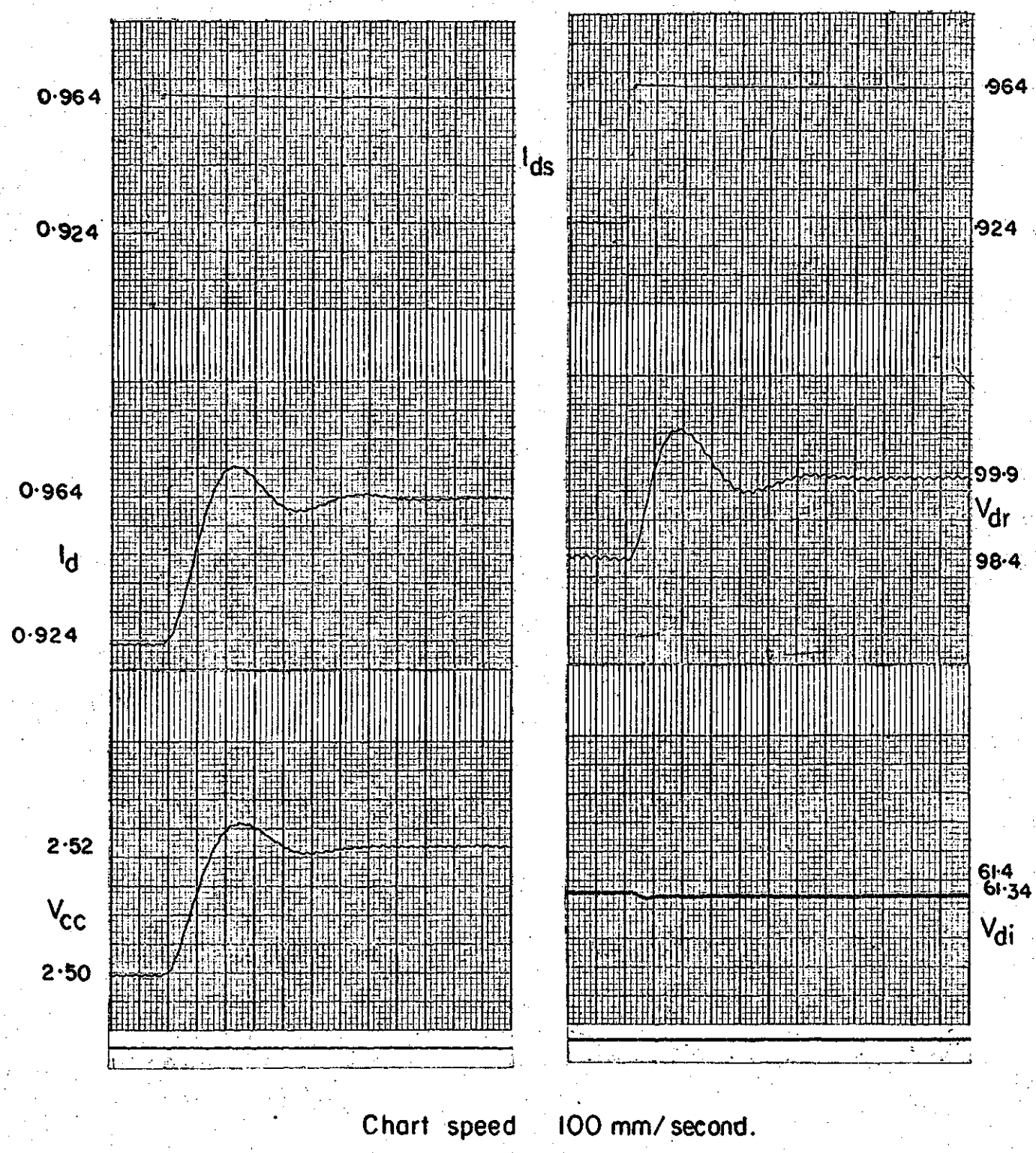

Figure 4.6 The d.c. line current, rectifier and inverter d.c. voltage changes for a+0.04 amp. current order step change recorded from the simulator.

after the step change is applied. The system performance for this disturbance has also been studied on the h.v.d.c. simulator. The line current and rectifier and inverter d.c. voltages recorded at the simulator are shown in Figure 4.11. The inverter commutation voltage change increases the inverter d.c. voltage which decreases the d.c. line current. The decreased d.c. current modifies the commutation reactance drop compensation decreasing the firing advance angle. This in turn increases the inverter d.c. voltage further decreasing the current. The drop in d.c. current increases the current error and hence increases the constant current controller output decreasing the rectifier firing delay angle. The rise in rectifier d.c. voltage increases the d.c. current. The settling time, rise time and percentage overshoot for the rectifier voltage from digital and analog studies are shown in Table 4.2. The system responses obtained from digital and analog studies are comparable in form and magnitude.

Table 4.2 Time domain performance of the simulator from digital and analog studies.

	Digital	Analog
Settling time	0.30 secs	0.33 secs
Rise time	0.07 secs	0.08 secs
Overshoot	25%	28.5%
Time to overshoot	0.15 secs	0.18 secs

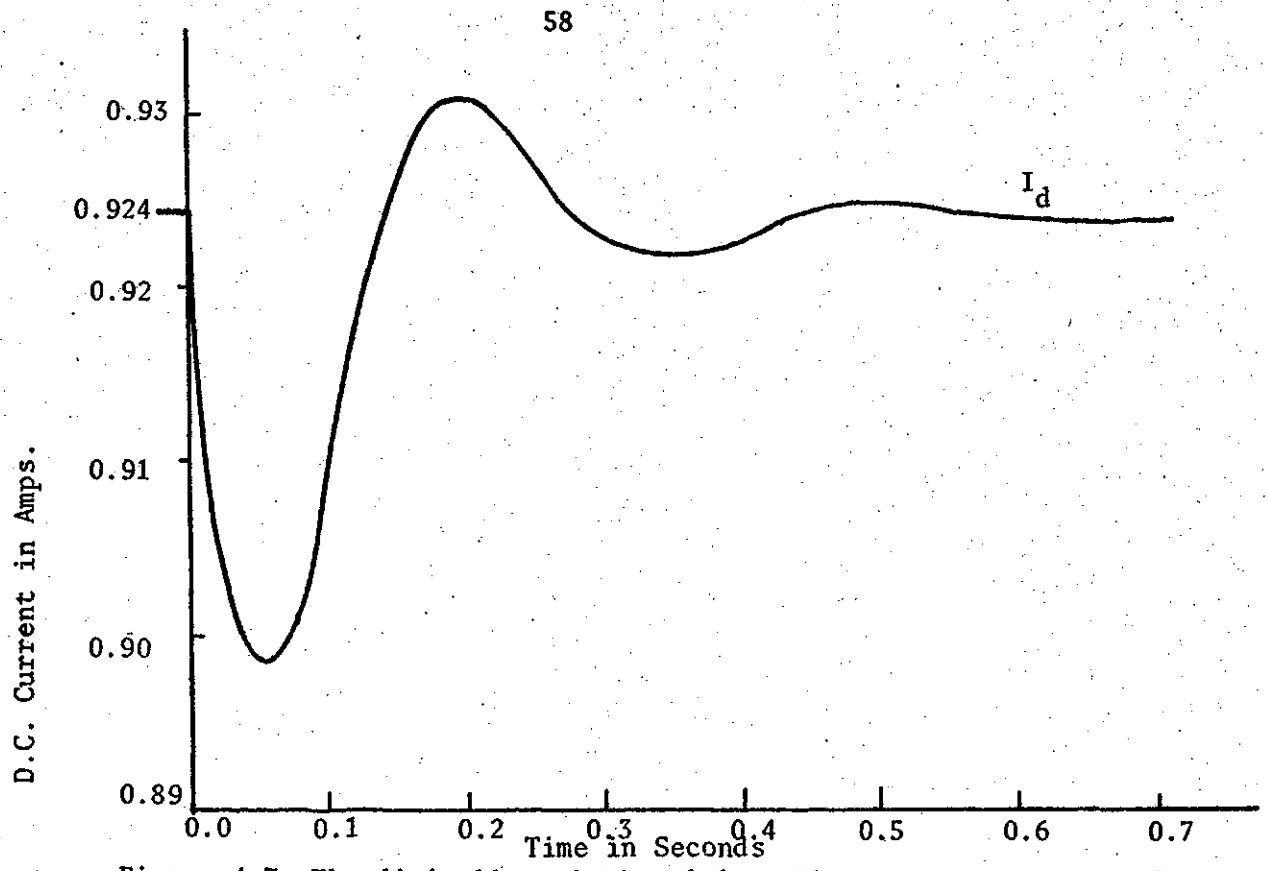

Figure 4.7 The digitally calculated d.c. line current response for a +2 percent inverter commutation voltage step change.

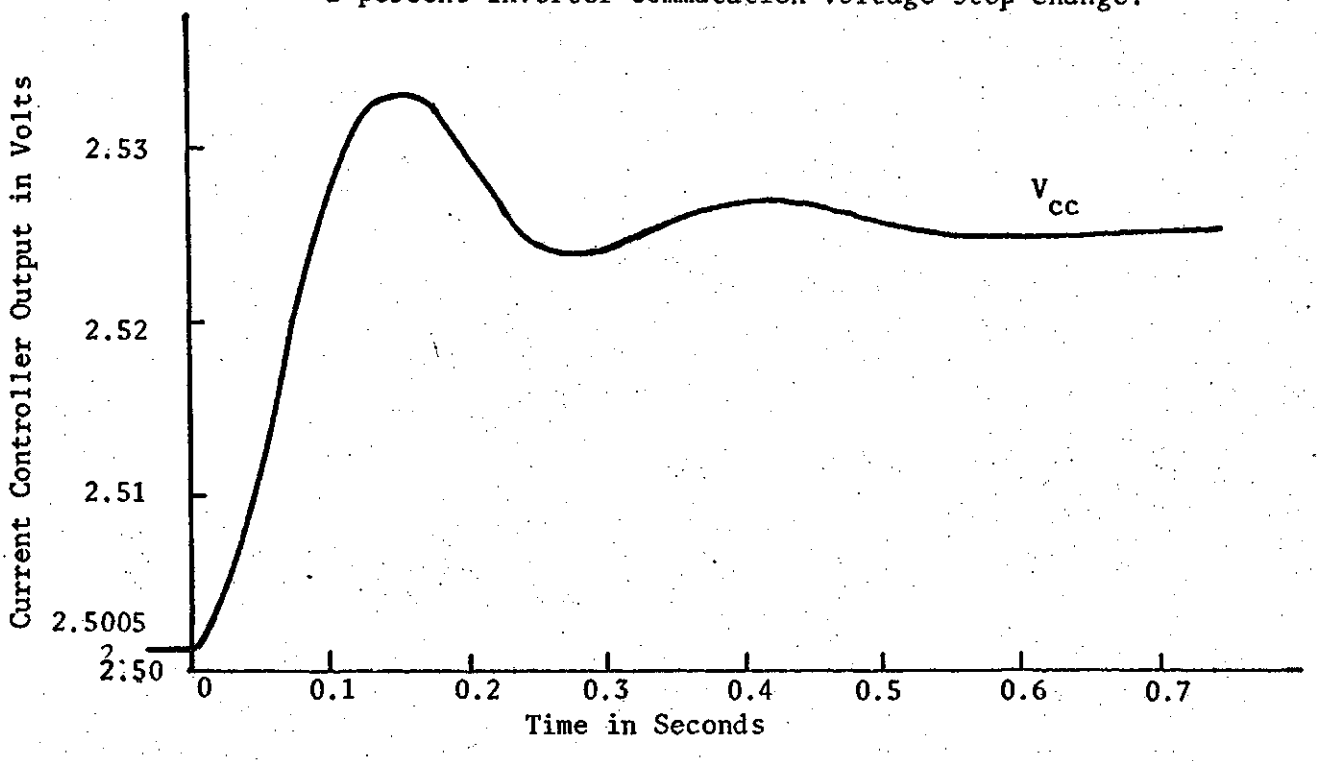

Figure 4.8 The digitally calculated current controller output response for α+2 percent inverter commutation voltage step change.

A five electrical degree rectifier delay angle lower limit is provided in the simulator. The digital computer program developed also includes this non-linearity. The system response to a 0.06 amps. current order step change is also digitally calculated and experimentally checked. The calculated d.c. line current for this study is shown in Figure 4.12. The convertor d.c. voltages and firing angles are shown in Figure 4.13. The rectifier firing delay angle decreases and remains constant at 5 electrical degrees for 0.075 secs due to high constant current controller output V_{cc}. The d.c. line current and the convertor voltages recorded during the simulator study are shown in Figure 4.14. The digital model results compare favourably with those obtained from the simulator study.

The performance of a simulated 500 mile H.V.D.C. transmission line has also been examined. The system wasassumed to be equipped with individual phase controllers discussed in Paragraph 2.4.1. The system parameters are listed in Appendix I. It is noticed that the commutation reactance drop compensation positive feedback exceeds the damping effect of the d.c. line resistance and the system is therefore unstable. The commutation reactance drop compensation is not essential at the rectifier station and the control system is modified accordingly. The reactance to resistance ratio of this system is quite different from the reactance to resistance ratio of the simulator d.c. line. Therefore the system was not studied experimentally. The analytical results are also given in Appendix I.

The state space technique has been used to develop a mathematical model of the h.v.d.c. simulator. A root locus for varying constant current controller amplifier gain has been calculated and plotted. The system transient responses have been calculated using an I.B.M. 360/50 digital computer and have been recorded from the h.v.d.c. simulator experiments. The system responses obtained from analytical studies and simulator experiments are similar in form and magnitude, which establishes the validity of the mathematical model in the operating range considered.

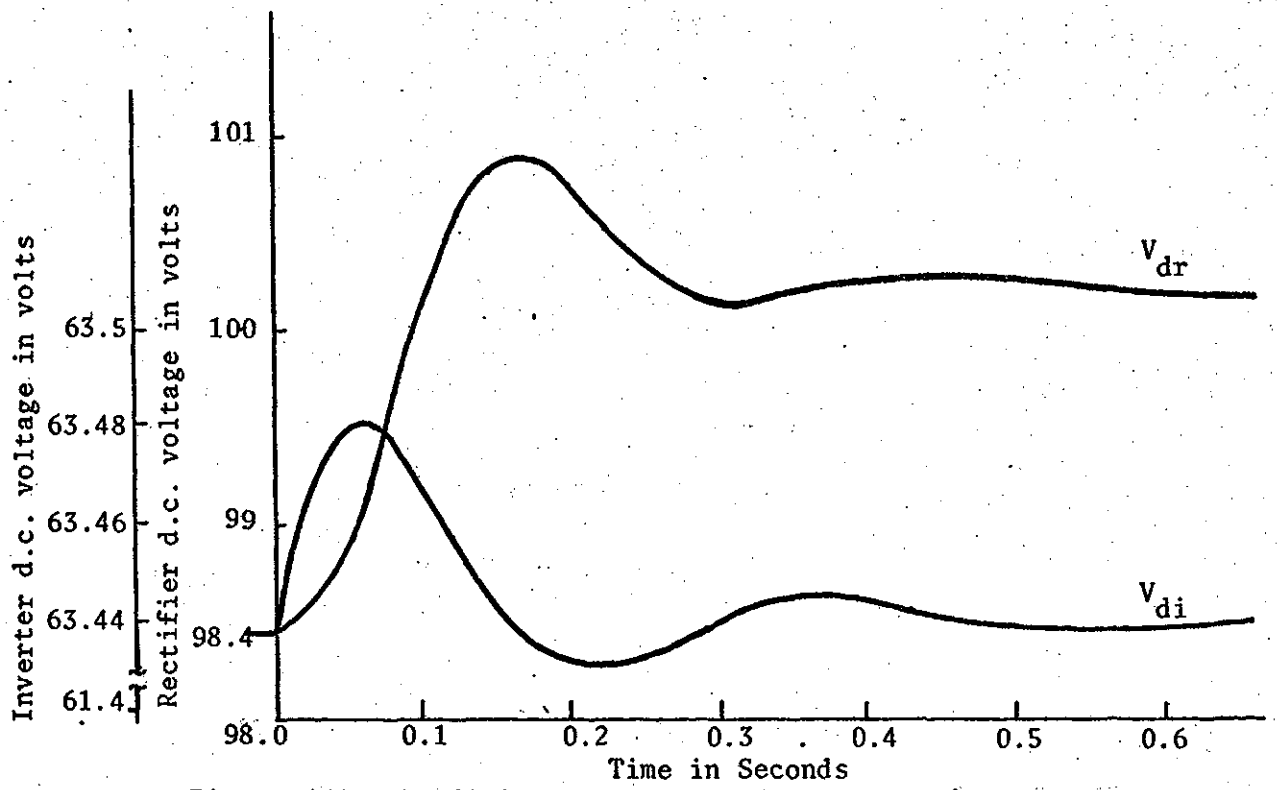

Figure 4.9 The digitally calculated convertor d.c. voltage changes for α+2 percent inverter commutation voltage step change.

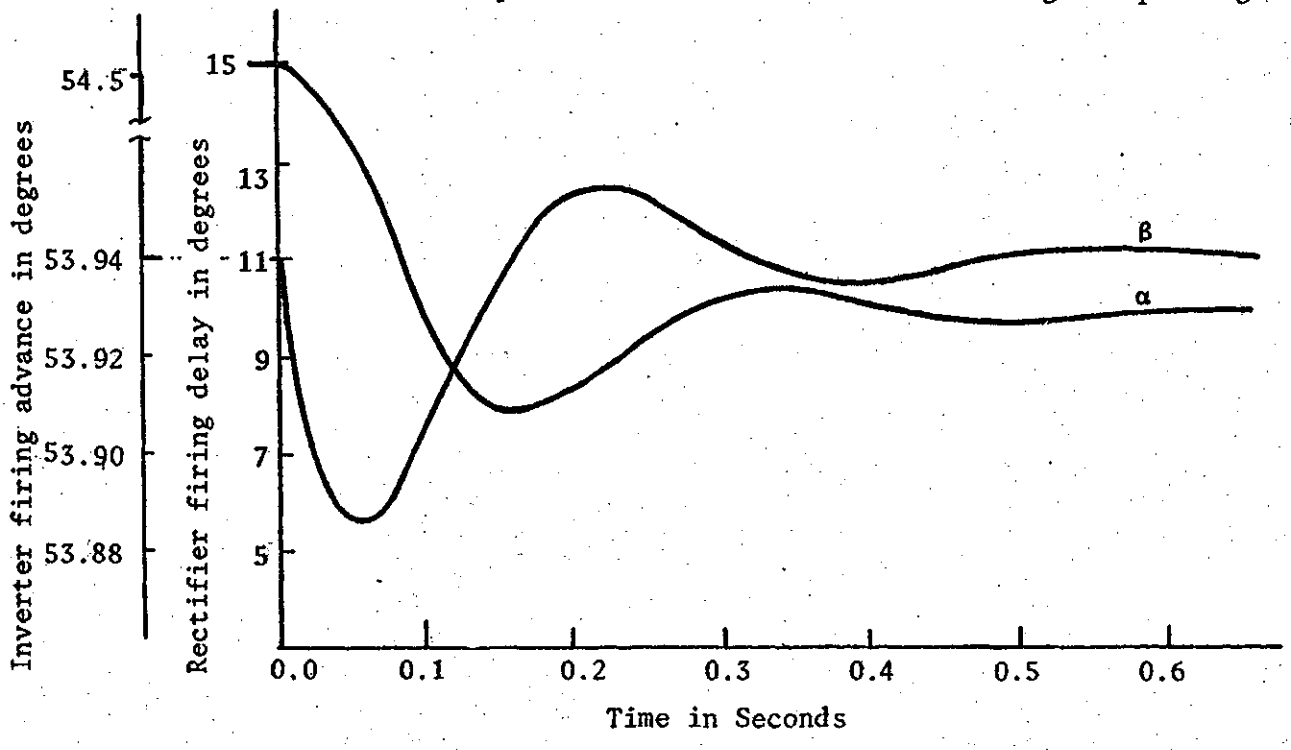

Figure 4.10 The digitally calculated convertor firing angle changes for α+2 percent inverter commutation voltage step change.

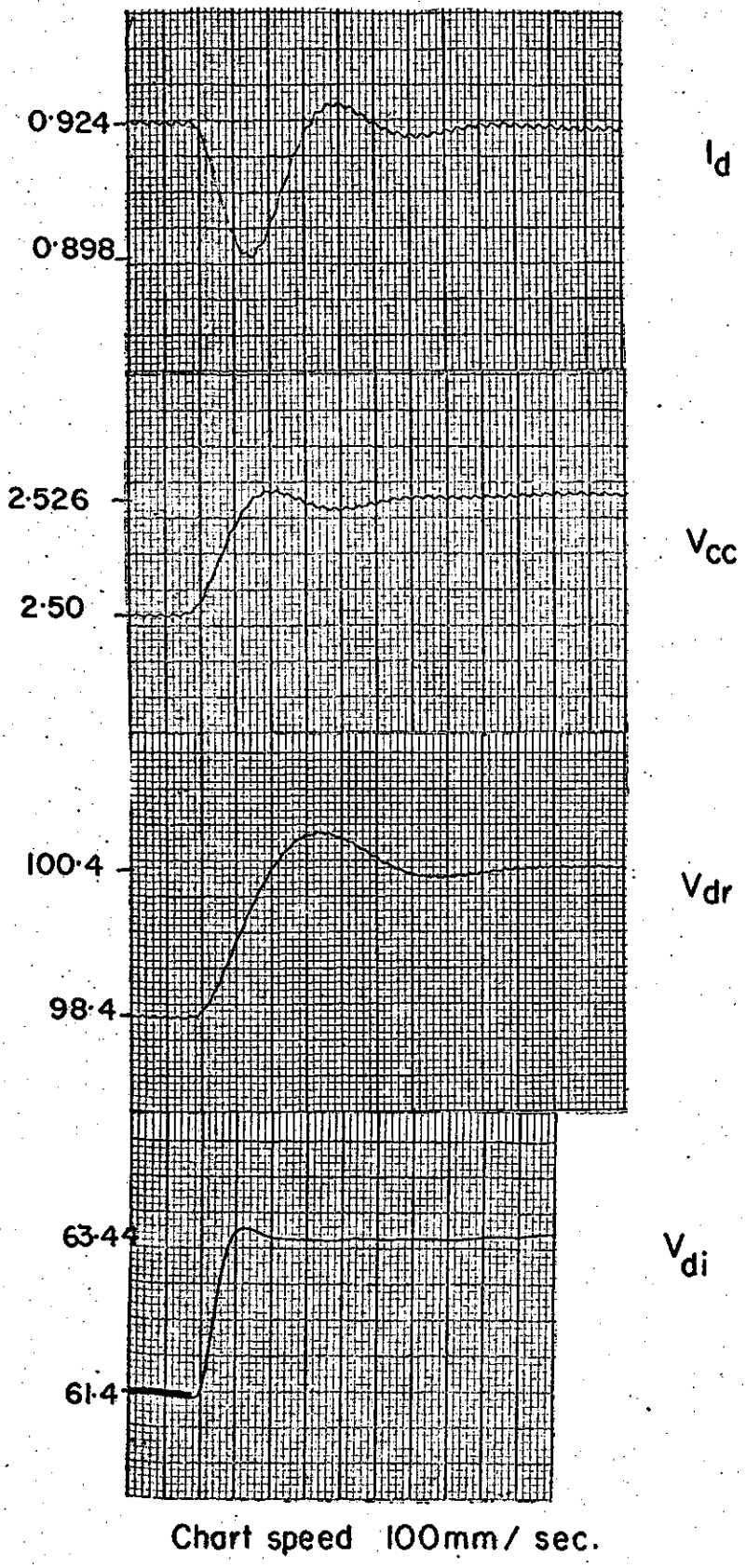

Figure 4.11 The d.c. line current, current controller output, rectifier and inverter d.c. voltage changes for α+2 percent inverter commutation voltage step change recorded from the simulator.

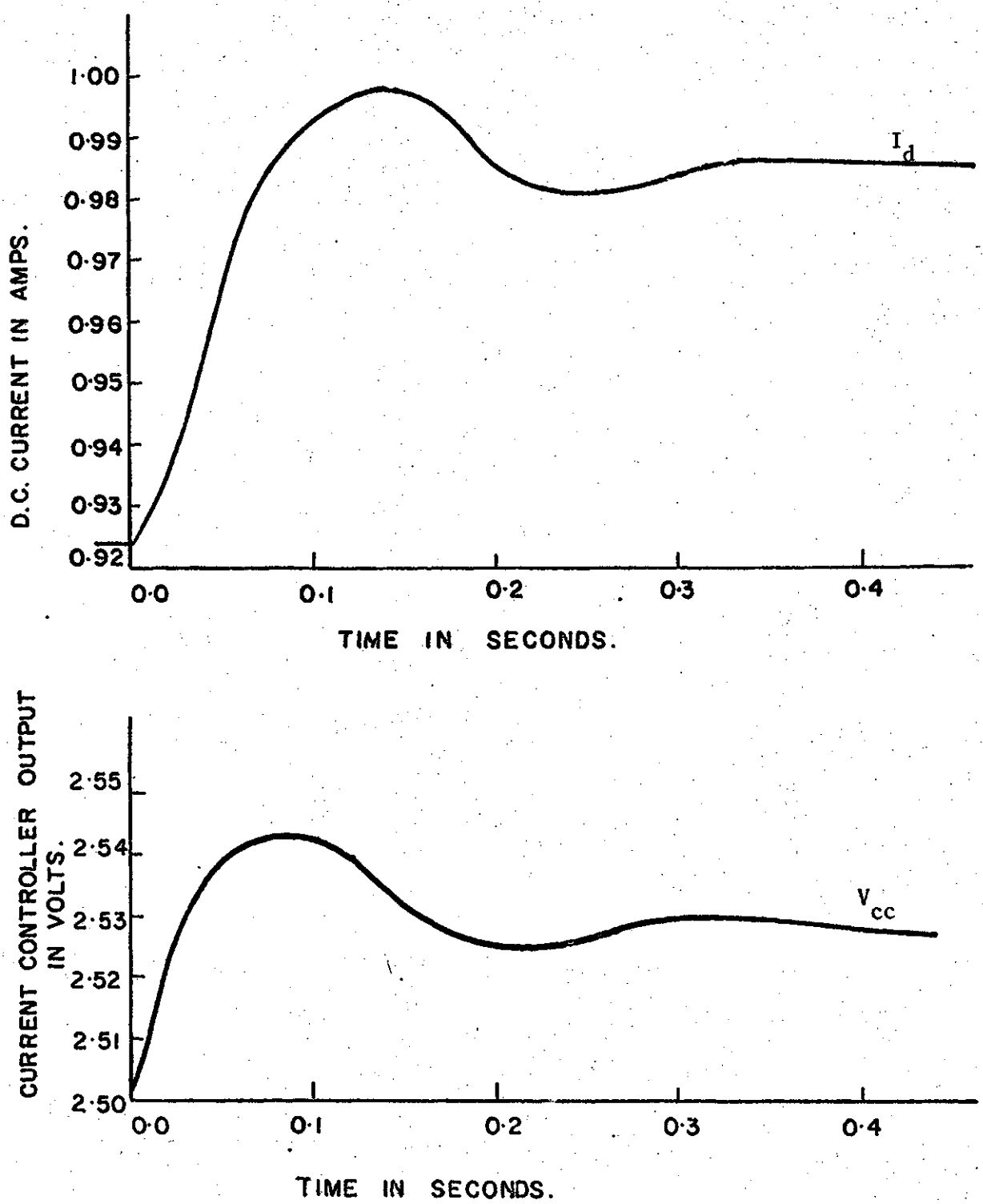

Figure 4.12 The digitally calculated d.c. line current and current controller output response for a +0.06 amp. current order step change.

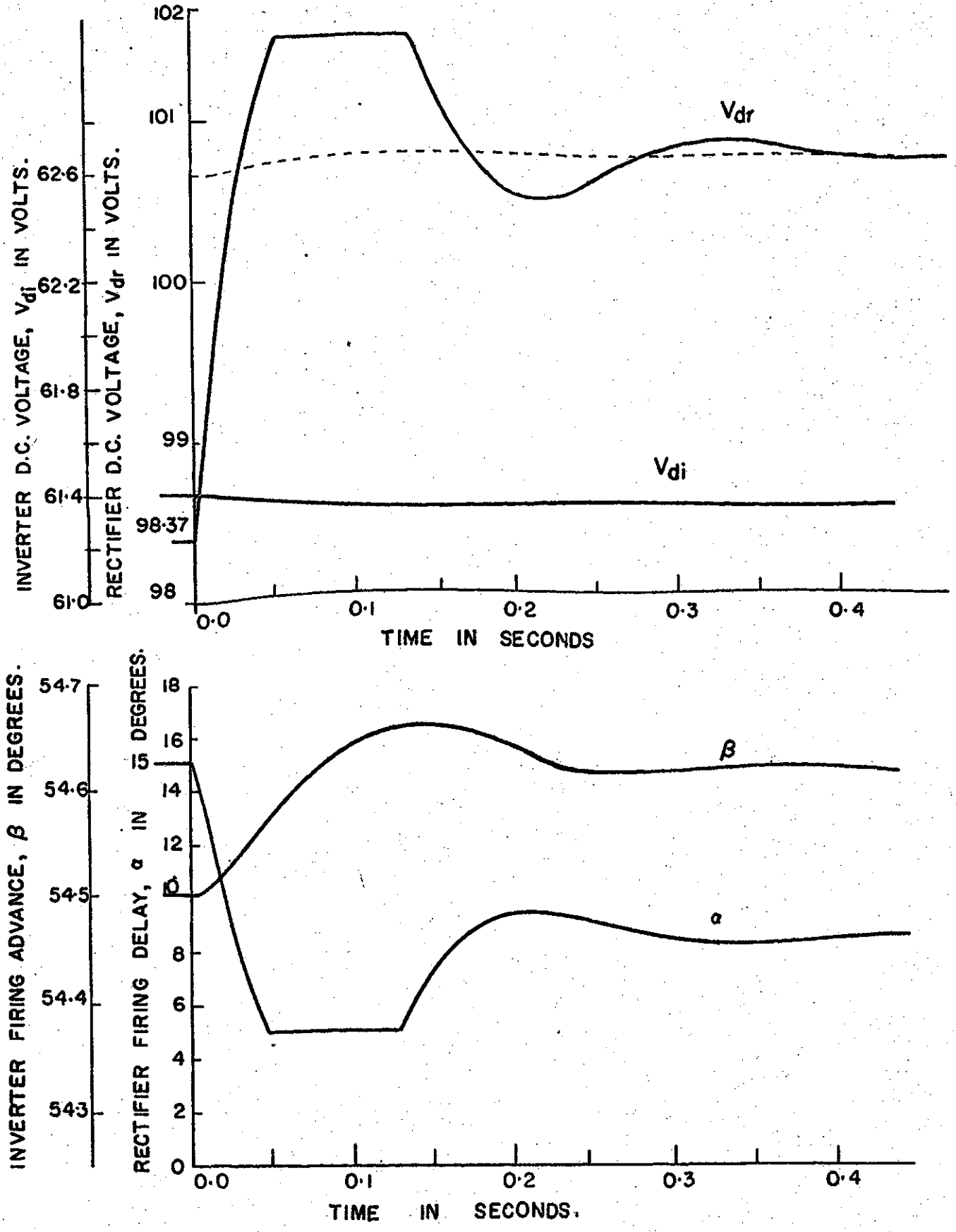

Figure 4.13 The digitally calculated convertor voltage and firing angle changes for α+0.06 amp. current order step change.

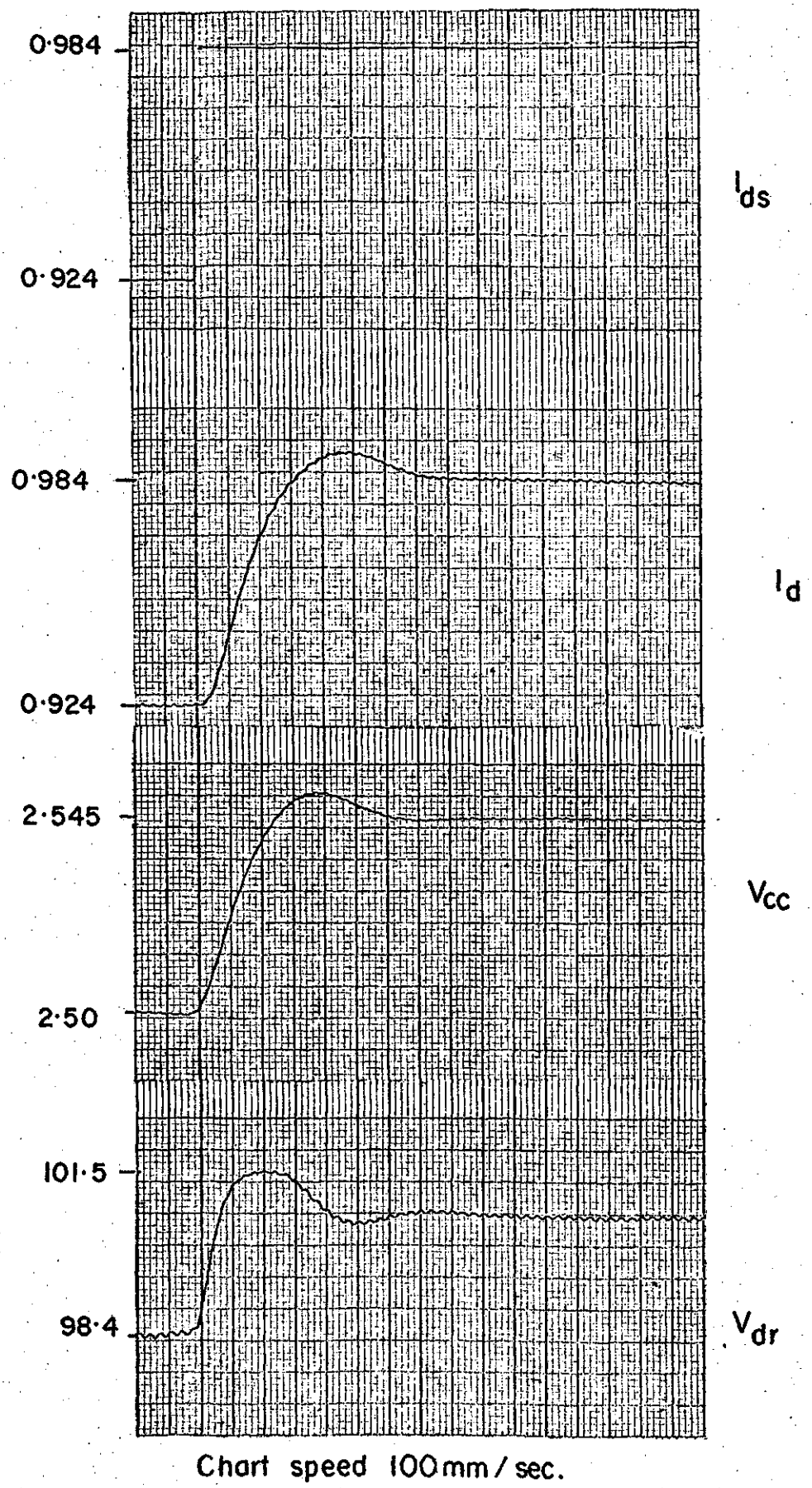

Figure 4.14 The d.c. line current, current controller output and rectifier d.c. voltage changes for α+0.06 amp. current order step change recorded from the simulator.

5. OPTIMAL AND SUBOPTIMAL CONTROL OF A H.V.D.C. SIMULATOR

The performance quality of an h.v.d.c. transmission system is judged from the current or power settling time and overshoot during a disturbance. The current or power deviation in the steady state should also be small. A number of techniques such as state-regulator, tracking, energy minimization have been developed and applied to improve the system performance for a specified criterion. The optimization may not be achieved due to the difficulties of realizability, availability of components and economics.[42,43] In these techniques a mathematical performance criterion called the cost function is estabiished and minimized by Pontryagin's principle or dynamic programming to achieve an approximately ideal performance.[39-42]

H.V.D.C. controllers have been designed in the past by Bode and Nyquist plots.[7-13] The method is laborious and time consuming and the performance may or may not be optimal.[42] The state-regulator technique was used to optimize the h.v.d.c. simulator performance to maintain the d.c. line current at the ordered value. A suboptimal controller was also designed and used on the simulator.

5.1 Optimal Control Theory

The optimization consists of minimizing the cost function describing the system performance criterion. A feedback signal derived from all the system states is provided to the controller for optimal operation. The input vector is a null vector if the system inputs are steady. The modified system state equations

are given by

$$[\dot{x}(t)] = [A][x(t)] + [E][\omega(t)] \qquad 5.1$$

Where $[x(t)]$ - nx1 state vector

$[A]$ - nxn state coefficient matrix

$[E]$ - nxm control coefficient matrix

$[\omega(t)]$ - mx1 control vector.

The state-regulator cost function $J(\omega)$ is given by

$$J(\omega) = \frac{1}{2}\int_0^\infty \left[(x^T(t)\ Q\ x(t)) + (\omega^T(t)\ R\ \omega(t))\right] dt \qquad 5.2$$

Where $x^T(t)$ and $\omega^T(t)$ are transposes of $x(t)$ and $\omega(t)$ respectively.

Q - nxn state penalty matrix

R - mxm control weighting matrix

Equation 5.2 penalizes the large deviation in the system states and high value elements of the control vector more than the smaller values. The optimization problem is to minimize the cost function satisfying the equality constraint of equation 5.1. A costate vector p(t) similar to a Lagrange multiplier is used in optimal control theory to include the equality constraint. The Hamiltonian H based on Pontryagin's principle is given by

$$H = \frac{1}{2}(x^T(t)\ Q\ x(t)) + \frac{1}{2}(\omega^T(t)\ R\ \omega(t)) + p^T(t)\ (Ax(t) + E\omega(t)) \qquad 5.3$$

The nx1 costate vector $p(t) = K\,x(t)$

K is the nxn positive definite symmetric Riccati matrix.

In addition to satisfying equation 5.1 and minimizing the cost function, the following canonical equations must be satisfied for optimal control of a system.[39]

$$\frac{\partial H}{\partial p(t)} = \dot{x}(t) \tag{5.4}$$

$$\frac{\partial H}{\partial \omega(t)} = 0 \tag{5.5}$$

$$\frac{\partial H}{\partial x(t)} = -\dot{p}(t) \tag{5.6}$$

The Riccati matrix K and the control vector $\omega(t)$ are calculated from equations 5.7 and 5.8.

$$\dot{K} = -KA - A^{T}K + KER^{-1}E^{T}K - Q \tag{5.7}$$

$$\omega(t) = -R^{-1}E^{T}K\,x(t) \tag{5.8}$$

These equations are derived from equations 5.3 through 5.6 as shown in Appendix II. The control vector $\omega(t)$ is eliminated from equations 5.1 by substituting its value from equation 5.8. The modified state equations are given by

$$\dot{x}(t) = (A - ER^{-1}E^{T}K)\,x(t) \tag{5.9}$$

Equations 5.7 represents $\frac{n(n+1)}{2}$ independent nonlinear first order differential equations for a nth order system. The elements of the symmetric Riccati matrix K are used in equation 5.8 to calculate the

control input $\omega(t)$. The system stability is determined by the eigenvalues of the characteristic matrix $(A - ER^{-1}E^{T}K)$ of the modified state equations. The transient response of the system is calculated by solving equation

$$\dot{x}(t) = (A - ER^{-1}E^{T}K)\, x(t) + B\, u(t) \qquad 5.10$$

Where $u(t)$ is the input vector as defined in Chapter 4.

5.2 Optimal Controller Design

The simulator block diagram of Figure 3.16 and the proposed control input to the rectifier controller is shown in Figure 5.1. A control input can also be provided at the inverter station. Since the d.c. line current is controlled at the rectifier station, the advantages of the control input to the inverter controller will be negligible. The control signal ω_1 is applied through a lag network to the summing junction at the rectifier constant current controller output in the studies reported in this thesis. The system equations including the control signal at the rectifier station are given by

$$\frac{d\Delta I_{dr}}{dt} = \frac{-(R_1 - \frac{6}{\pi}\omega L_r)}{L_1}\, \Delta I_{dr} - \frac{100}{L_1}\, \Delta V_c^1 + \frac{300}{\pi}\, \frac{K_2}{K_p}\, \frac{1}{L_1}\, \Delta V_{cc}^1 + \frac{300}{\pi L_1}\, \frac{K_2}{K_p}\, \Delta V_\omega^1 \qquad 5.11$$

Where $\Delta V_\omega^1 = \dfrac{\omega_1}{(s + 1000)}$

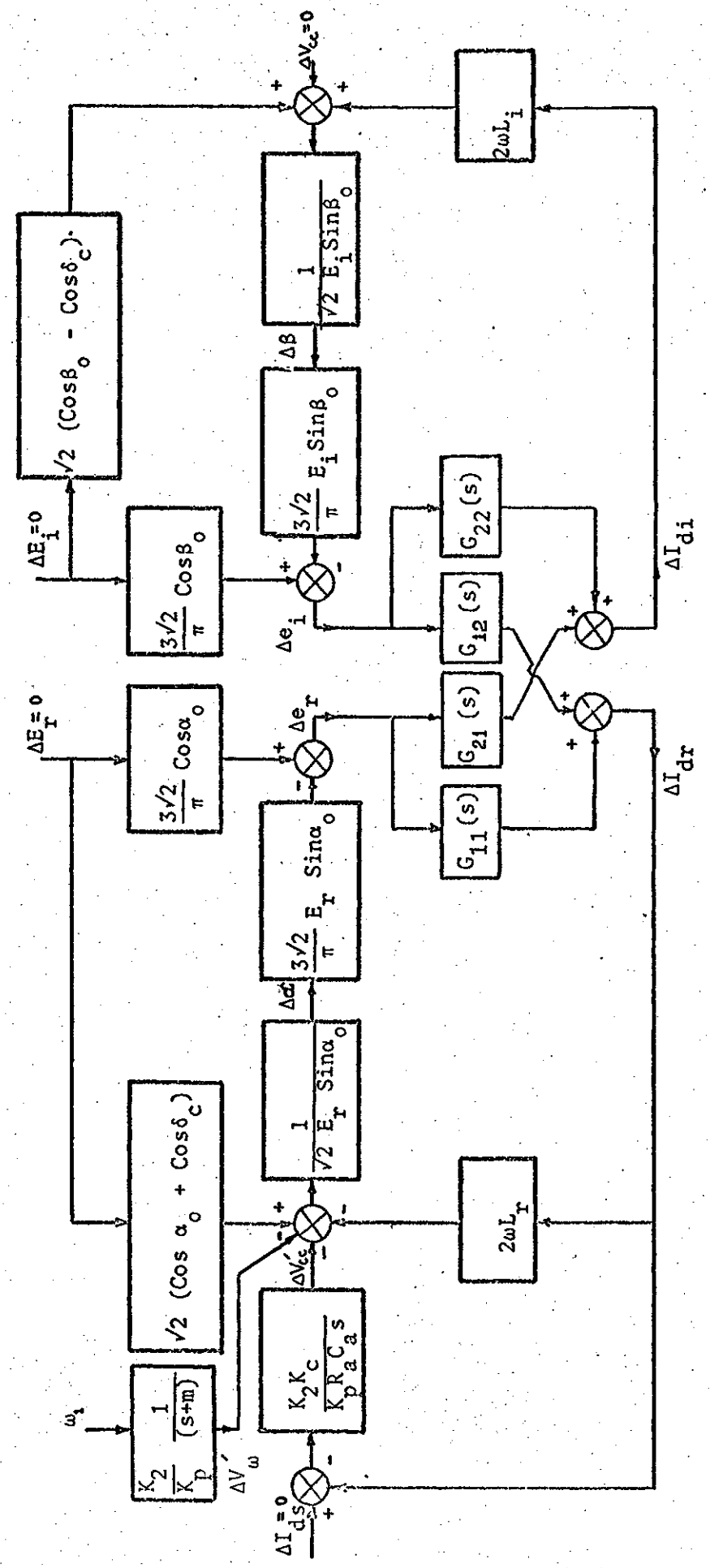

Figure 5.1 Block diagram of the simulator equipped with an optimal controller.

$$\frac{d\Delta I_{di}}{dt} = \frac{-(R_2 - \frac{6}{\pi}\omega L_i)}{L_2} \Delta I_{di} + \frac{100}{L_2} \Delta V_c^1 \qquad 5.12$$

$$\frac{d\Delta V_c^1}{dt} = \frac{1}{100C} \Delta I_{dr} - \frac{1}{100C} \Delta I_{di} \qquad 5.13$$

$$\frac{d\Delta V_{cc}^1}{dt} = \frac{-K_c K_a}{100} \Delta I_{dr} \qquad 5.14$$

$$\frac{d\Delta V_\omega^1}{dt} = -m\ \Delta V_\omega^1 + \omega_1 \qquad 5.15$$

Where $\Delta V_c^1 = \frac{\Delta V_c}{100}$; $\Delta V_{cc}^1 = \frac{\Delta V_{cc}}{100}$ and $\Delta V_\omega^1 = \frac{\Delta V_\omega}{100}$.

Defining ΔI_{dr}, ΔI_{di}, ΔV_c^1, ΔV_{cc}^1 and ΔV_ω^1 as the system state variables x_1, x_2, x_3, x_4 and x_5 respectively, the state equations 5.11 through 5.15 are given by

$$[\dot{x}] = [A][x] + [E][\omega] \qquad 5.16$$

Where $[x] = [x_1 \quad x_2 \quad x_3 \quad x_4 \quad x_5]^T$ 5.17

$$[\omega] = \omega_1 \qquad 5.18$$

$$[A] = \begin{bmatrix} \frac{-(R_1 - \frac{6}{\pi}\omega L_r)}{L_1} & 0 & \frac{100}{L_1} & \frac{300}{\pi L_1}\frac{K_2}{K_p} & \frac{300}{\pi L_1}\frac{K_2}{K_p} \\ 0 & \frac{-(R_2 - \frac{6}{\pi}\omega L_i)}{L_2} & \frac{100}{L_2} & 0 & 0 \\ \frac{1}{100C} & -\frac{1}{100C} & 0 & 0 & 0 \\ \frac{-K_c K_a}{100} & 0 & 0 & 0 & 0 \\ 0 & 0 & 0 & 0 & -m \end{bmatrix}$$

and $[E] = [0 \quad 0 \quad 0 \quad 0 \quad 1]^T$

The control input loop transfer function of $\frac{1}{s+1000}$ is used to provide a small time lag to enhance the optimal controller response. The characteristic matrix A for the h.v.d.c. simulator is given by

$$[A] = \begin{bmatrix} -23.98975 & 0 & -129.87013 & 10320.79688 & 10320.79688 \\ 0 & -23.98975 & 129.87013 & 0 & 0 \\ 5681.81652 & -5681.81652 & 0 & 0 & 0 \\ -0.17864 & 0 & 0 & 0 & 0 \\ 0 & 0 & 0 & 0 & -1000 \end{bmatrix}$$

The penalty matrices Q and R are selected from a number of trials (see Appendix III). The following values provided the best system characteristics.

$$[Q]=\begin{bmatrix} 20 & 0 & 0 & 0 & 0 \\ 0 & 20 & 0 & 0 & 0 \\ 0 & 0 & 10 & 0 & 0 \\ 0 & 0 & 0 & 20 & 0 \\ 0 & 0 & 0 & 0 & 20 \end{bmatrix} \qquad [R]= 0.1 \qquad 5.20$$

The d.c. currents are to be controlled and the controller voltages affect the valve firing delays which in turn affect the d.c. voltages and currents. Therefore heavy penalties are applied to these variables in the selected Q matrix.

The fifteen Riccati equations of the simulator are formulated from equation 5.7 by substituting for the A, E, Q and R matrices defined above. The elements of the Riccati matrix K are zero at $t \to \infty$. The Riccati equations are solved backwards in time from t = 10 secs using the Runge-Kutta method for an integration interval of 0.001 secs. One of the many solutions of the Riccati equations is given by

$$[K] = \begin{bmatrix} 0.540637 & -0.463907 & 0.007672 & 0.272476 & 2.571946 \\ -0.463907 & 0.520344 & -0.005094 & -1.086940 & -1.947429 \\ 0.007672 & -0.005094 & 0.021112 & -0.756757 & -0.410363 \\ 0.272476 & -1.086940 & -0.756757 & 3731.545898 & 23.726196 \\ 2.571946 & -1.947429 & -0.410363 & 23.726196 & 23.731277 \end{bmatrix} \quad 5.21$$

Sylvester's criterion[36] was applied to check if the Riccati matrix K is positive definite or not. The determinant of K and the principal minors of the determinant were calculated and were found to be positive. The control input ω_1 as obtained from equation 5.8 is given by

$$\omega_1 = -25.71946\, x_1 + 19.47429\, x_2 + 4.10363\, x_3 - 237.26196\, x_4 - 237.31277\, x_5 \qquad 5.22$$

The state space equations of the h.v.d.c. simulator equipped with an optimal controller are given by

$$\begin{aligned}\left[\dot{x}\right] &= \left[A - ER^{-1}E^{T}K\right]\left[x\right] + \left[B\right]\left[U\right] \\ &= \left[G\right]\left[x\right] + \left[B\right]\left[U\right] \end{aligned} \qquad 5.23$$

Where

$$\left[G\right] = \begin{bmatrix} -23.98975 & 0 & -129.87013 & 10320.79688 & 10320.79688 \\ 0 & -23.98975 & 129.87013 & 0 & 0 \\ 5681.81642 & -5681.81642 & 0 & 0 & 0 \\ -0.17864 & 0 & 0 & 0 & 0 \\ -25.71946 & 19.47429 & 4.10363 & -237.26196 & -1237.31277 \end{bmatrix}$$

$$[B] = \begin{bmatrix} -172.75 & 0 & 0 \\ 0 & -172.75 & 0 \\ 0 & 0 & 0 \\ 0 & 0 & -17.8640 \\ 0 & 0 & 0 \end{bmatrix} \qquad 5.25$$

and $[U] = [\Delta E_r^1 \quad \Delta E_i^1 \quad \Delta I_{ds}]^T$

$$\Delta E_r^1 = \frac{\Delta E_r}{100}\ ; \qquad \Delta E_i^1 = \frac{\Delta E_i}{100}$$

Equation 5.23 is used for stability analysis in complex and time domains.

For stability studies in the complex domain, the eigenvalues of the characteristic equation $|G - \lambda I| = 0$ are calculated using the I.B.M. Scientific Subroutine programs HSBG and ATEIG. The dominant eigenvalues are shifted to -27.8908844 ± j 23.4443207 which corresponds to a damping factor and damping ratio of 0.765 and -27.89 as compared to 0.52 and -12.0 of the original system. The Riccati matrix, control input and the dominant eigenvalues for different combinations of Q and R matrices are given in Appendix III.

The fourth order Runge-Kutta method and a time interval of 0.001 secs were used to calculate the time domain optimal system responses. The system was considered to be operating at 0.924 amps

d.c. line current, commutation voltages of 76.5 volts and 10 and 15 electrical degrees inverter deionization margin angle and rectifier delay angle respectively as in paragraph 4.4. A 0.04 amps current order step change was applied. The commutation voltages were assumed to remain constant. The digitally calculated d.c. line current due to the current order change is shown in Figure 5.2. The line current settles at 0.964 amps - the updated current order after a transient period of 0.132 secs. The rise time is 0.09 secs and approximately 2 percent overshoot occurs 0.16 secs after the step change is applied. The constant current controller output is also plotted in Figure 5.2. The changes in rectifier and inverter firing angles and d.c. voltages during the transient are shown in Figures 5.3 and 5.4 respectively. The original system responses reported in Chapter 4 are also plotted for comparison. The system response is significantly improved by the optimal controller. The optimal and original system performance is compared in Table 5.1.

Table 5.1 Digitally calculated time domain performance of the d.c. simulator equipped with (i) original and (ii) optimal controllers.

	Original	Optimal
Settling time	0.27 sec	0.132 sec
Rise Time	0.05 sec	0.09 sec
Overshoot	25%	2%
Time to Overshoot	0.11 sec	0.16 sec

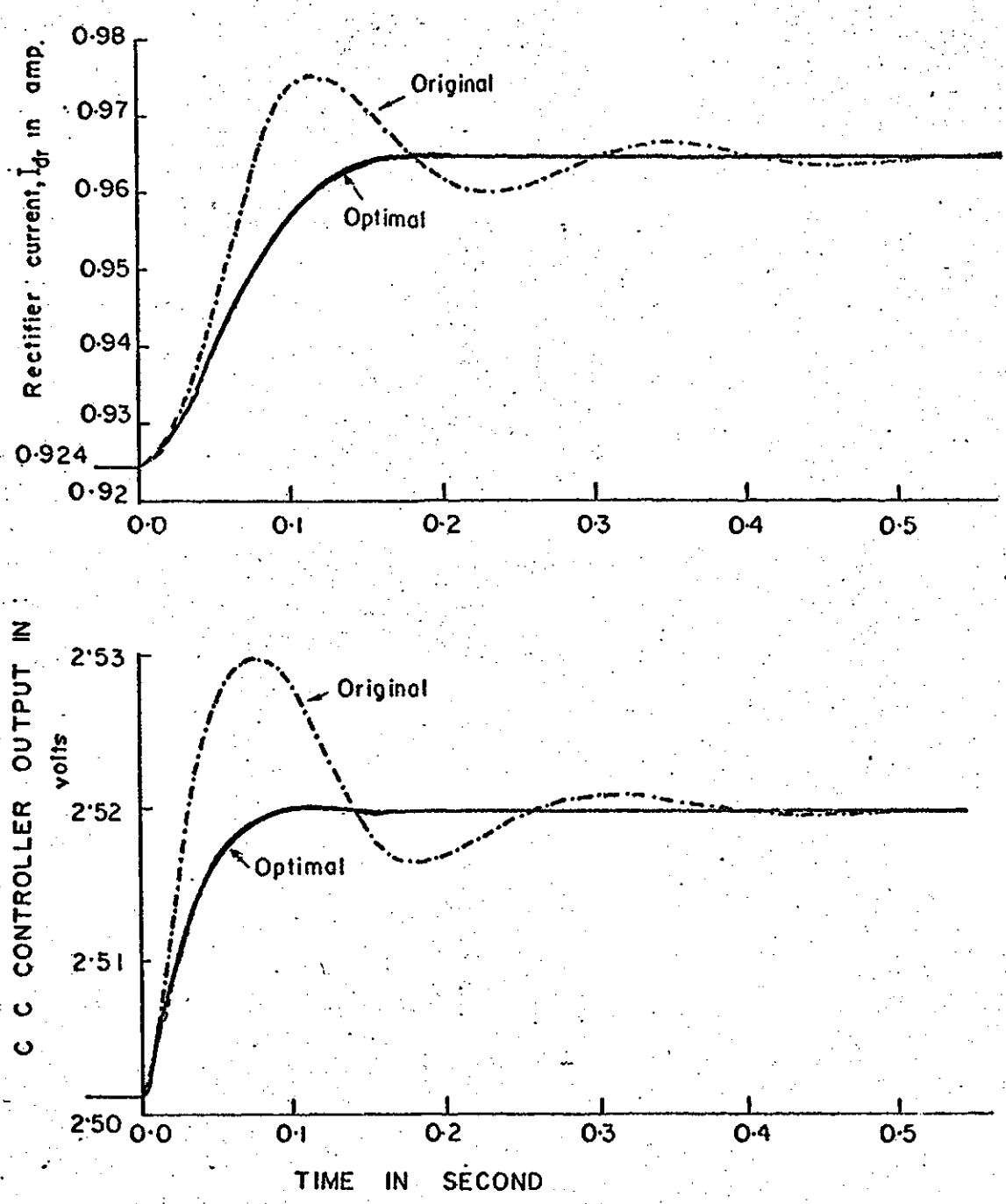

Figure 5.2 The digitally calculated d.c. line current and current controller output response of the simulator equipped with optimal controller for a+0.04 amp. current order step change

A two percent step increase of inverter commutation voltage was considered for system response quality. The rectifier commutation voltages and d.c. line current order are 76.5 volts and 0.924 amps respectively and do not change during the disturbance. The digitally calculated d.c. line current during the disturbance is shown in Figure 5.5. The line current settles within ±0.5 percent of the set value after a transient period of 0.18 secs. The minimum line current of approximately 1.6 percent overshoot occurs 0.055 secs after the step change is applied. The constant current controller output is also shown in Figure 5.5. The changes in rectifier and inverter firing angles and d.c. voltages are shown in Figures 5.6 and 5.7 respectively. The original system responses reported in Chapter 4 are also plotted for comparison. The rectifier voltage settles at the new value of 100.4 volts after a transient period of 0.11 secs. The rise time is 0.085 secs and approximately 3% overshoot occurs. The system response is significantly improved by the optimal controller in this case also. The optimal and original system performance is compared in Table 5.2.

Table 5.2 Digitally calculated time domain performance of the d.c. simulator equipped with (i) original and (ii) optimal controller.

	Original	Optimal
Settling time	0.30 sec	0.11 sec
Rise time	0.07 sec	0.085 sec
Overshoot	25%	3%
Time to Overshoot	0.15 sec	0.17 sec

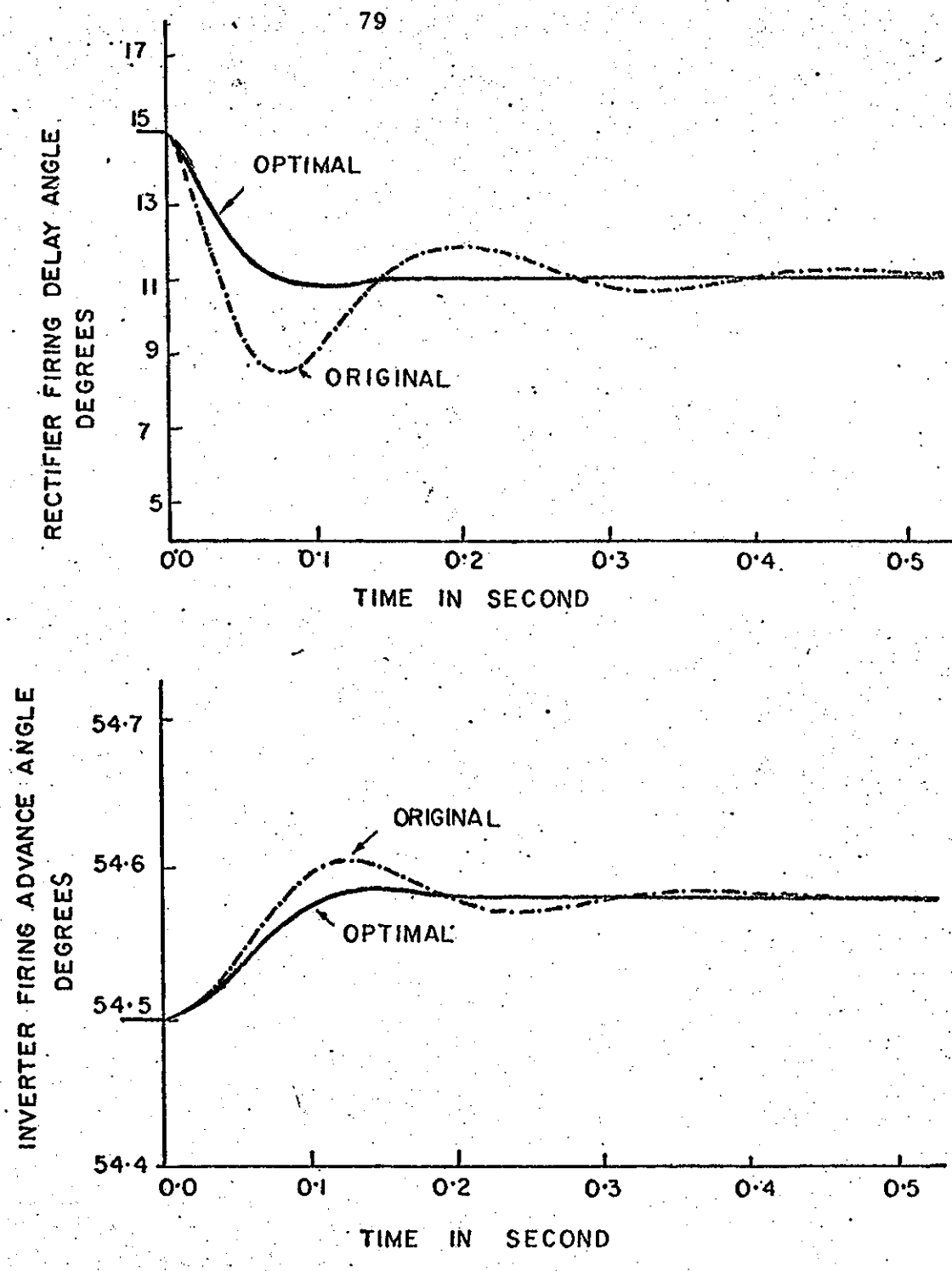

Figure 5.3 The digitally calculated convertor firing angle changes for α+0.04 amp. current order step change.

5.3 Suboptimal Control of H.V.D.C. Simulator

All system states are measured and used for optimal control. It is not possible to conveniently measure all the system states in a practical h.v.d.c. system. The on-line computation of the unavailable state signals is an attractive alternative.[42] The knowledge of the remote states of a h.v.d.c. transmission system such as inverter current and d.c. transmission line midpoint voltage will have to be transmitted over communication channels. This is expensive and introduces a phase shift in the state information provided to the controller. A suboptimal controller using the system states available at the rectifier only was designed and used for studies on the simulator and by digital modelling.

The current controller output state is the dominant element of the control input defined by equation 5.22. The inverter and rectifier currents were similar in form and magnitude in the system being studies. The inverter and the rectifier current feedback gains are combined and used with the rectifier current state. The d.c. transmission line mid-point voltage state is not used in forming the control input. The modified control input ω_1^1 obtained from equation 5.22 and Riccati matrix K^1 obtained from equation 5.21 are given by

$$\omega_1^1 = -6.24517\, x_1 - 237.26196\, x_4 - 237.31277\, x_5 \qquad 5.26$$

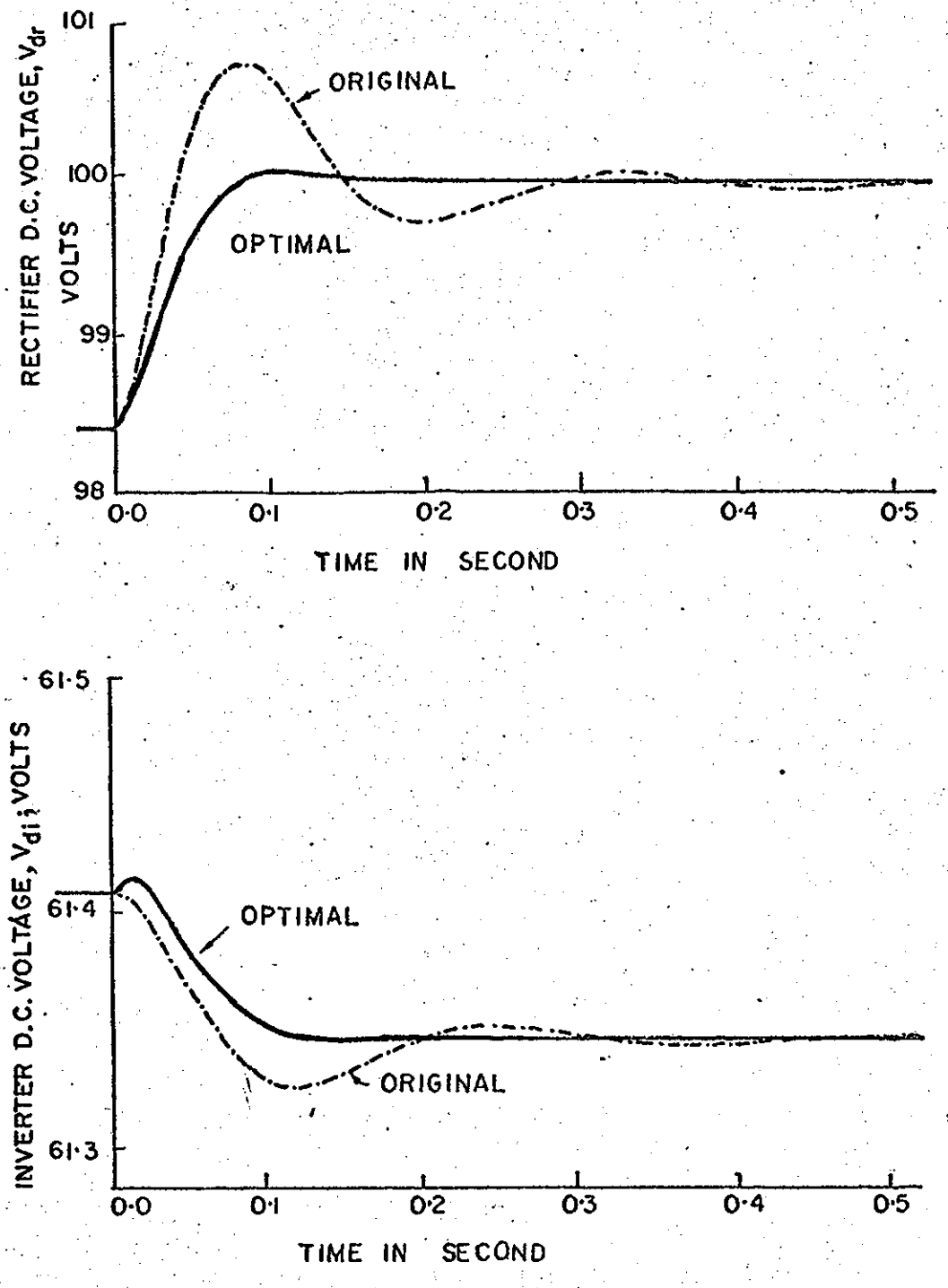

Figure 5.4 The digitally calculated convertor voltage changes for a +0.04 amp. current order step change.

$$[K^1] = \begin{bmatrix} 0.540637 & -0.463907 & 0.007672 & 0.272476 & 0.624517 \\ -0.463907 & 0.520344 & -0.005094 & -1.086940 & 0 \\ 0.007672 & -0.005094 & 0.021112 & -0.756757 & 0 \\ 0.272476 & -1.086940 & -0.756757 & 3731.545898 & 23.726196 \\ 0.624517 & 0 & 0 & 23.726196 & 23.731277 \end{bmatrix} \quad 5.27$$

The system state equations are therefore given by

$$[\dot{x}] = [A - ER^{-1}E^TK^1][x] + [B][U]$$

$$= [G^1][x] + [B][U] \quad 5.28$$

Where

$$[G^1] = \begin{bmatrix} -23.98975 & 0 & -129.87013 & 10320.79688 & 10320.79688 \\ 0 & -23.98975 & 129.87013 & 0 & 0 \\ 5681.81641 & -5681.81641 & 0 & 0 & 0 \\ -0.17864 & 0 & 0 & 0 & 0 \\ -6.24517 & 0 & 0 & -237.26196 & -1237.31277 \end{bmatrix}$$

$$[B] = \begin{bmatrix} -172.75 & 0 & 0 \\ 0 & -172.75 & 0 \\ 0 & 0 & 0 \\ 0 & 0 & -17.8640 \\ 0 & 0 & 0 \end{bmatrix}$$

The dominant eigenvalues of this system are -25.6419373 $\pm$ j22.2673492 and corresponds to a damping factor and damping ratio of 0.755 and -25.6419373. The eigenvalue, damping factor and the damping ratio are quite close to those of the optimal system. Therefore, the suboptimal system performance is expected to be very similar to that of the optimal system.

A suboptimal controller based on equation 5.26 was designed and used on the simulator as shown in Figure 5.8. The system was considered to be operating at 0.924 amps d.c. line current, 76.5 volts commutation voltages and 54.5 and 15 electrical degrees inverter firing advance angle and rectifier firing delay angle respectively. A step change of 0.04 amps current setting was applied. The commutation voltages have been assumed to remain constant. The digitally calculated d.c. line current due to the current order change is shown in Figure 5.9. The line current settles at 0.964 amps - the updated current order - after a transient period of 0.146 secs. The rise time is 0.11 secs and approximately 1 percent overshoot occurs 0.17 secs after the step change is applied. The constant current controller output is also plotted in Figure 5.9. The changes in rectifier and inverter firing angles and d.c. voltages during the transient are shown in Figures 5.10 and 5.11 respectively. The d.c. line current, constant current controller output, and the rectifier voltage recorded at the simulator due to the current setting step change are shown in Figure 5.12. The digital and analog studies of the simulator performance are compared in Table 5.3.

Table 5.3 Time domain performance of the d.c. simulator from digital and analog studies.

	Digital	Analog
Settling time	0.146 secs	0.18 sec
Rise time	0.11 sec	0.12 sec
Overshoot	1%	3%
Time to overshoot	0.17 sec	0.20 sec

These studies provide reasonably similar results. The performance of original, optimal and suboptimal systems is compared in Table 5.4.

Table 5.4 Time domain performance of the d.c. simulator equipped with (i) original ,(ii) optimal and (iii) suboptimal controllers.

	Original		Optimal	Suboptimal	
	Digital	Analog	Digital	Digital	Analog
Settling time	0.27 sec	0.29 sec	0.132 sec	0.146 sec	0.18 sec
Rise time	0.05 sec	0.055 sec	0.09 sec	0.11 sec	0.12 sec
Overshoot	25%	24%	2%	1%	3%
Time to overshoot	0.11 sec	0.13 sec	0.16 sec	0.17 sec	0.20 sec

A two percent step increase of inverter commutation voltages was also considered to evaluate the performance of the system equipped with

a suboptimal controller. The rectifier commutation voltages and d.c. line current order were 76.5 volts and 0.924 amps respectively and were not changed during the disturbance. The digitally calculated d.c. line current and constant current controller output during the disturbance is shown in Figure 5.13. The changes in rectifier and inverter firing angles and d.c. voltages are shown in Figures 5.14 and 5.15 respectively. The d.c. line current, constant current controller output, rectifier and inverter voltages recorded at the simulator are shown in Figure 5.16. The performance of the original, optimal and suboptimal system is compared in Table 5.5.

Table 5.5 Time domain performance of the d.c. simulator equipped with (i) original, (ii) optimal and (iii) suboptimal controllers.

	Original		Optimal	Suboptimal	
	Digital	Analog	Digital	Digital	Analog
Settling time	0.30 sec	0.33 sec	0.11 sec	0.125 sec	0,145 sec
Rise time	0.07 sec	0.08 sec	0.085 sec	0.087 sec	0.105 sec
Overshoot	25%	28.5%	3%	1%	5%
Time to overshoot	0.15 sec	0.18 sec	0.17 sec	0.18 sec	0.20 sec

These results also indicate that the performance of the suboptimally controlled system is similar to that of the optimally controlled system.

The state regulator technique of optimization has been described and used for optimal controller design of a h.v.d.c. scheme. A suitable combination of state penalty and control weighing matrices has been selected to provide near critical system damping. The transient response of the system equipped with optimal controller has been digitally calculated

for (i) a current order and (ii) an inverter commutation voltage step change. A suboptimal controller using the states available at the rectifier station has also been designed and used on the h.v.d.c. simulator. The transient response of the simulator equipped with the suboptimal controller has been digitally calculated and also varified from the simulator tests.

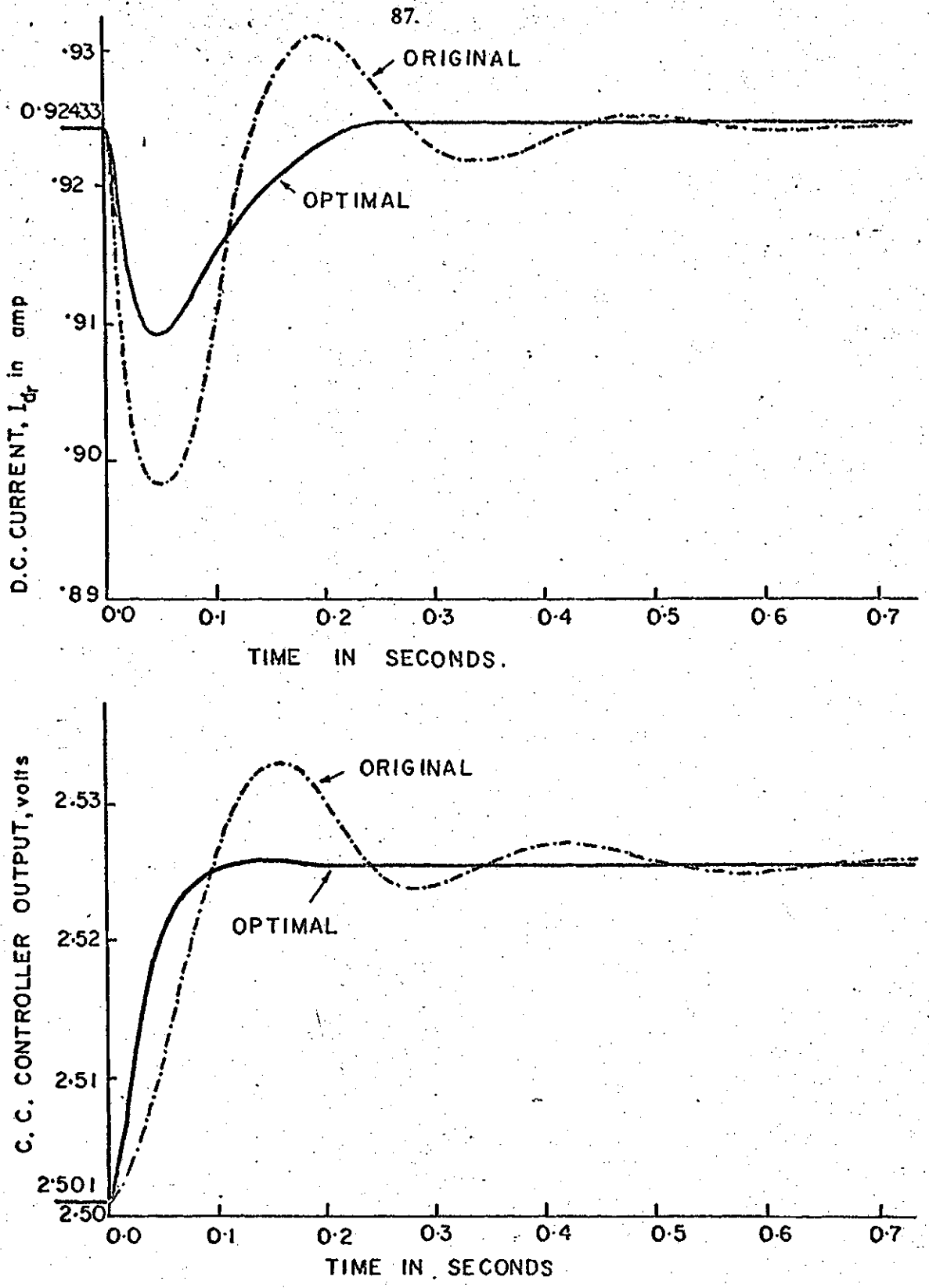

Figure 5.5 The digitally calculated d.c. line current and current controller output response of the simulator equipped with optimal controller for α+2 percent inverter commutation voltage step change.

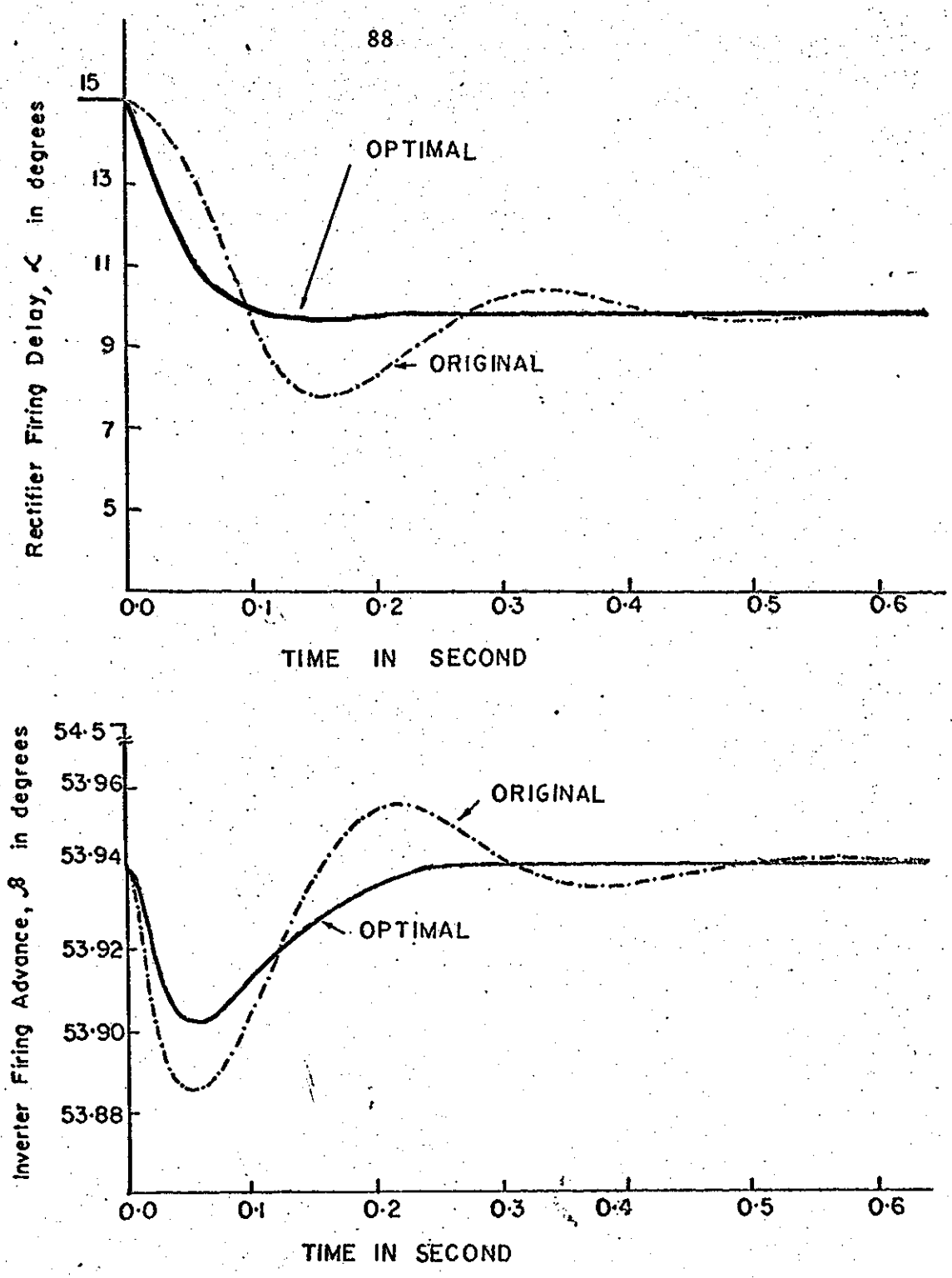

Figure 5.6 The digitally calculated convertor firing angle changes for α+2 percent inverter commutation voltage step change.

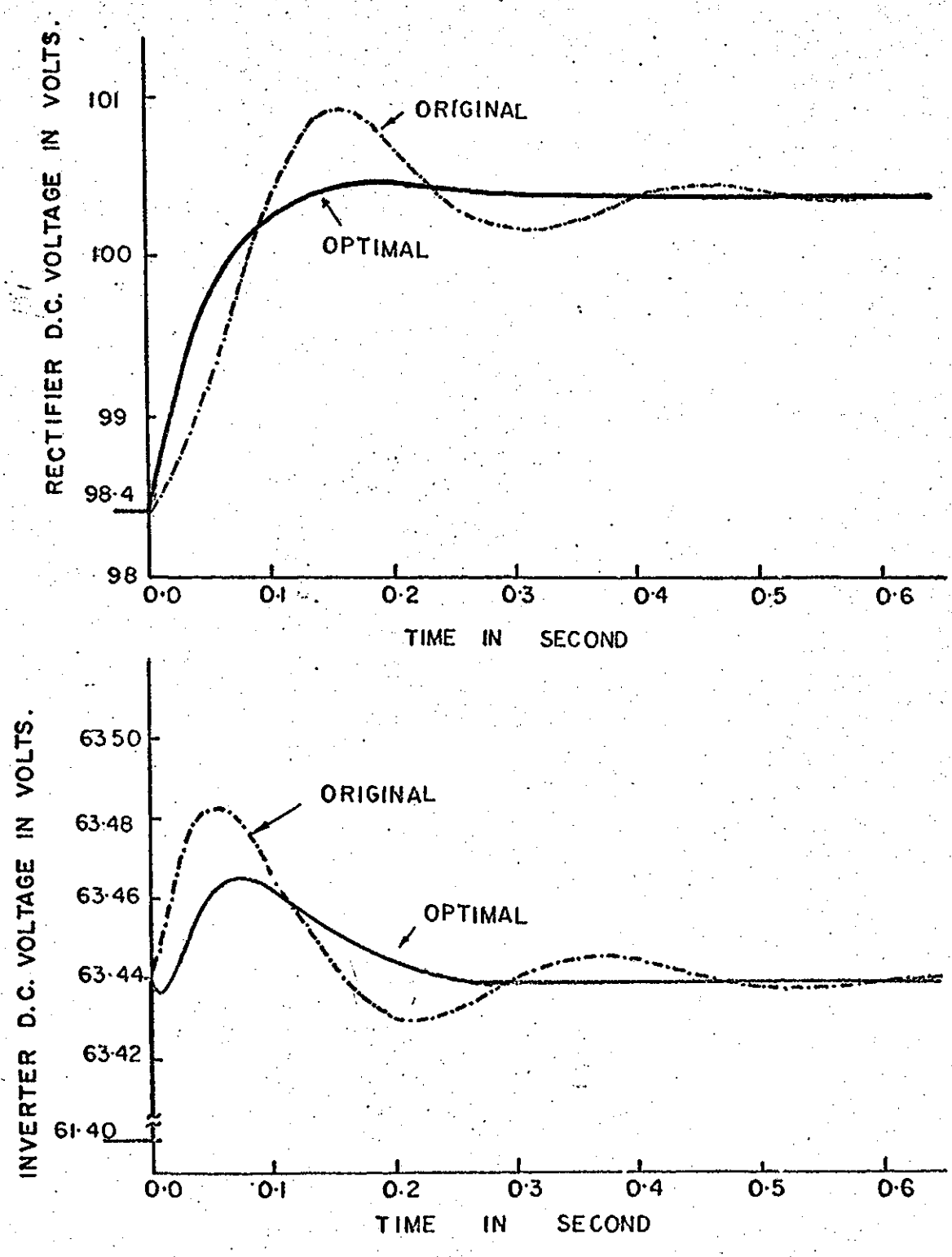

Figure 5.7 The digitally calculated convertor d.c. voltage changes for α+2 percent inverter commutation voltage step change.

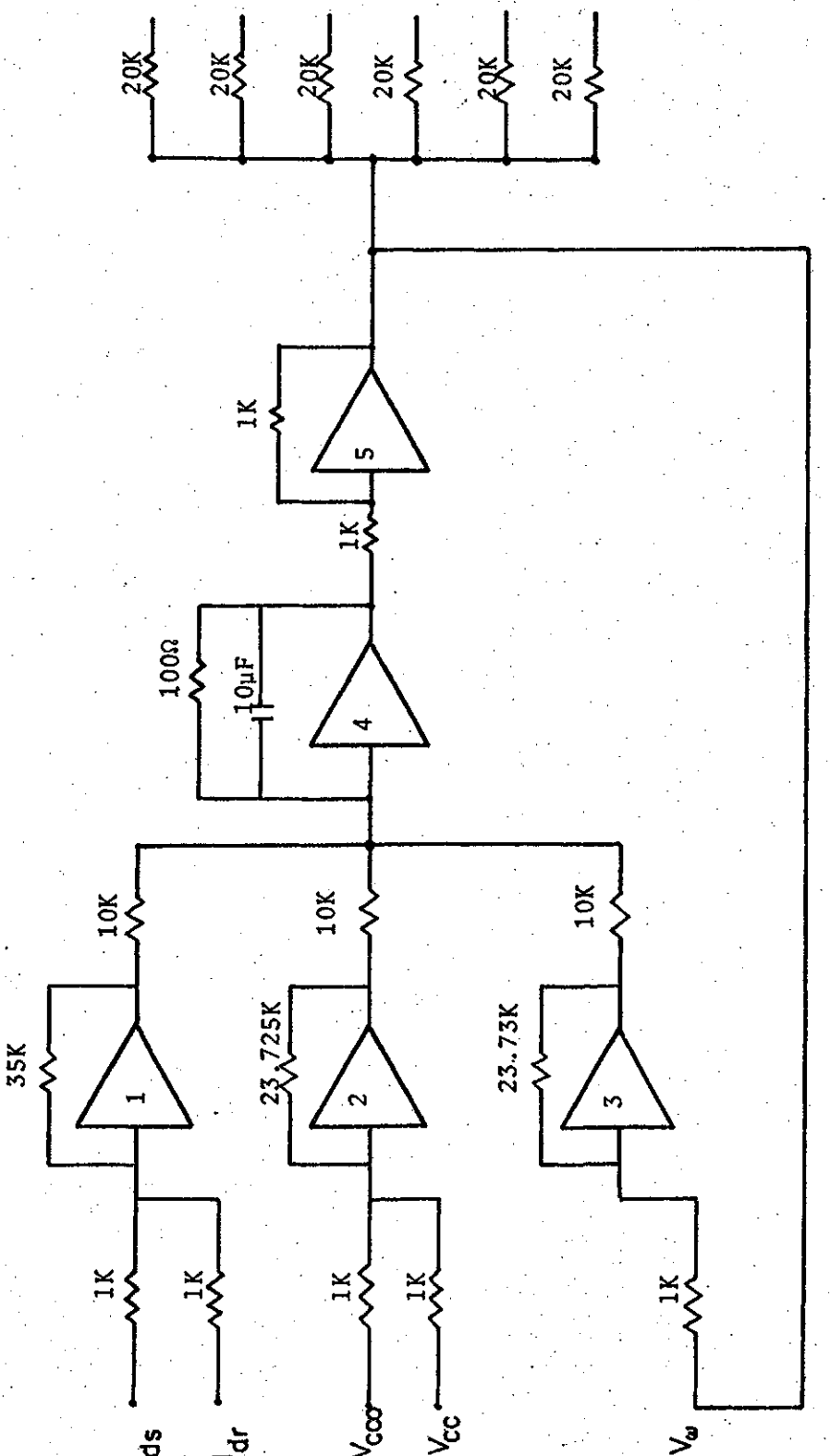

Figure 5.8 The simplified circuit diagram of the suboptimal controller used for the simulator constant current control.

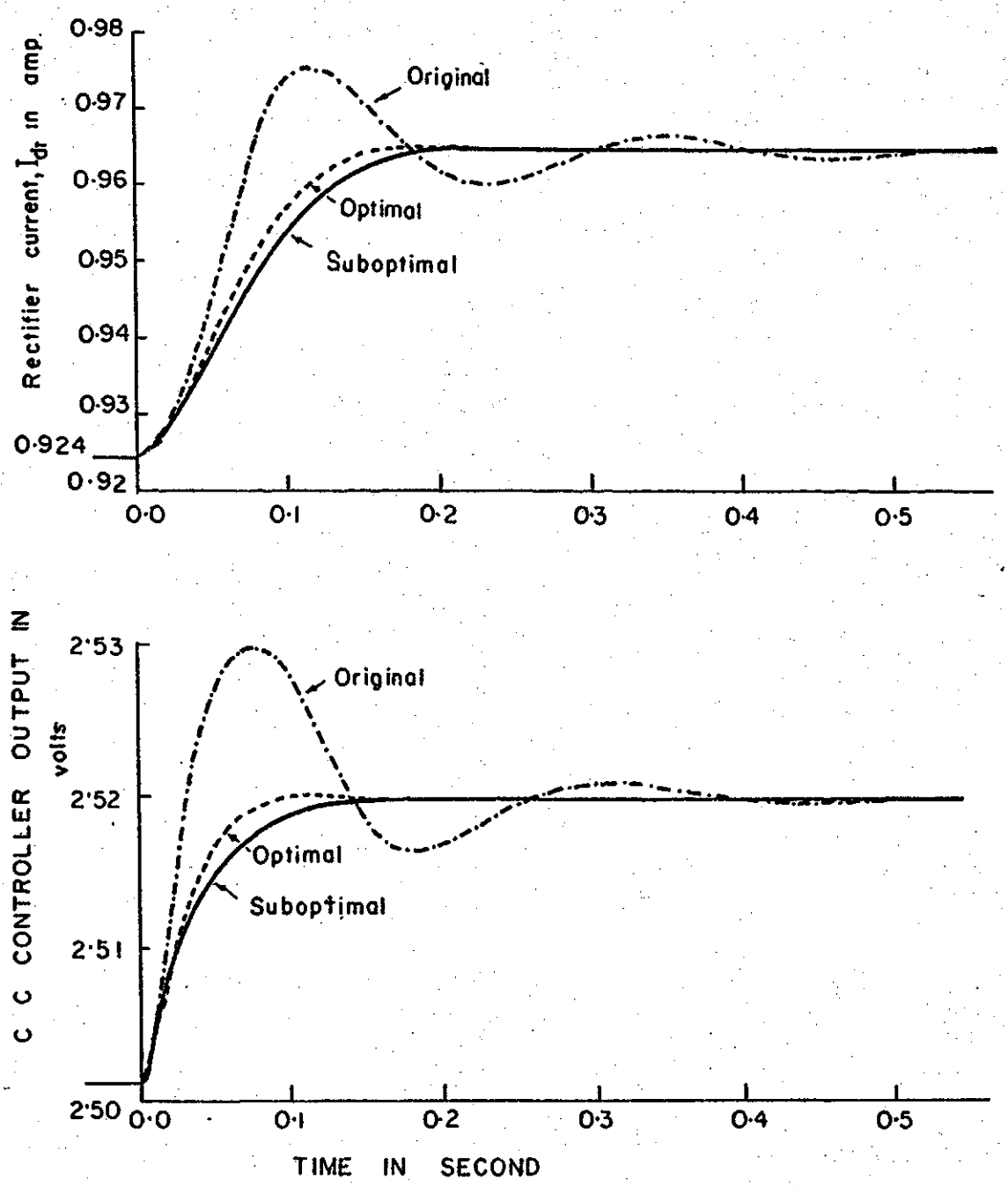

Figure 5.9 The digitally calculated d.c. line current and current controller output response of the simulator equipped with suboptimal controller for a+0.04 amp. current order step change

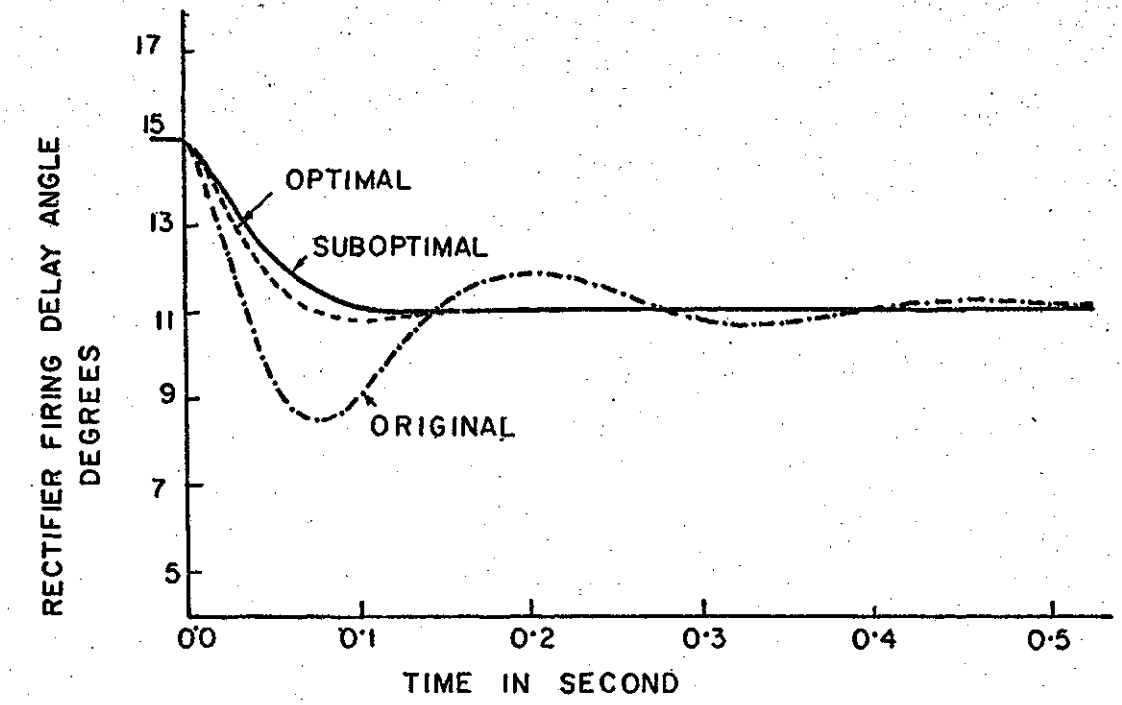

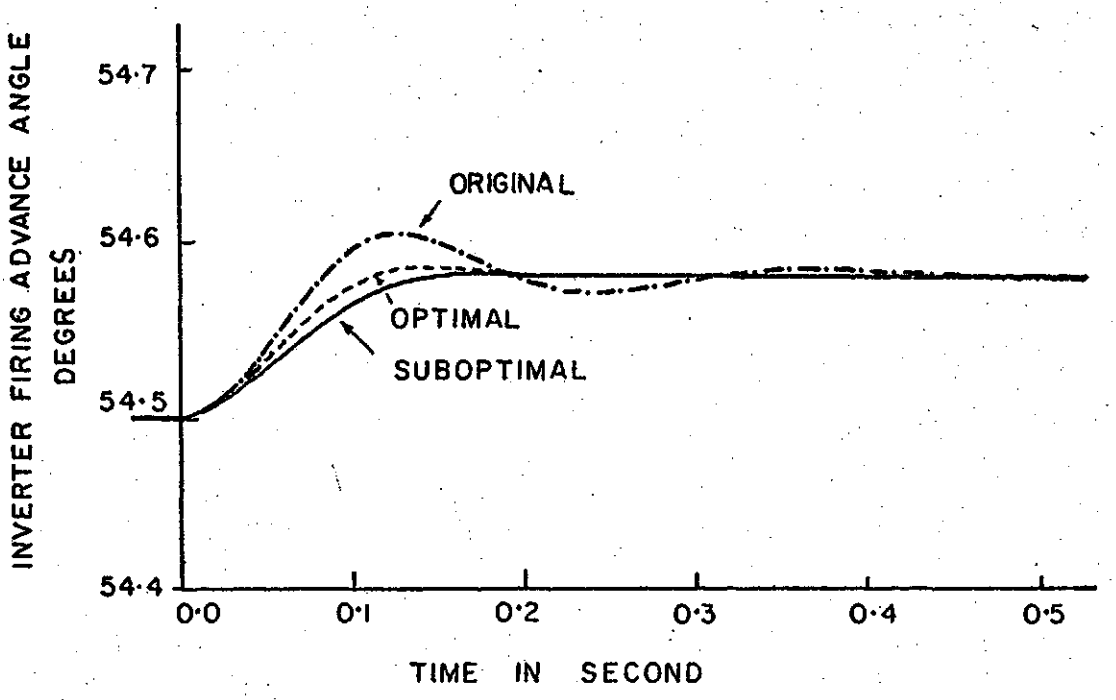

Figure 5.10 The digitally calculated convertor firing angle changes for α+0.04 amp. current order step change.

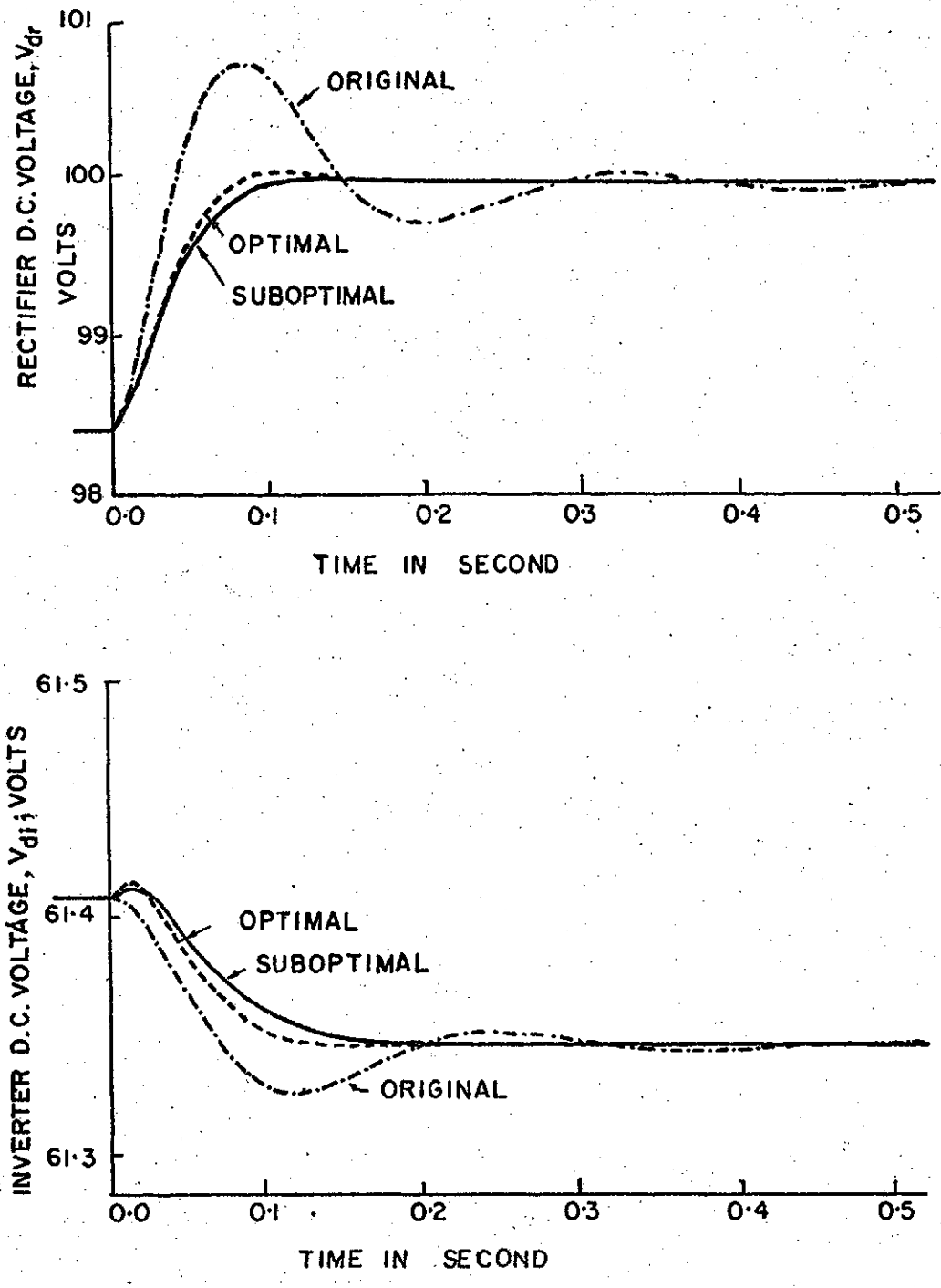

Figure 5.11 The digitally calculated convertor voltage changes for a+0.04 amp. current order step change.

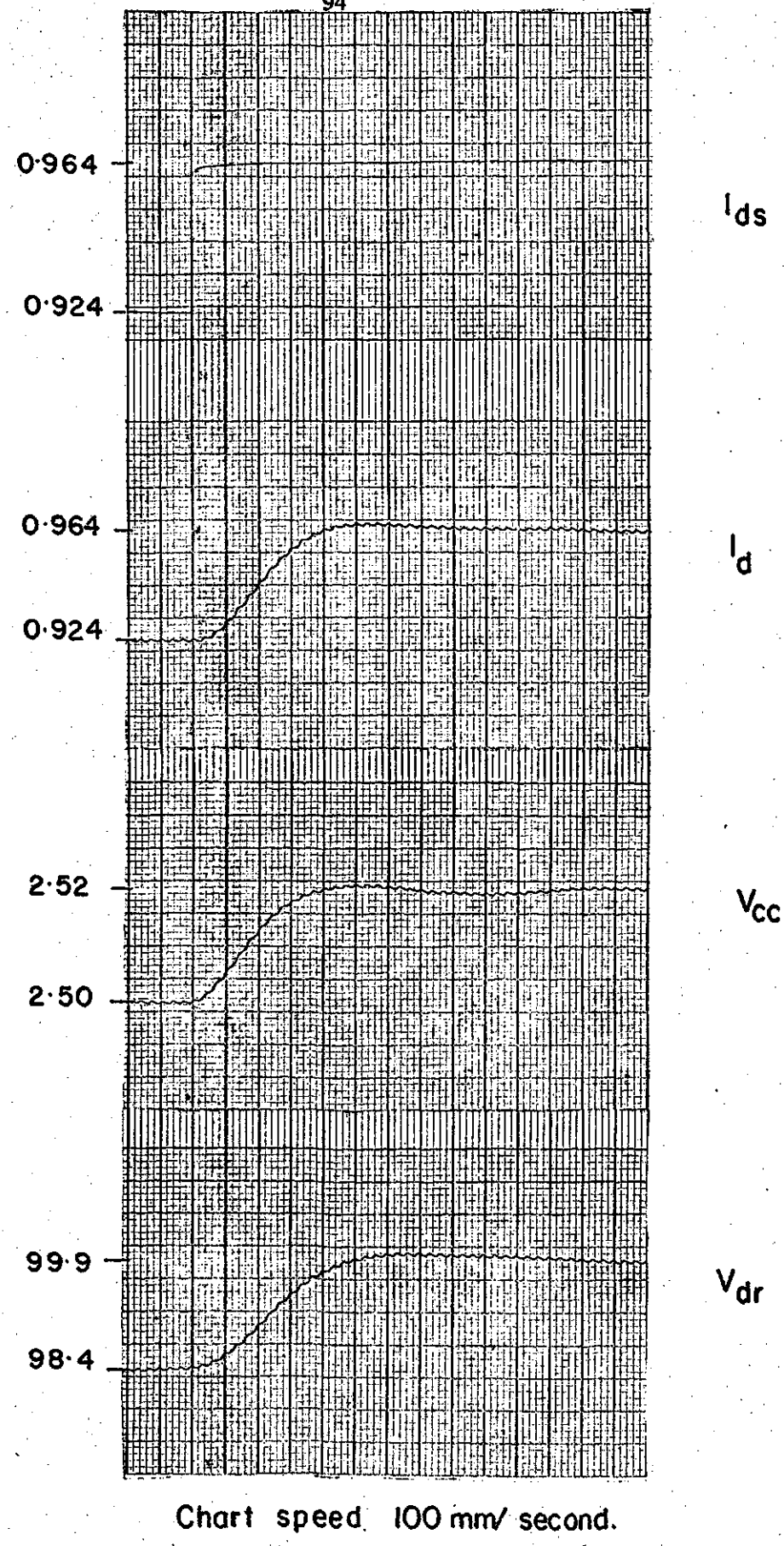

Figure 5.12 The d.c. line current, current controller output and rectifier voltage changes for a +0.04 amp. current order step change recorded from the simulator.

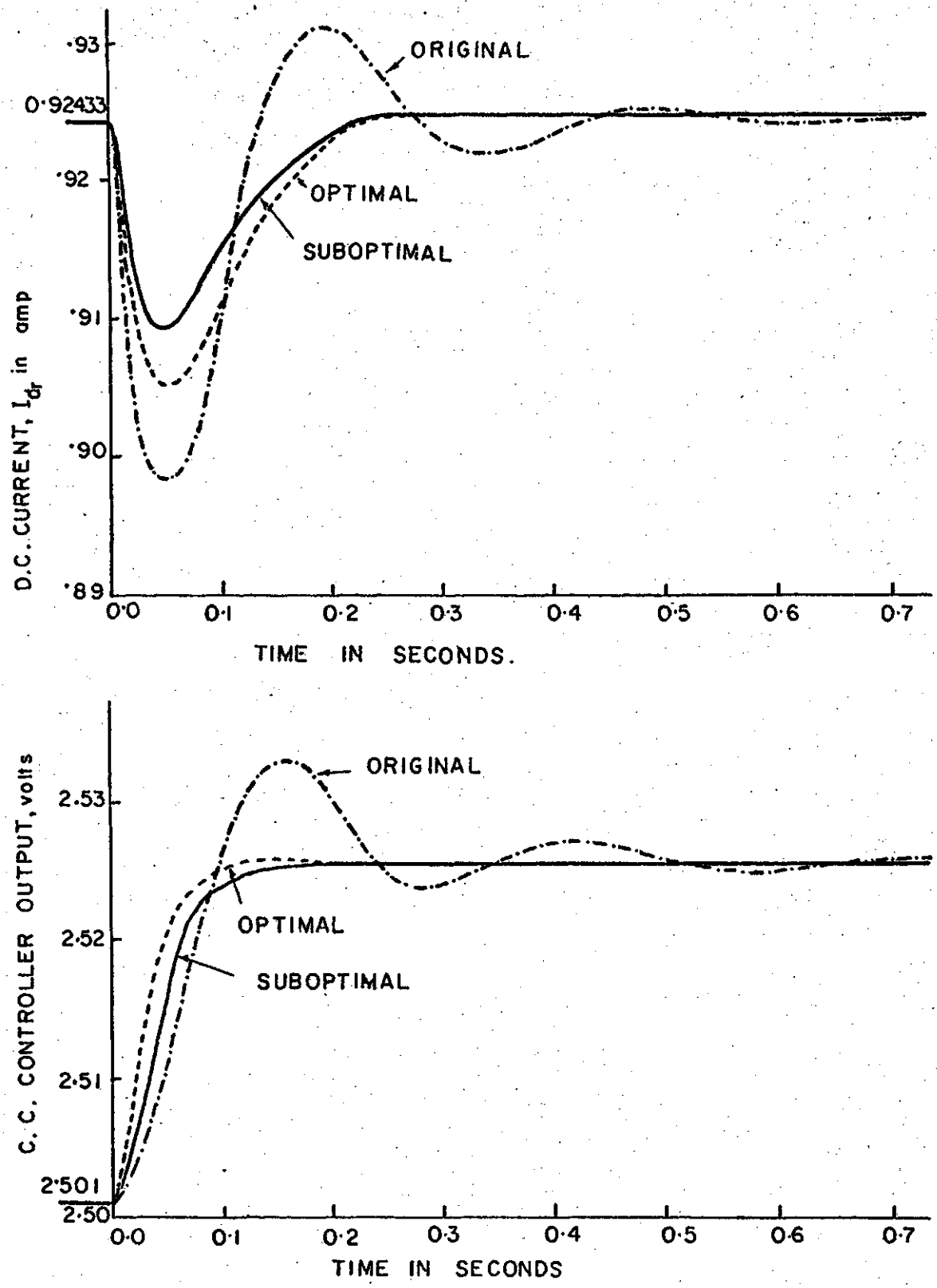

Figure 5.13 The digitally calculated d.c. line current and current controller output response of the simulator equipped with a suboptimal controller for α+2 percent inverter commutation voltage step change.

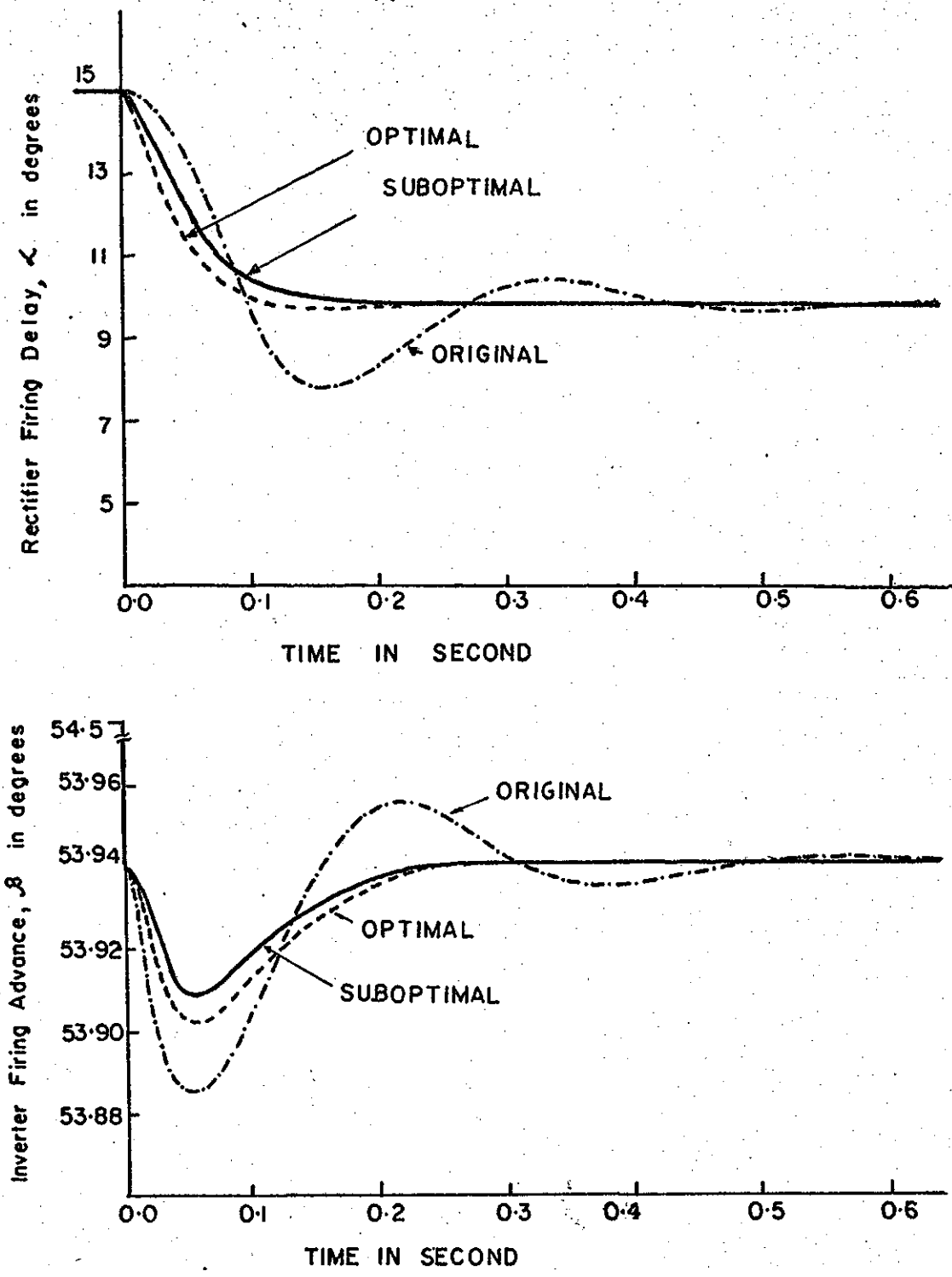

Figure 5.14 The digitally calculated convertor firing angle changes for α+2 percent inverter commutation voltage step change.

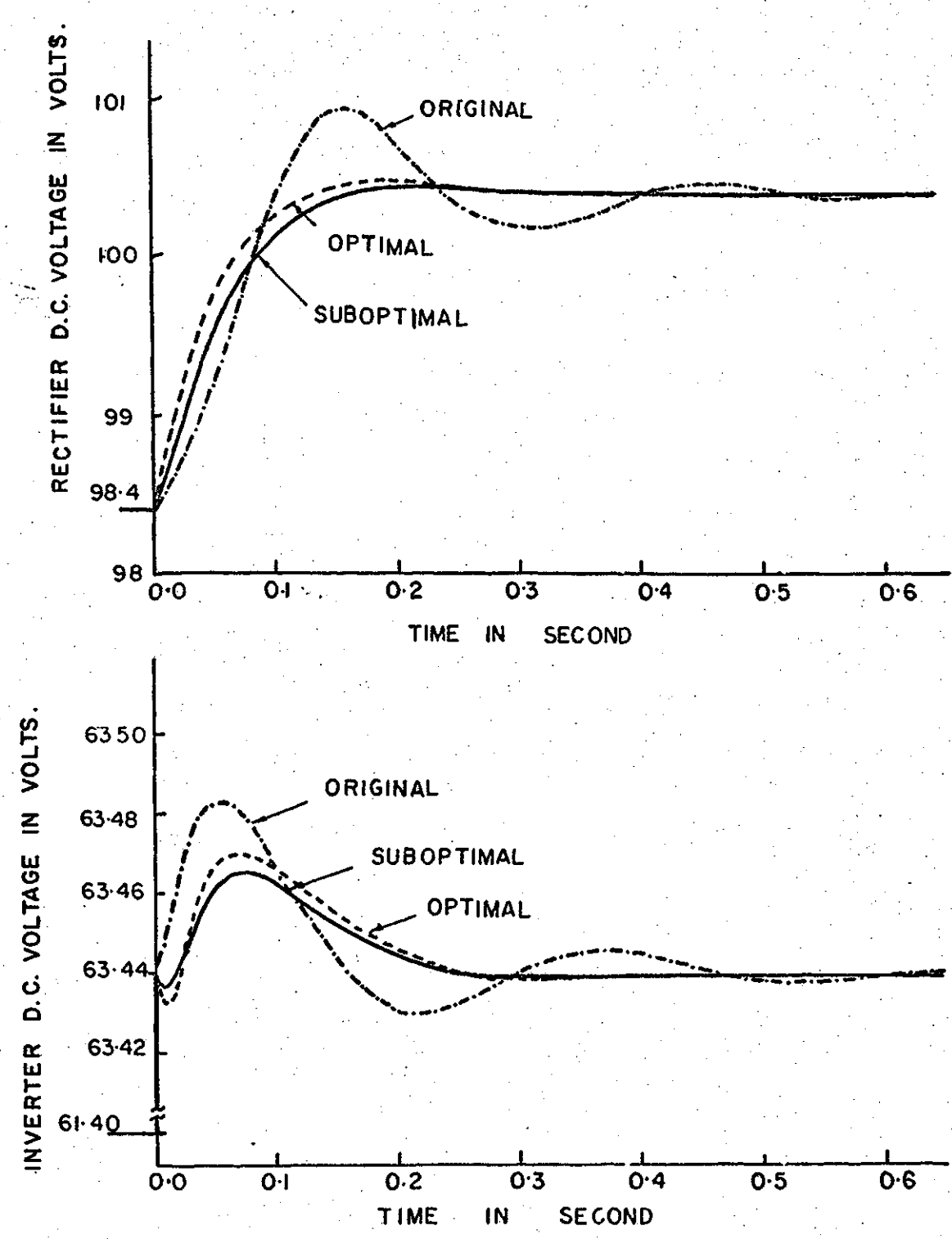

Figure 5.15 The digitally calculated convertor d.c. voltage changes for α+2 percent inverter commutation voltage step change.

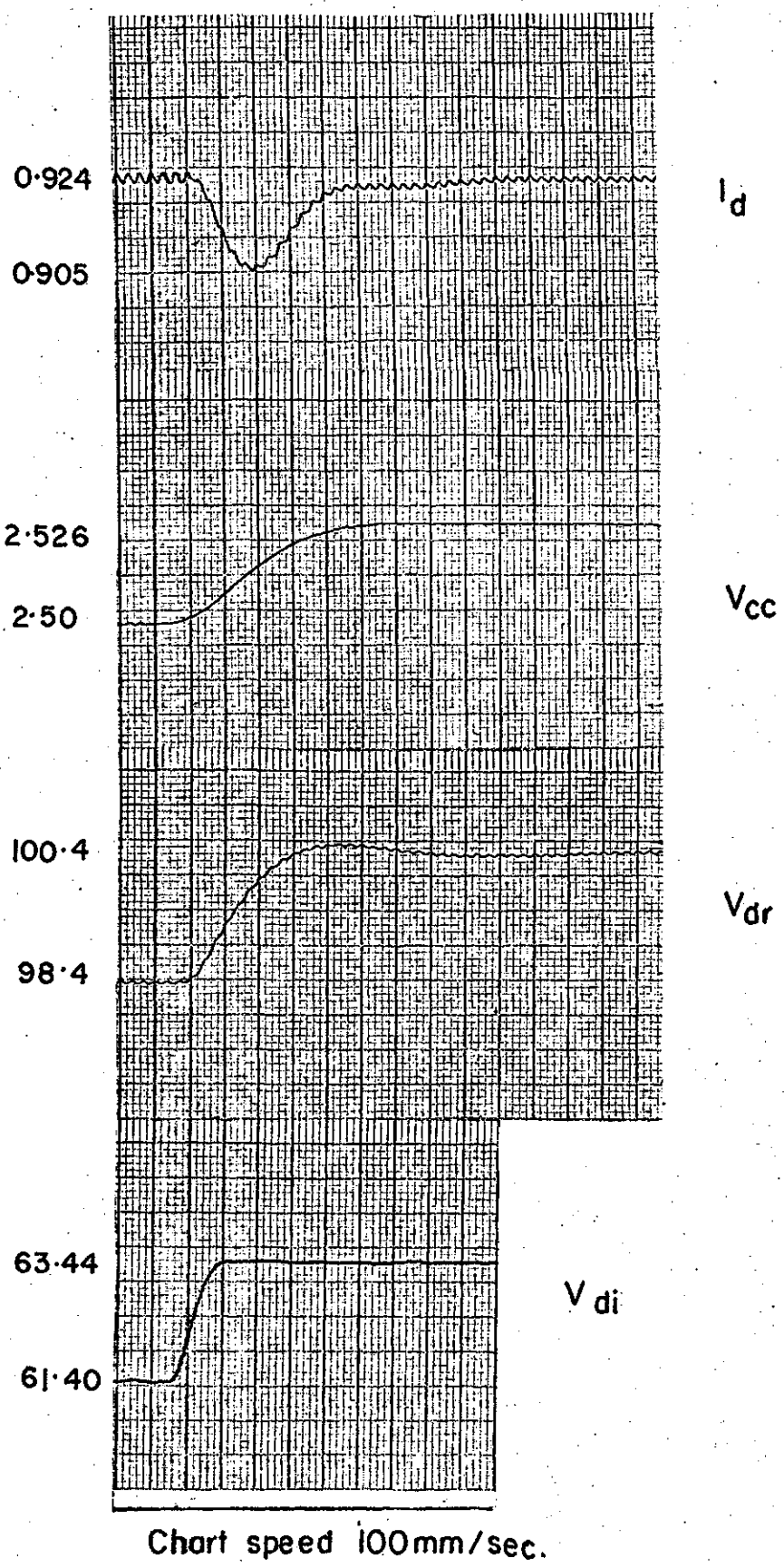

Figure 5.16 The d.c. line current, current controller output and convertor voltage changes for α+2 percent inverter commutation voltage step change recorded from the simulator.

6. ADDITIONAL STUDIES

The single bridge convertor output includes 6th, 12th, 18th, ... $6k^{th}$ order harmonics in addition to the d.c. voltage. The real time dynamic response is more accurately determined by considering the actual convertor voltage wave forms. The system dynamic performance was studied including the effect of harmonics in the convertor outputs. Two methods of modifying the current controller feedback loop to provide 7.5 current controller gain (corresponding to 0.707 damping ratio) for normal operation were examined. The current controller feedback loop was modified to include phase lead compensation. The modified state-space equations were derived, the compensator parameters were evaluated from the root-locus plots. The controller optimization by the tracking technique was examined for reducing the system response time. The digital and simulator system stability studies are included.

6.1 Stability Analysis - Effect of Voltage Harmonics

Convertor operation consists of consecutive two and three valve conduction modes. Typical rectifier and inverter voltages and the equivalent a.c./d.c. systems are shown in Figures 6.1. The dynamic performance is more accurately determined considering the actual exciting voltage wave forms and the system reactances in two and three valve conduction modes. The assumptions made in this analysis are:

(i) The transformer and a.c. system resistances are negligible.

(ii) Voltage drop across a conducting valve and the reverse current through a nonconducting valve are small and hence negligible.

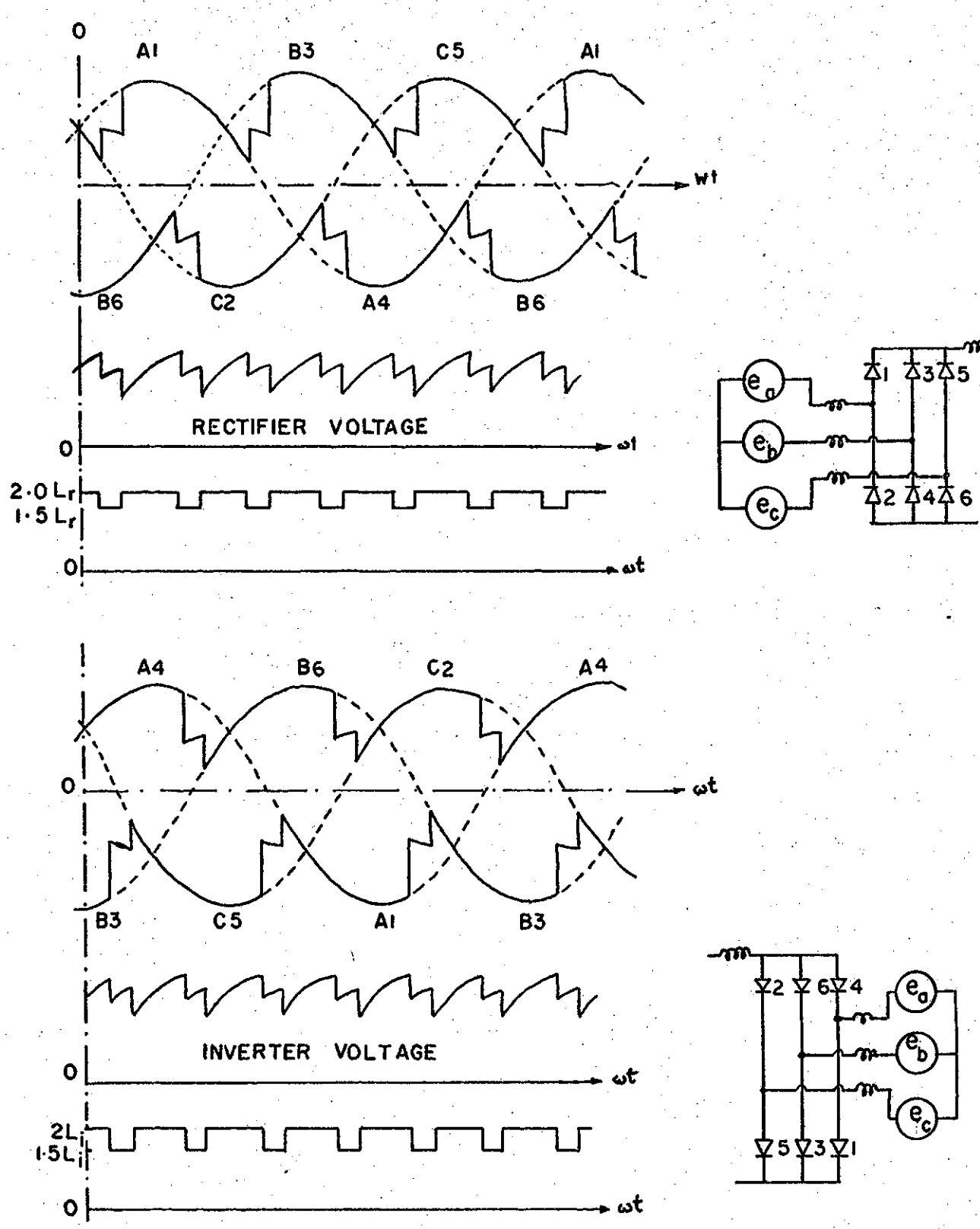

Figure 6.1 The typical convertor voltages and equivalent circuits for a.c./d.c. systems.

(iii) The a.c. system voltages e_a, e_b, and e_c are balanced.

The system inductances in two and three valve conduction modes are 2.0 and 1.5 times the per phase equivalent a.c. system inductance respectively. The equivalent source voltages in two and three valve conduction modes at the rectifier terminal are given by

$$e_{2r} = \sqrt{2}\, E_r \cos\{\omega t - (n-1)\cdot\tfrac{\pi}{3} + \tfrac{\pi}{6}\} \qquad 6.1$$

$$e_{3r} = \frac{\sqrt{3}}{\sqrt{2}}\, E_r \cos\{\omega t - (n-2)\cdot\tfrac{\pi}{3}\} \qquad 6.2$$

$n = 1, 2, 3, \ldots\ldots$

Where E_r is the line to line r.m.s. voltage of the rectifier transformer secondary at no load.

Subscripts 2 and 3 represent two and three valve conduction modes.

n denotes the valve firing counter.

The equivalent source voltages at the inverter terminal are similar except for a half cycle phase displacement. The equivalent network representing two and three valve conduction modes is shown in Figure 6.2.

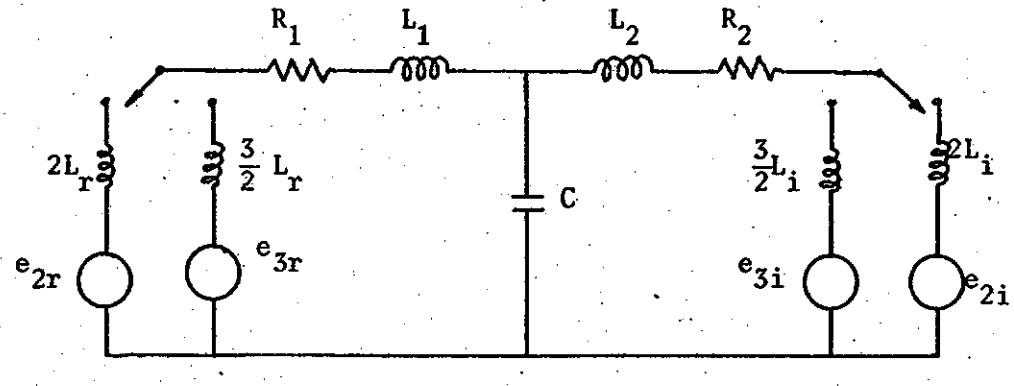

Figure 6.2 An equivalent circuit of the h.v.d.c. transmission system representing two and three valve conduction modes.

Where R_1 is the series combination of rectifier d.c. reactor resistance and equivalent line resistance.

R_2 is the series combination of the inverter d.c. reactor resistance and equivalent line resistance.

L_1 is the series combination of the rectifier d.c. reactor inductance and the equivalent inductance of the line.

L_2 is the series combination of the inverter d.c. reactor inductance and the equivalent inductance of the line.

L is the equivalent a.c. system inductance per phase.

Subscript r and i denote the associated rectifier and inverter quantities.

The system equations are given by

$$R_1 I_{dr} + (L_1 + KL_r) \frac{dI_{dr}}{dt} + V_c = e_r \qquad 6.3$$

$$R_2 I_{di} + (L_2 + KL_i) \frac{dI_{di}}{dt} - V_c = -e_i \qquad 6.4$$

$$\frac{dV_c}{dt} = \frac{1}{C} (I_{dr} - I_{di}) \qquad 6.5$$

Where K is 2.0 and 1.5 in two and three valve conduction modes respectively.

The voltage e_r is defined by equations 6.1 and 6.2 depending on the conduction mode. The voltage e_i is similarly defined. The commutation processes are given by

$$2L_r \frac{di_r}{dt} - L_r \frac{dI_r}{dt} = \sqrt{2}\, E_r \sin(\omega t - (n-2) \cdot \tfrac{\pi}{3}) \qquad 6.6$$

$$2L_i \frac{di_i}{dt} - L_i \frac{dI_i}{dt} = \sqrt{2}\, E_i \sin(\omega t - (n-2)\cdot\tfrac{\pi}{3} - \tfrac{\pi}{3}) \qquad 6.7$$

Where i and I are short circuit and d.c. line currents respectively.

The simulator dynamic performance equations 6.1 through 6.7 and the control equations 2.10 through 2.12 were digitally solved by Runge-Kutta method for a step change of 0.04 amps current order (from 0.924 amp to 0.964 amp). The d.c. current due to the current order change is shown in Figure 6.3. The average current compares favourably with that calculated from the average d.c. excitation voltages as shown in Figure 4.3. The superimposed oscillation magnitudes are approximately two percent of the average value in this case and are due to the convertor output voltage harmonics. Harmonic filters are provided on most practical high voltage d.c. lines and the effective excitation is the average d.c. voltage. The harmonic exciting voltages can be neglected in system studies in view of the low magnitude of the harmonic currents.

6.2 Modified Constant Current Controller Feedback.

Two methods of modifying the constant current controller feedback loop to provide 7.5 current controller gain (corresponding to 0.707 damping ratio) for normal operation are shown in Figure 6.4.

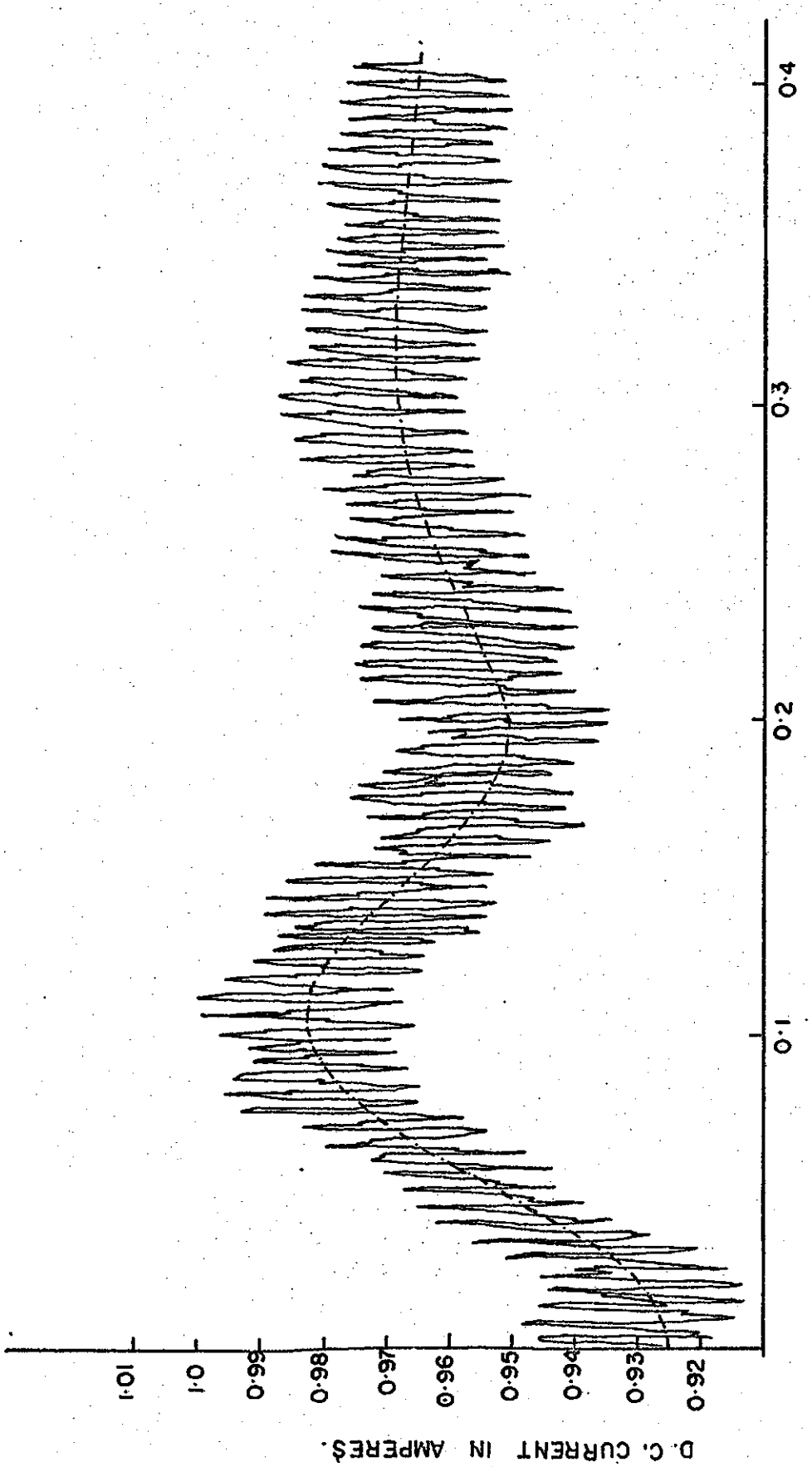

Figure 6.3 The digitally calculated d.c. line current changes for a+0.04 amp. current order step change.

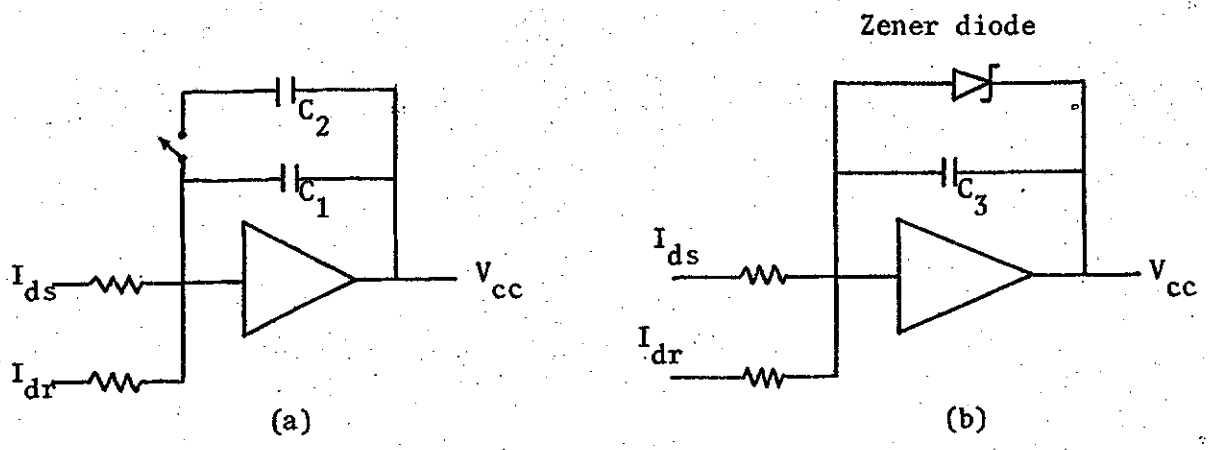

Figure 6.4 Modified current controller feedback arrangement.

The size of the feedback capacitor c_1 was selected to provide an amplifier gain of 10 for simulator starting. When the line current rose to the set value I_{ds} the additional capacitor c_2 was switched in parallel with c_1. The rating of c_2 was selected such that the parallel combination provides 7.5 current controller gain corresponding to 0.707 damping ratio. The second method tried consisted of providing the capacitor c_3 such that the amplifier gain was 7.5. The voltage output of the amplifier was limited to 9.1 volts by the zener diode connected as shown in Figure 6.4(b). The 9.1 volts current controller output limit ensured at least five electrical degrees rectifier firing delay during the simulator starting also. The zener diode was ineffective during normal operation.

The system response of the simulator equipped with a 7.5 gain current controller was calculated for a step increase of 0.04 amp d.c. current order (from 0.924 amps to 0.964 amps). The d.c. current changes

and convertor voltages for this study are shown in Figure 6.5. A two percent increase of inverter commutation voltage was also considered as before. The d.c. current changes and convertor voltages are shown in Figure 6.8. These studies were also repeated on the simulator and the analog results are shown in Figure 6.9 and 6.10 respectively. The digital and analog performance is compared in Table 6.1. The d.c. line current rise time in this case is higher than when the compared system is equipped with a 10 amplifier gain controller. The settling-time and percentage overshoot are comparatively smaller.

6.3 Modified H.V.D.C. Controller

The current controller feedback loop modification to include phase lead compensation usually reduces the output overshoot and time delays. The constant current controller including the phase lead compensation is shown in Figure 6.6. The state space equations for the d.c. transmission system including the modified controller werederived. The desirable compensator parameters were evaluated from the root-locus plots. The transient response of the simulator was digitally evaluated and simulator test results were obtained to confirm digital model validity.

6.3.1 Dynamic equations and stability analysis

The series R-C branch of the constant current controller feedback loop shown in Figure 6.6 provides the phase lead compensation. The modified current controller transfer function is given by

Table 6.1 Time domain performance of the d.c. simulator for the current controller gains of (i) 10 and (ii) 7.5.

	Step Change in Current Order				Step Change in Inverter Commutation Voltage			
	Gain = 10		Gain = 7.5		Gain = 10		Gain = 7.5	
	Digital	Analog	Digital	Analog	Digital	Analog	Digital	Analog
Settling time in seconds	0.27	0.29	0.20	0.24	0.30	0.33	0.21	0.22
Rise time in seconds	0.05	0.055	0.13	0.13	0.07	0.08	0.15	0.17
Overshoot in percent	25	24	5	5	25	28.5	4	1
Time to overshoot in seconds	0.11	0.13	0.26	0.30	0.15	0.18	0.27	0.30

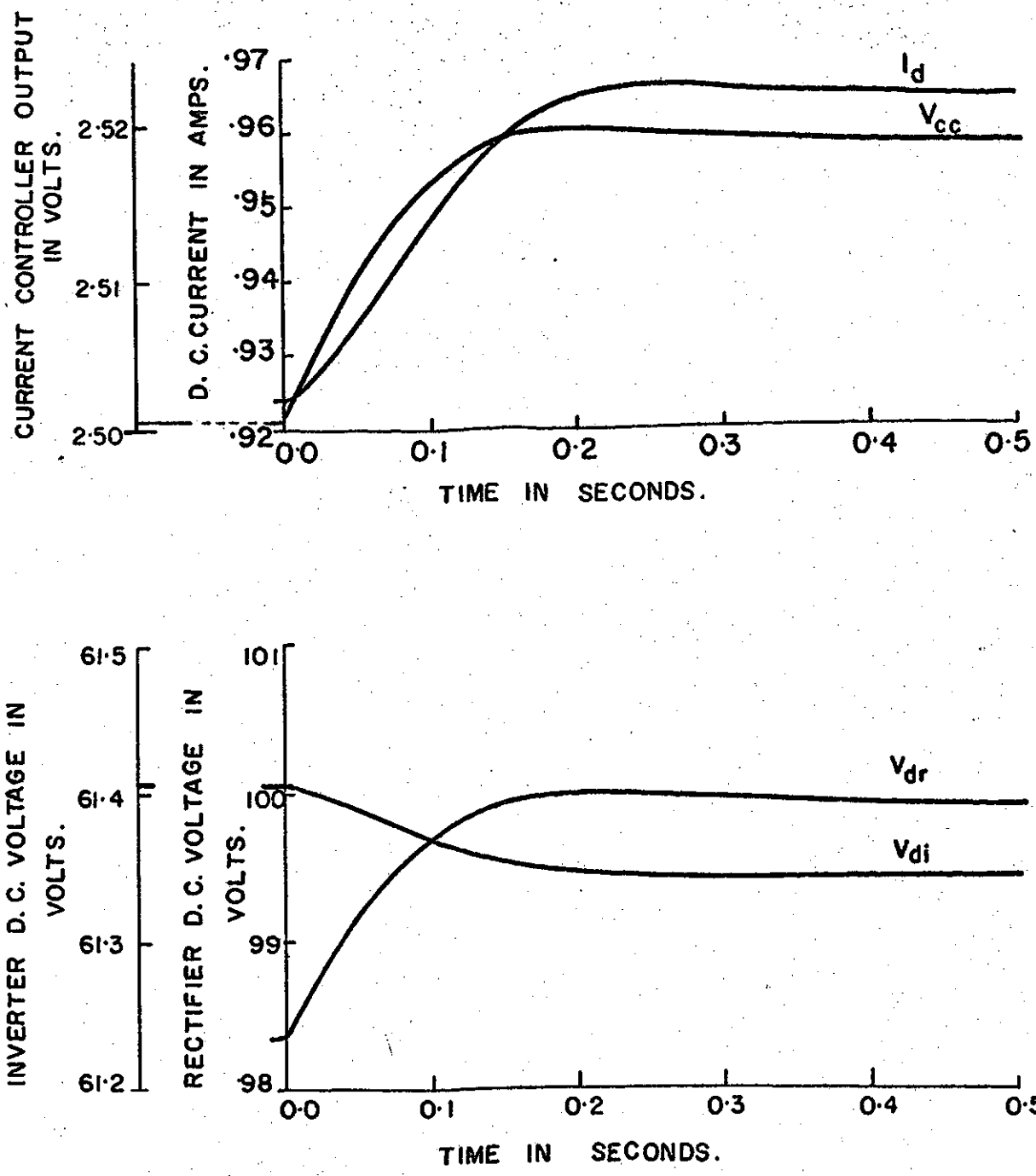

Figure 6.5 The d.c. current, current controller output and convertor voltage changes for a +0.04 amp. current order step change.

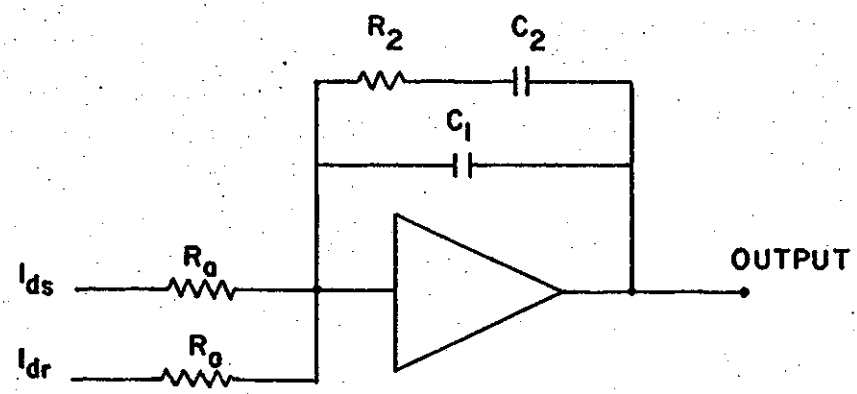

Figure 6.6 Modified integral controller with phase lead compensation.

$$G(s) = \frac{K_a}{s} \frac{(1 + sT)}{(1 + saT)} \qquad 6.8$$

$$T = R_2C_2 \qquad 6.9(a)$$

$$a = \frac{C_1}{C_1 + C_2} \qquad 6.9(b)$$

$$K_a = \frac{1}{R_a(C_1 + C_2)} \qquad 6.9(c)$$

Where 'a' is a constant

T is the time constant in seconds

K_a is the current controller gain.

The magnitude of a is less than 1 and is usually kept low to obtain low noise to signal ratio. A small time constant is provided for a relatively high bandwidth operation.[35]

The d.c. transmission system equipped with the modified current controller is represented by the block diagram of Figure 3.16 except that the current controller block $\frac{K_2K_c}{K_pR_aC_as}$ is replaced by

$$\frac{K_2K_c}{K_p\,R_a\,(C_1+C_2)s}\;\frac{(1+sT)}{(1+saT)}.$$

The system state space equations are given by

$$\begin{bmatrix}\dot{x}_1\\ \dot{x}_2\\ \dot{x}_3\\ \dot{x}_4\\ \dot{x}_5\end{bmatrix} = \left[\begin{array}{ccccc:c:c} \frac{-(R_1-\frac{6}{\pi}\omega L_r)}{L_1} & 0 & \frac{-1}{L_1} & \frac{3}{\pi}\frac{K_2}{K_p}\frac{1}{L_1} & 0 & \\ 0 & \frac{-(R_2-\frac{6}{\pi}\omega L_i)}{L_2} & \frac{1}{L_2} & 0 & 0 & \\ \frac{1}{C} & \frac{-1}{C} & 0 & 0 & 0 & \\ 0 & 0 & 0 & 0 & 1 & \\ \frac{K_cK_a}{a}\left(\frac{R_1-\frac{6}{\pi}\omega L_r}{L_1}-\frac{1}{T}\right) & 0 & \frac{K_cK_a}{a}\frac{1}{L_1} & -\frac{3}{\pi}\frac{K_cK_aK_2}{aK_pL_1} & \frac{1}{aT} & \end{array}\right]\begin{bmatrix}x_1\\ x_2\\ x_3\\ x_4\\ x_5\end{bmatrix}$$

$$+\begin{bmatrix} \frac{3\sqrt{2}}{\pi}\frac{1}{L_1}\cos\delta_c & 0 & 0\\ 0 & \frac{-3\sqrt{2}}{\pi}\frac{\cos\delta_c}{L_2} & 0\\ 0 & 0 & 0\\ 0 & 0 & 0\\ \frac{K_cK_a}{a}\cos\delta_c & 0 & \frac{K_cK_a}{aT}\end{bmatrix}\begin{bmatrix}\Delta E_r\\ \Delta E_i\\ \Delta I_{ds}\end{bmatrix} \qquad 6.10$$

ΔI_{dr}, ΔI_{di}, ΔV_c, ΔV_{cc} and $\Delta \dot{V}_{cc}$ are the five system state variables x_1, x_2, x_3, x_4 and x_5 respectively. Equation 6.12 is an extension of equation 4.18 and includes the additional state variable $x_5 = \Delta \dot{V}_{cc}$. The eigenvalues of the characteristic equation were calculated for amplifier gain $K_a = 10$, a = 0.1 and 0.2 and T increasing from 0.01 to 0.14. The root locus plots are shown in Figure 6.11 and the system instability regions are listed in Table 6.2.

Table 6.2 System instability regions.

a	System unstable for T
0.1	(i) Less than or equal to 0.018 secs. (ii) Greater than or equal to 0.042 secs. but less than or equal to 0.10 secs.
0.2	(i) Less than or equal to 0.01 secs. (ii) Greater than or equal to 0.025 secs. but less than or equal to 0.042 secs.

The values of a and T corresponding to a 0.707 damping ratio for the dominant roots are 0.2 and 0.018 respectively. The parameters of the current controller feedback loop for a=0.2 and T=0.018 secs as calculated using equations 6.9(a), 6.9(b) and 6.9(c) are C_1 = 1.34 μF, R_2 = 3.36 kohm and C_2 = 5.36 μF.

A step change of 0.04 amps current order (from 0.924 amps to 0.964 amps) was applied. The calculated d.c. line current and the current controller output due to the current order change are shown in Figure 6.12. The line current settles at the new value of 0.964 amps

after a transient period of 0.142 secs. The rise time is 0.065 secs and approximately 6 percent overshoot occurs 0.135 secs after the step change is applied. The changes in rectifier and inverter firing angles and d.c. voltages during the transient are shown in Figure 6.13. The simulator current controller feedback loop was modified to include phase lead compensation and the current order step change study was repeated. The simulator line current and d.c. voltage changes recorded are shown in Figure 6.14.

A two percent step increase in inverter commutation voltage was also considered. The digital results for d.c. current and current controller output are shown in Figure 6.15. The changes in convertor firing angles and d.c. voltages are shown in Figure 6.16. The simulator results for a similar change are shown in Figure 6.17.

The performance of the system using (i) integral and (ii) integral with phase lead compensation current controllers is compared in Table 6.3. It is observed that integral controller with phase lead compensation reduces the overshoot and rise and settling times compared to the integral controller.

6.4 Optimization by the Tracking Technique.

The tracking technique in optimization theory determines a control signal that minimizes the error between the desired and actual outputs.[39] The system state space equations are already defined in Chapter 4. The tracking cost function $J(\omega)$ is given by

Table 6.3 Time domain performance of the d.c. simulator equipped with (i) integral (ii) integral with phase lead compensation current controllers.

	Step change in current order				Step change in inverter commutation voltage			
	Integral		Phase lead		Integral		Phase lead	
	Digital	Analog	Digital	Analog	Digital	Analog	Digital	Analog
Settling time in seconds	0.27	0.29	0.142	0.15	0.30	0.33	0.19	0.23
Rise time in seconds	0.05	0.055	0.065	0.07	0.07	0.08	0.067	0.07
Overshoot in percent	25	24	6	7	25	28.5	7.5	10
Time to overshoot in seconds	0.11	0.13	0.135	0.14	0.15	0.18	0.15	0.20

$$J(\omega) = \frac{1}{2} \int_0^\infty \left[e^T(t)\ Q\ e(t) + \omega^T\ (t)\ R\ \omega(t) \right] dt \qquad 6.11$$

This cost function is similar to the cost function defined by equation 5.2 except for the error vector e(t) which is given by

$$e(t) = Z(t) - y(t) \qquad 6.12$$

$$y(t) = C\ \ x(t) \qquad 6.13$$

$$Z(t) = Z_o \qquad 6.14$$

Where Z_o is the mx1 desired output vector
$y(t)$ is the mx1 output vector
C is the mxn output-input coefficient matrix.

Including the effect of the desired output, the costate vector is given by

$$p(t) = K(t)\ x(t) - g(t) \qquad 6.15$$

Where K(t) is the nxn Riccati Matrix
g(t) is the nx1 column vector due to desired output.

The canonical equations 5.4 through 5.6 provide the following set of equations:

$$\dot{K} = -KA - A^TK + K\ E\ R^{-1}\ E^TK - C^TQC \qquad 6.16$$

$$g = -\left[(A - E\ R^{-1}\ E^TK)^T\right]^{-1}\ C^TQZ_o \qquad 6.17$$

$$\omega = -R^{-1}\ E^T\ (K\ x - g) \qquad 6.18$$

The Riccati matrix K is calculated from equation 6.16 and the control vector ω is calculated from equations 6.17 and 6.18. The system equations are therefore given by

$$\dot{x} = Ax + E\omega$$

$$= (A - E\,R^{-1}\,E^{T}K)x + E\,R^{-1}\,E^{T}g \qquad 6.19$$

The tracking control system block diagram is shown in Figure 6.7.

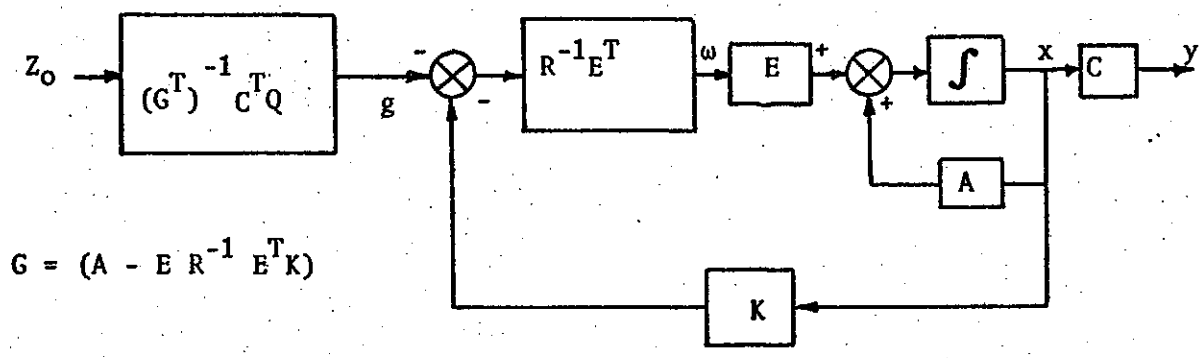

Figure 6.7. Tracking control system block diagram.

For the d.c. simulator system

$$\left[Z_o\right] = \begin{bmatrix} \Delta I_{dr_o} \\ \Delta I_{di_o} \end{bmatrix} \qquad \left[y\right] = \begin{bmatrix} \Delta I_{dr} \\ \Delta I_{di} \end{bmatrix}$$

$$\left[C\right] = \begin{bmatrix} 1 & 0 & 0 & 0 \\ 0 & 1 & 0 & 0 \\ 0 & 0 & 0 & 0 \\ 0 & 0 & 0 & 0 \end{bmatrix}$$

Where ΔI_{dr_o} and ΔI_{di_o} are the desired current order changes. The following values of Q and R were selected from a number of trials.

$$[Q] = \begin{bmatrix} 1 & 0 & 0 & 0 \\ 0 & 1 & 0 & 0 \\ 0 & 0 & 1 & 0 \\ 0 & 0 & 0 & 1 \end{bmatrix} \quad [R] = 0.01$$

The calculated Riccati matrix K is given by

$$[K] = \begin{bmatrix} 0.1127 & -0.1009 & 0.0008 & 0.2385 \\ -0.1009 & 0.1049 & -0.0004 & -0.1211 \\ 0.0008 & -0.0004 & 0.0045 & -0.0842 \\ 0.2385 & -0.1211 & -0.0842 & 5.0608 \end{bmatrix}$$

The feedforward gains calculated from equations 6.17 are

$$[(G^T)^{-1} C^T Q] = \begin{bmatrix} -0.07037 \\ -0.07037 \end{bmatrix}$$

The system solution is obtained by using equations 6.19 for a step change of +0.04 amp. current order (from 0.924 amps to 0.964 amps). The digitally calculated d.c. line current due to the current order change is shown in Figure 6.18. The line current settles at the set value of 0.964 amps after a transient period of 0.020 secs. The rise time is 0.016 secs and approximately 2 percent overshoot occurs 0.03 sec

after the step change is applied. The current controller output is also plotted in Figure 6.18. The current controller output reaches a peak at 0.01 sec as expected. The convertor voltage and firing angle changes are shown in Figure 6.19.

The calculated performance of original, state-regulator optimal, phase-lead compensated and tracking optimal d.c. simulator systems is compared in Table 6.4.

Table 6.4 Time domain performance of the d.c. simulator equipped with (i) original (ii) state-regulator optimal (iii) phase lead compensated and (iv) tracking optimal controllers.

	Original	State-regulator Optimal	Phase-lead Compensated	Tracking Optimal
Settling time	0.27 sec	0.132 sec	0.142 sec	0.020 sec
Rise time	0.05 sec	0.09 sec	0.065 sec	0.016 sec
Overshoot	25%	2%	6%	2%
Time to overshoot	0.11 sec	0.16 sec	0.20 sec	0.03 sec.

These results indicate that the tracking optimization provides the fastest d.c. line current response. The current controller output and rectifier voltage changes are quite violent and may be objectionable for operating a high voltage d.c. system. The system response speed can be reduced by changing the penalty matrices Q and R.

Two modified current controller feedback loops have been used and simulator successfully started with 7.5 amplifier gain corresponding to 0.707 damping ratio. The system performance was examined using the digital computer and the simulator. The effects of direct voltage harmonics on the transient behaviour of the simulator was also examined. The suitability of a phase lead compensated controller has been investigated. A suitable phase lead compensated controller parameters have been calculated and the system performance has been examined. The possibility of control optimization by the tracking technique has also been investigated and was found to reduce the rise time, settling time and overshoot considerably.

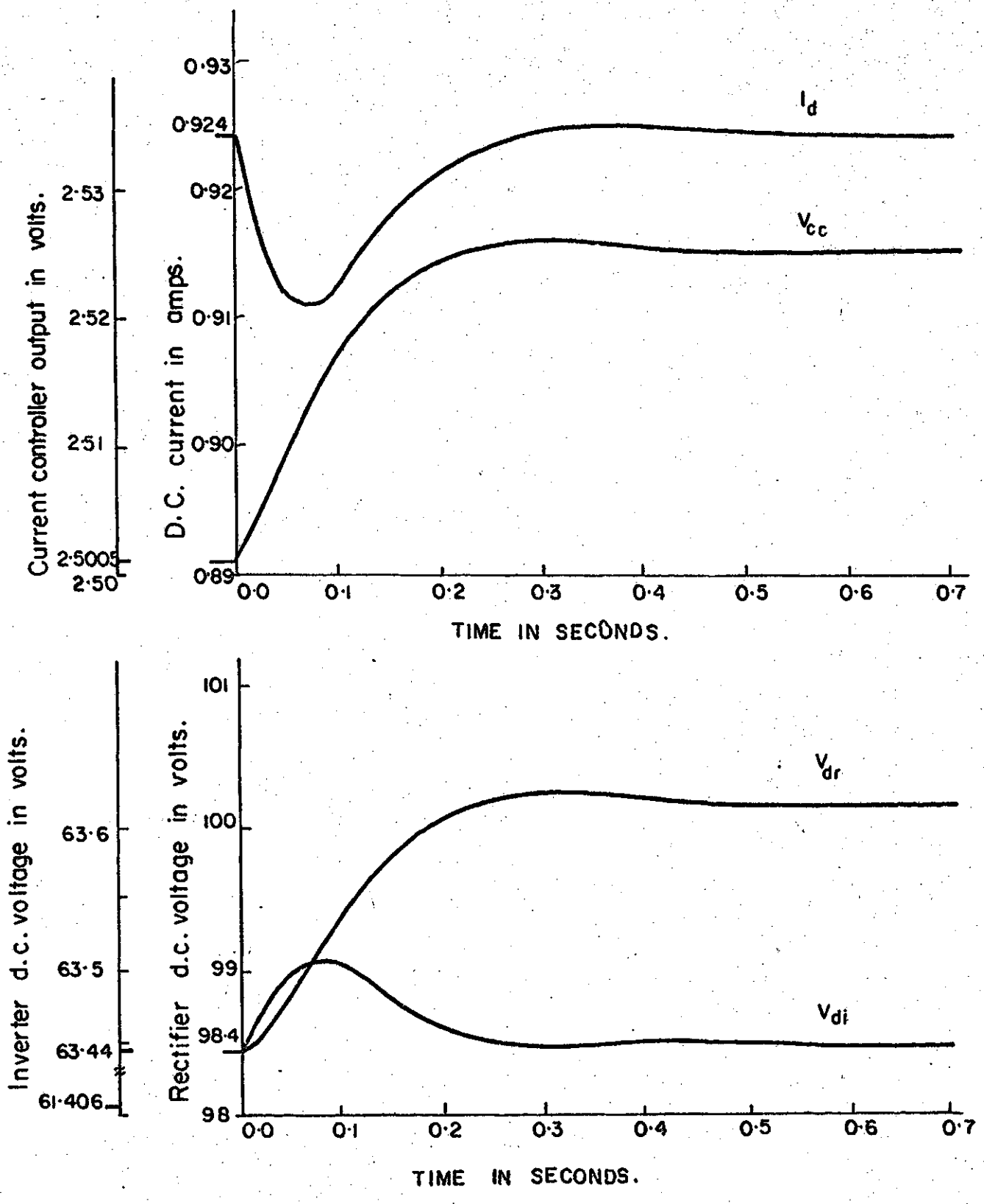

Figure 6.8 The digitally calculated d.c. line current, current controller output and convertor d.c. voltage changes for a+2 percent inverter commutation voltage step change.

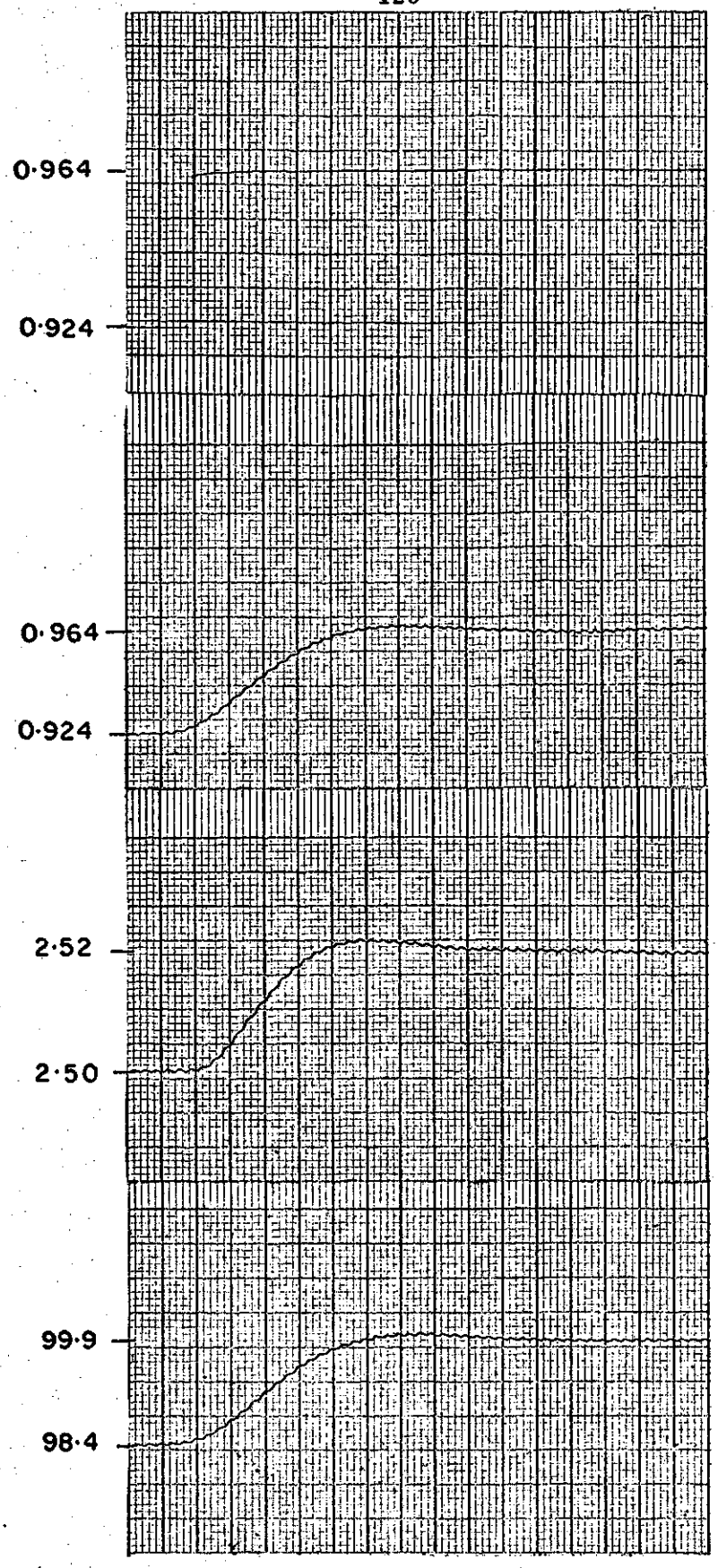

Figure 6.9. The d.c. line current, current controller output and rectifier d.c. voltage changes for a +0.04 amp. current order step change recorded from the simulator.

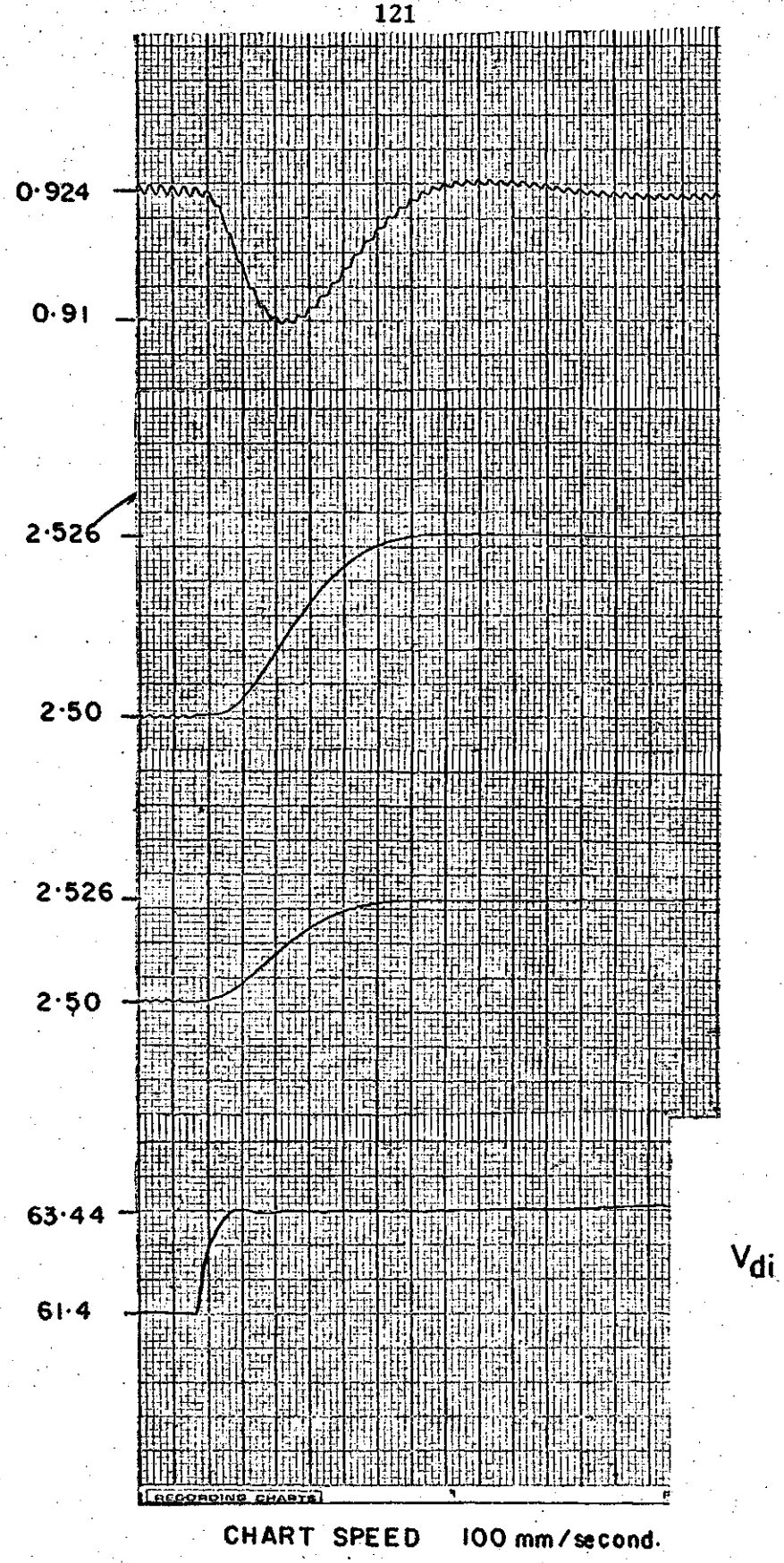

Figure 6.10 The d.c. line current, current controller output and convertor voltage changes for α+2 percent inverter commutation voltage step change recorded from the simulator.

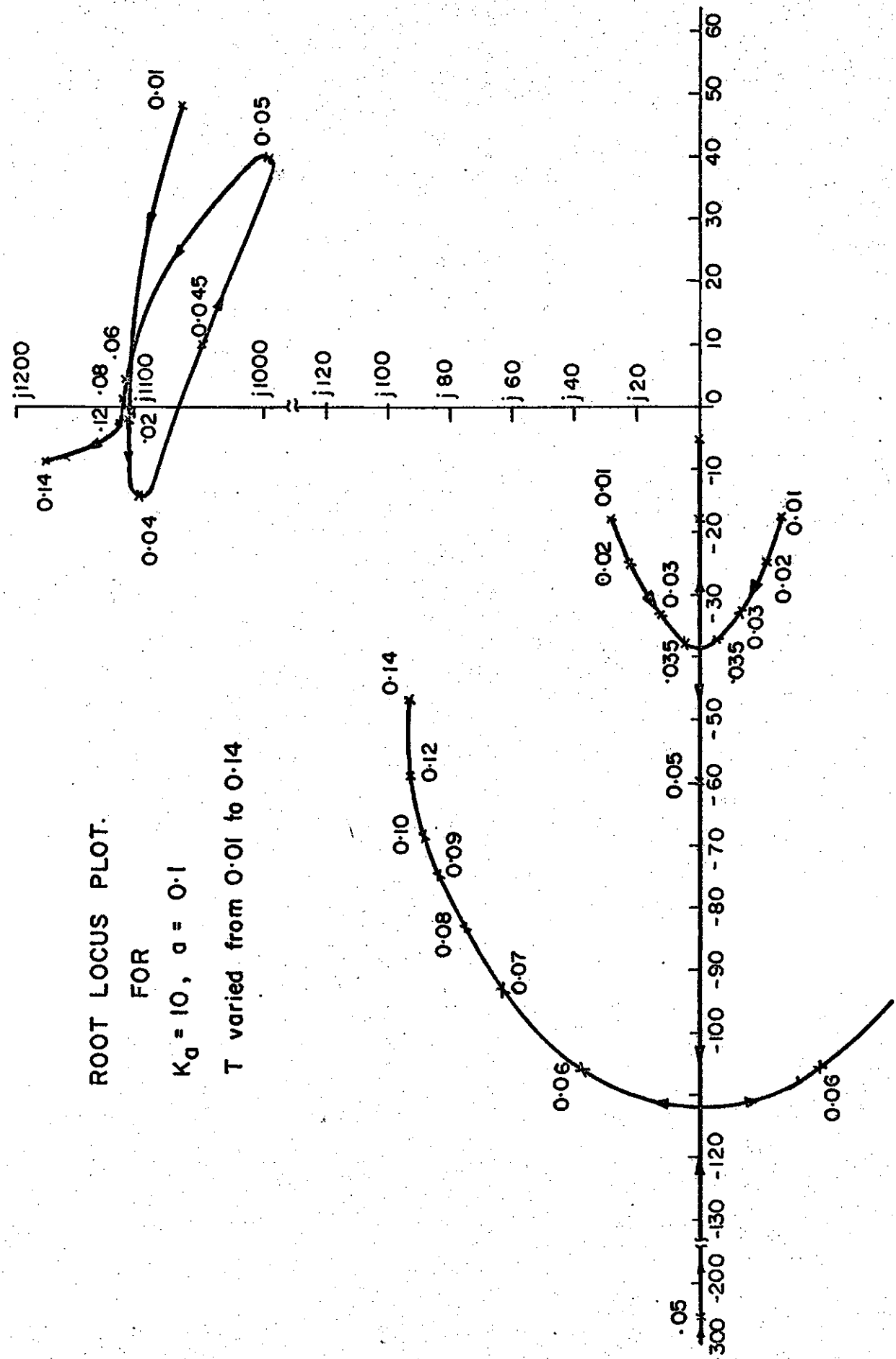

Figure 6.11 (a) Root locus plot for variable compensator parameters.

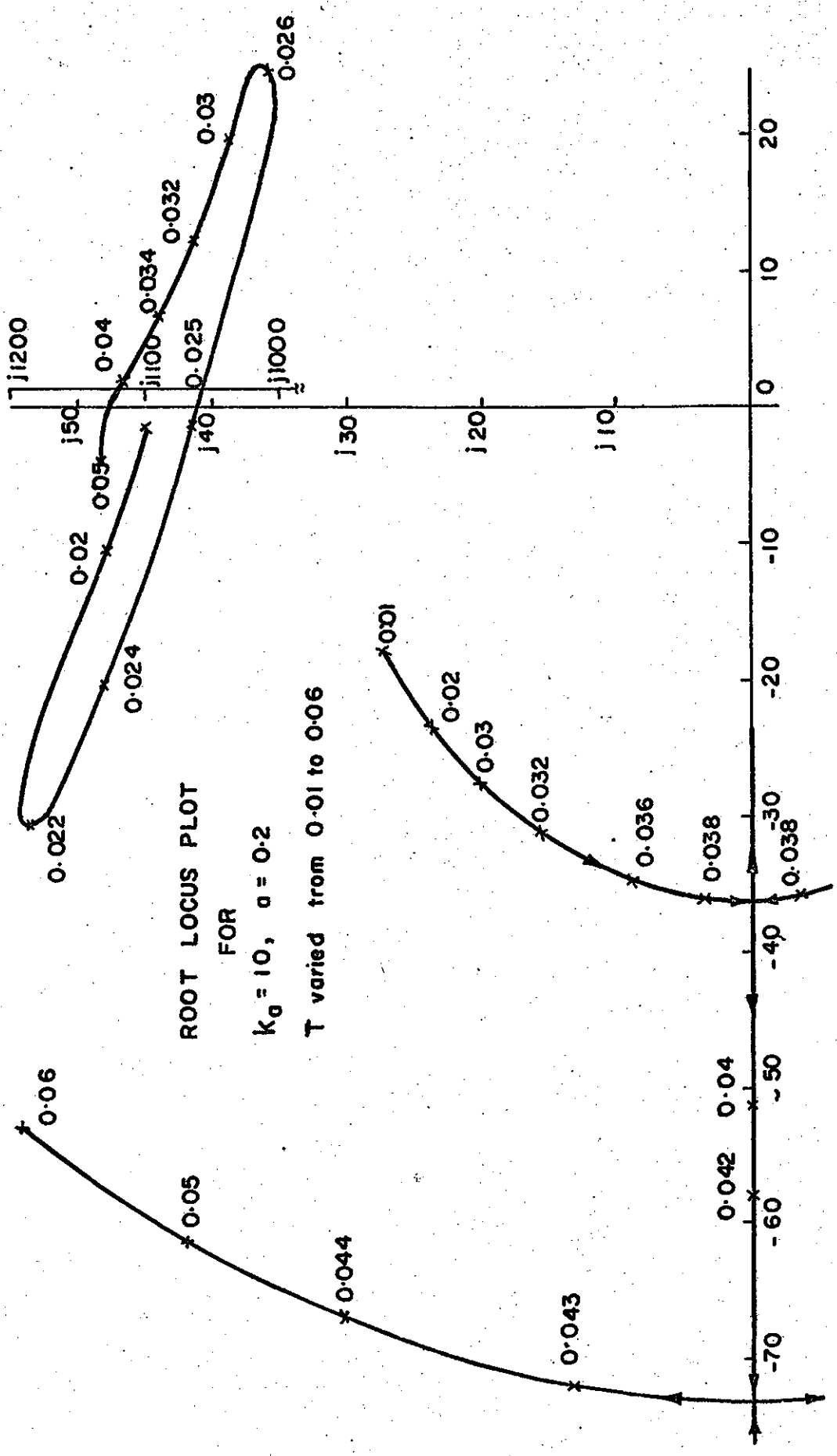

Figure 6.11 (b) Root locus plot for variable compensator parameters.

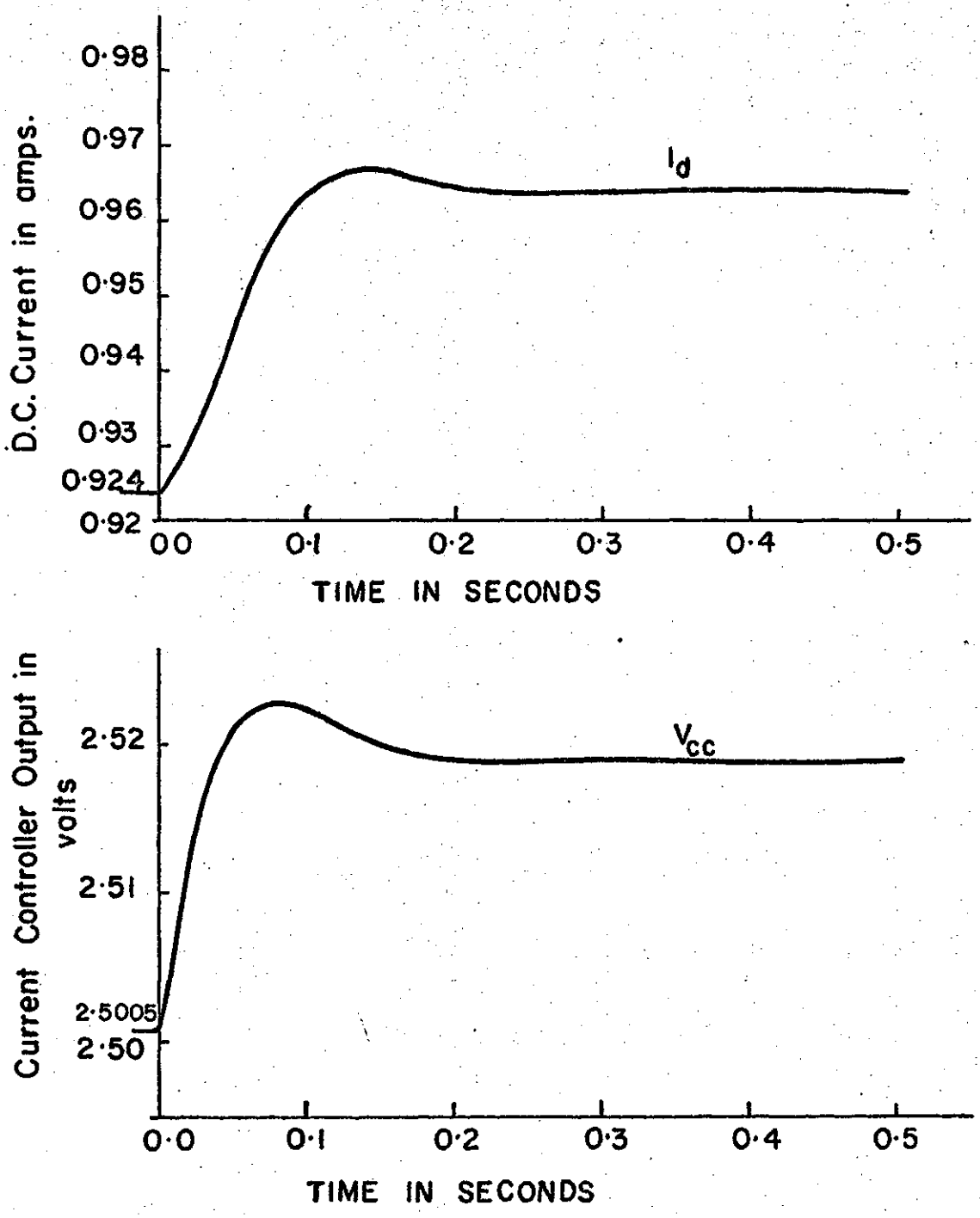

Figure 6.12 The digitally calculated d.c. line current and current controller output for a +0.04 amp. current order step change.

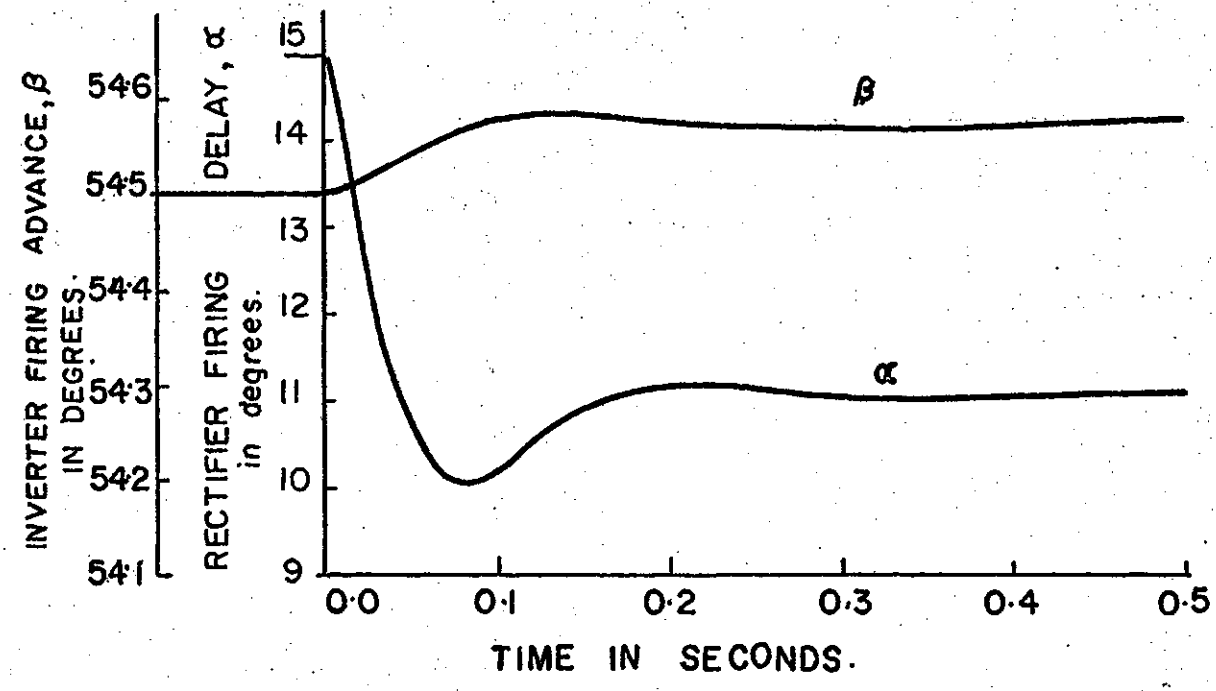

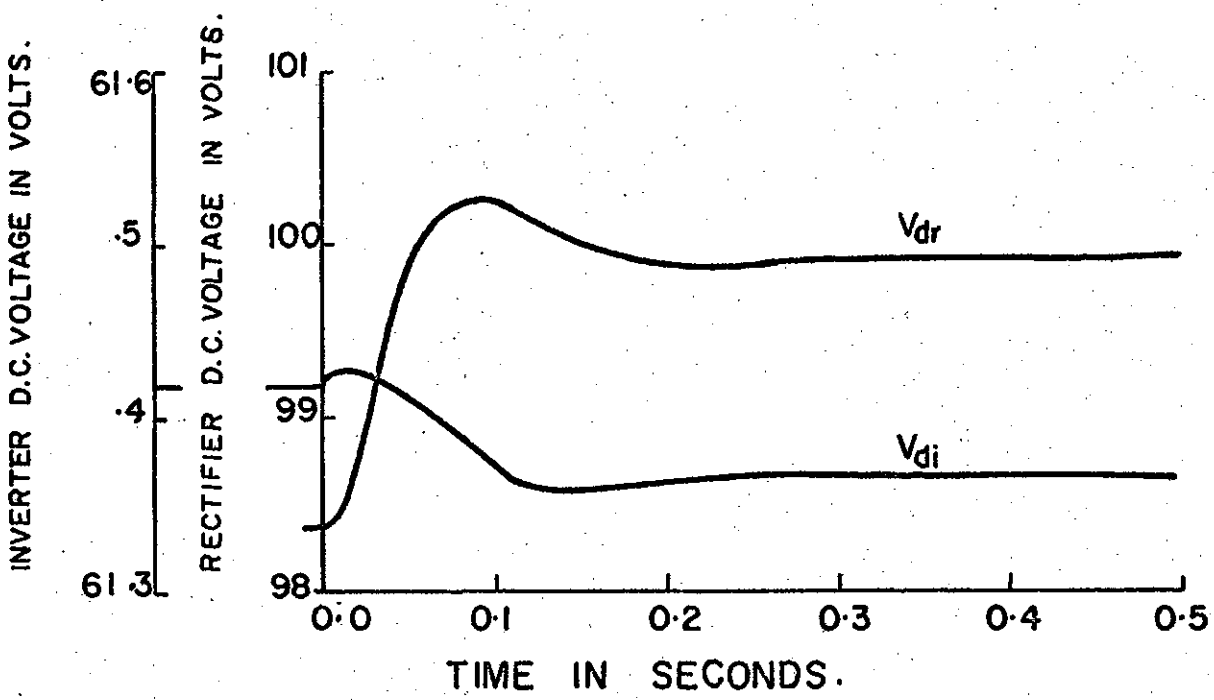

Figure 6.13 The digitally calculated convertor firing angle and d.c. voltage changes for a +0.04 amp. current order step change.

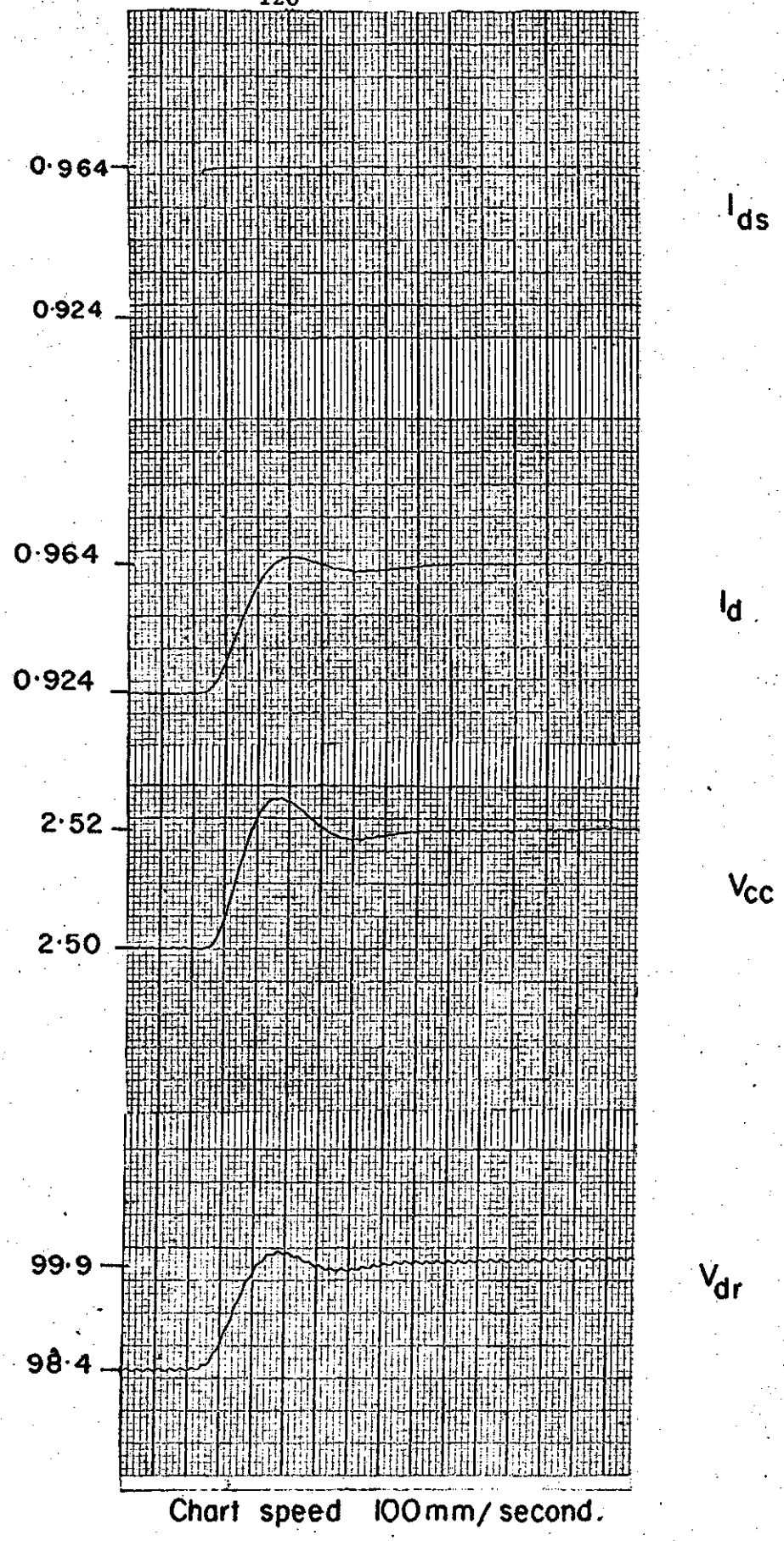

Figure 6.14 The d.c. line current, current controller output and rectifier d.c. voltage changes for a+0.04 amp. current order step change recorded from the simulator.

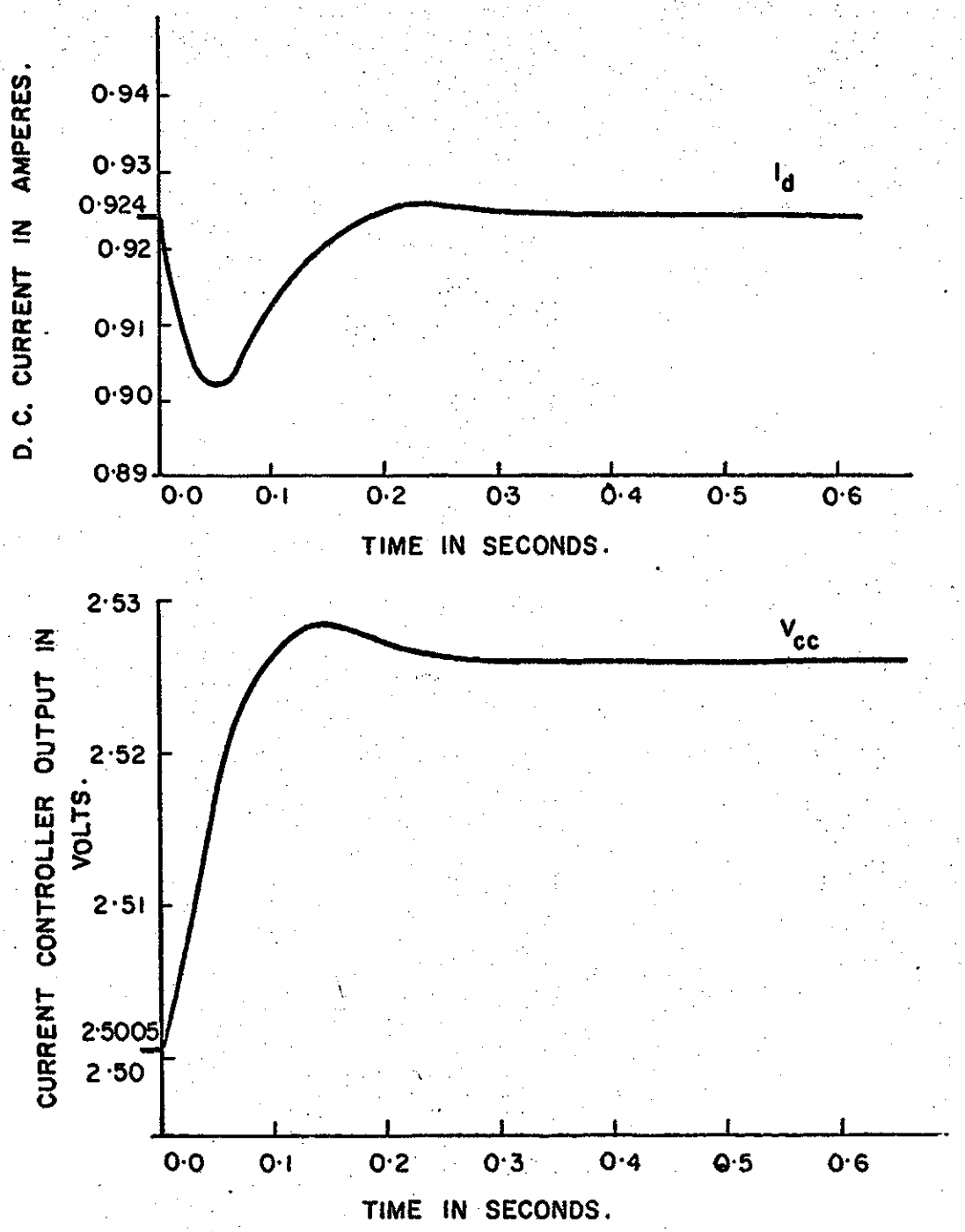

Figure 6.15 The digitally calculated d.c. line current and current controller output response for α+2 percent inverter commutation voltage step change.

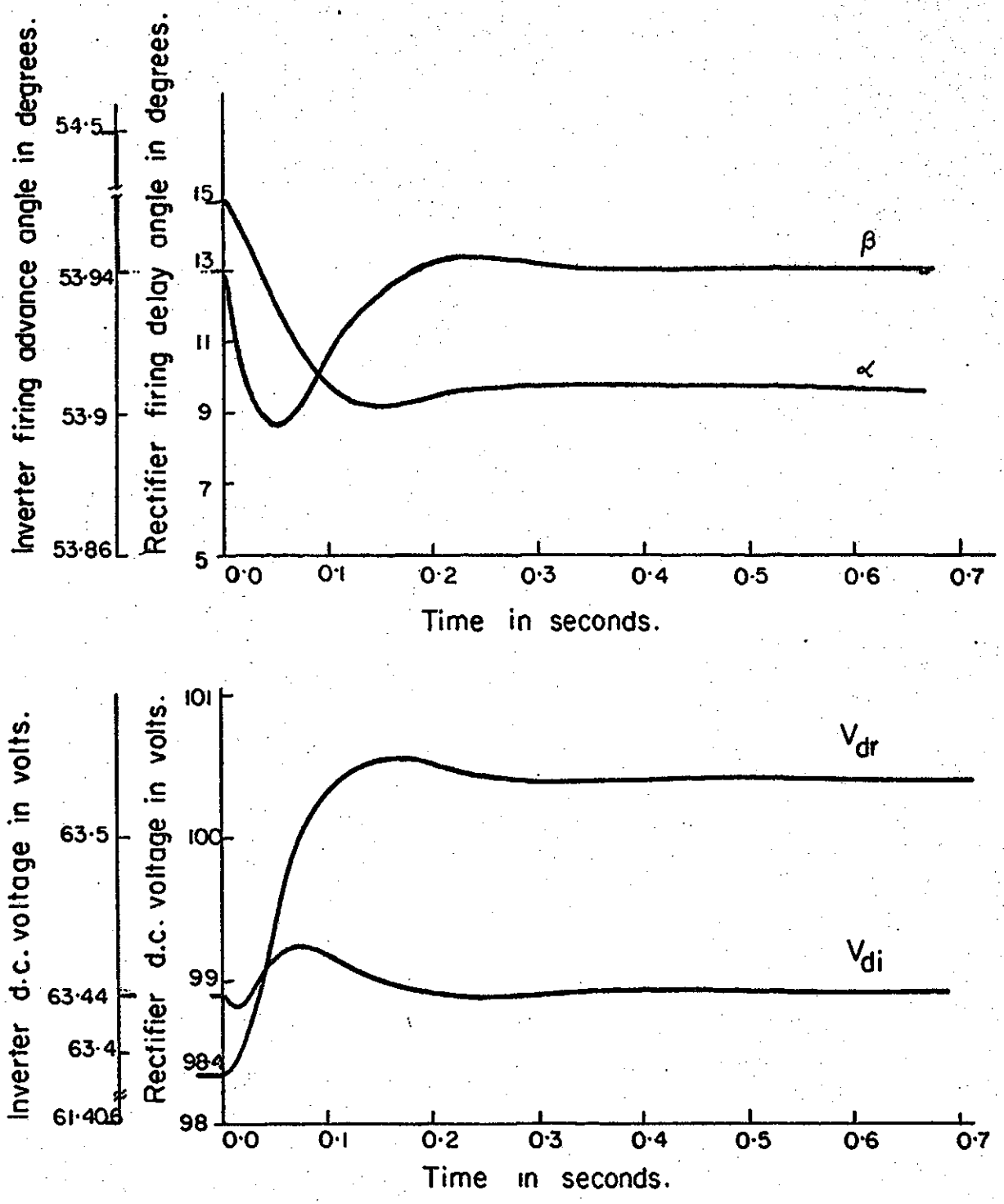

Figure 6.16 The digitally calculated convertor firing angle and d.c. voltage changes for α+2 percent inverter commutation voltage step change.

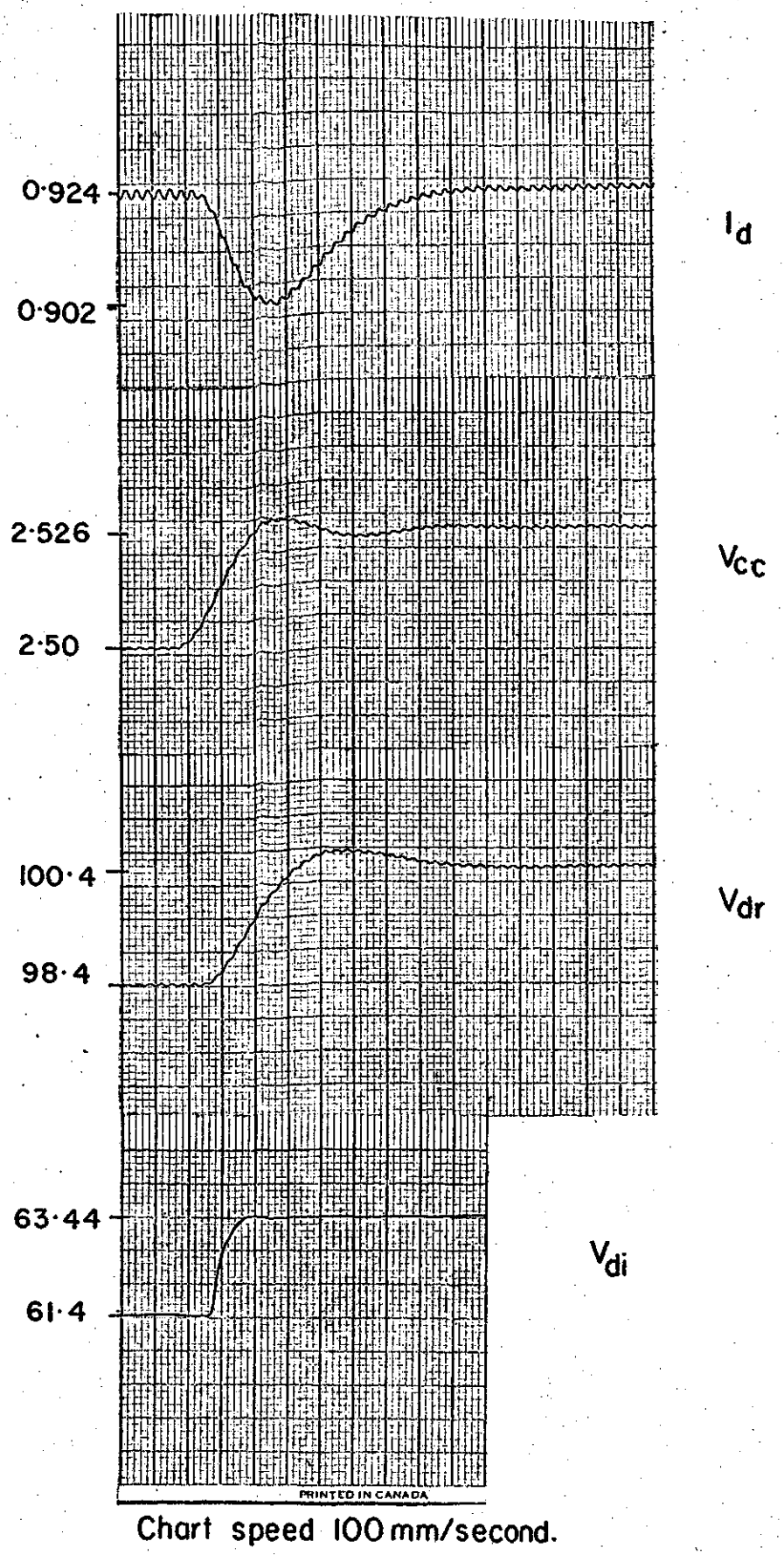

Figure 6.17 The d.c. line current, current controller output and convertor voltage changes for α+2 percent inverter commutation voltage step change recorded from the simulator.

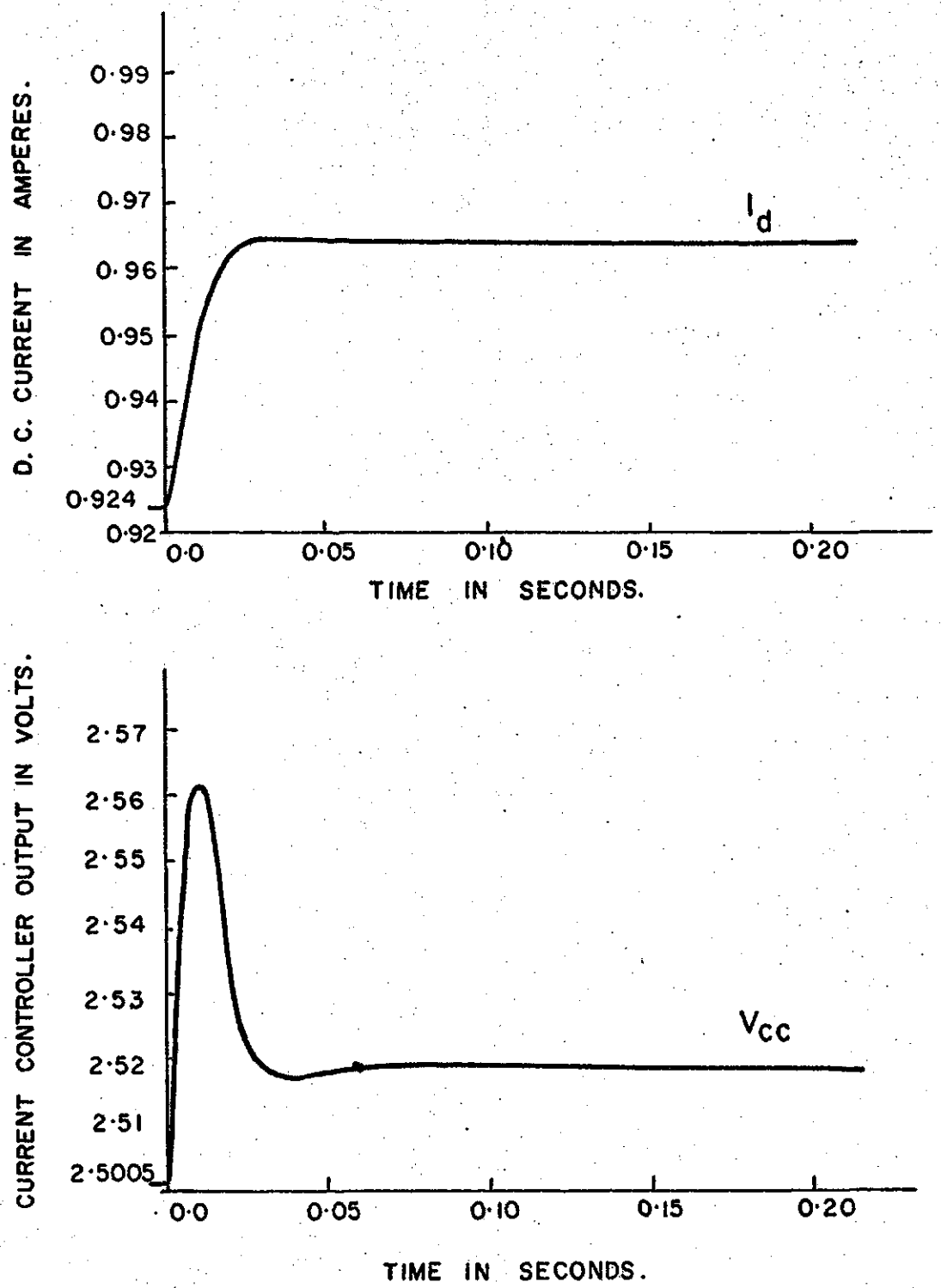

Figure 6.18 The digitally calculated d.c. line current and current controller output response of the simulator equipped with tracking controller for a +0.04 amp. current order step change.

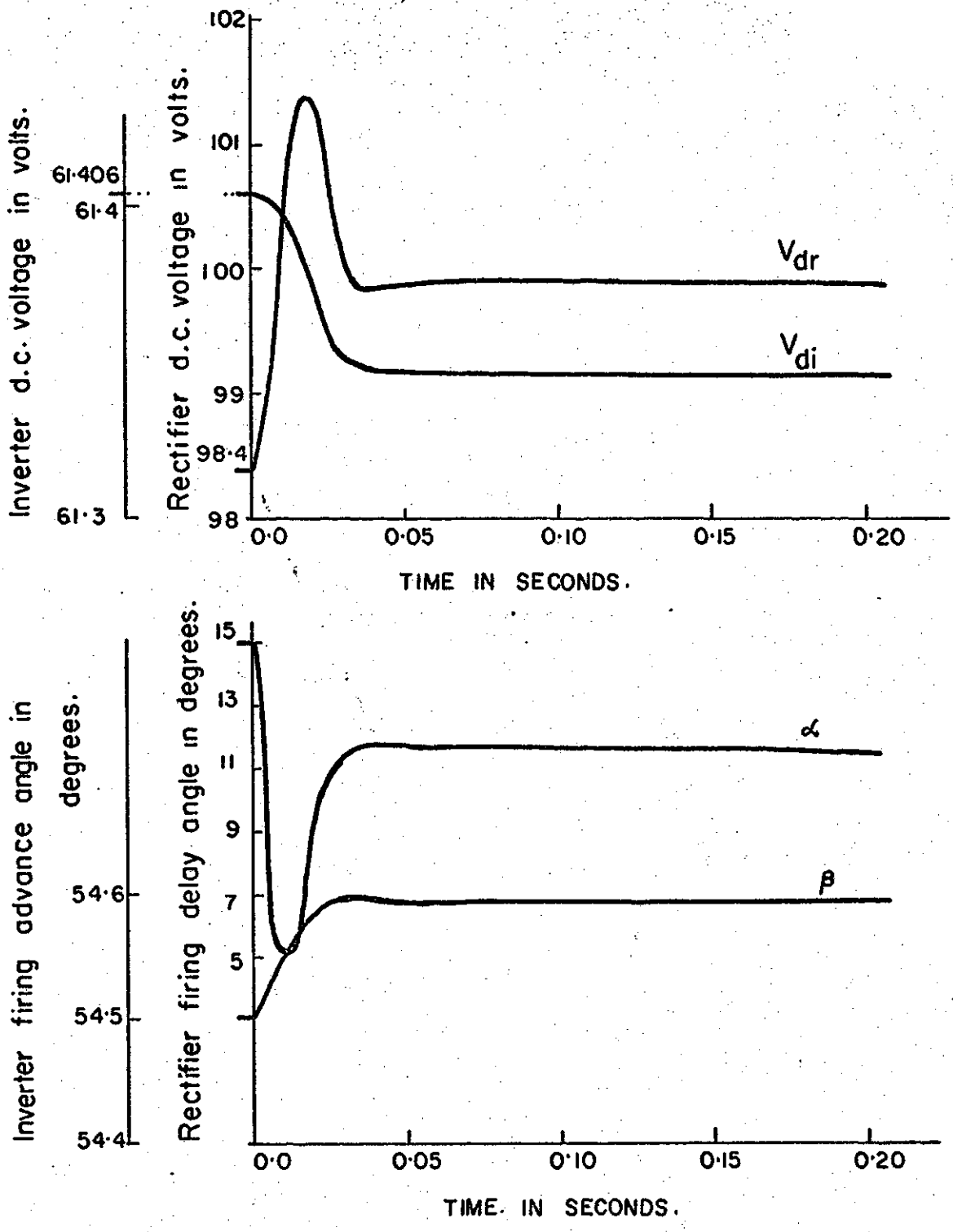

Figure 6.19 The digitally calculated convertor d.c. voltage and firing angle changes for α+0.04 amp. current order step change.

7. CONCLUSION

A brief review of the historical development of h.v.d.c. transmission and its control techniques has been presented. The small signal equations are presented for system dynamic performance studies. A h.v.d.c. simulator equipped with individual phase controllers is described. The constant current controller synthesis and state-space system analysis techniques are briefly discussed.

A block diagram model and the transfer function of the simulator equipped with an integral type constant current controller have been developed. The small signal system equations have been transformed to the state-space form. The dynamic response of the system following a step change of (i) current order and (ii) inverter commutation voltage has been digitally calculated from the state-space model. These studies have also been repeated on the simulator. The dynamic simulator response compares favourably with the digital results which establishes the mathematical model validity in the region studied.

The state-regulator optimal control technique consisting of an all state feedback regulator has been used to improve the system dynamic performance. All system states cannot be conveniently measured and therefore a suboptimal controller using the rectifier station state signals only has been tried. The performance of the system equipped with the suboptimal controller was digitally calculated. The suboptimal controller was designed and used in simulator studies. The system performance is improved and the digital and simulator results are similar.

The system performance can also be improved by a proper selection of the controller feedback loop parameters. The 7.5 integral current controller gain corresponding to 0.707 damping would improve system performance but this saturates the control amplifier during simulator starting and the rectifier valves fail to fire. Two methods of modifying the current controller feedback loop for successful starting and providing 7.5 gain during system operation have been demonstrated. The digital and analog studies of the system using 7.5 current controller gain included in this thesis indicate an increase in rise time and a decrease in overshoot. The effect of including phase lead compensation in the current controller feedback loop has been examined and the controller feedback network parameters determined by root-locus plots for 0.707 damping ratio. The feedback loop of the current controller has been modified and performance of the system using phase lead compensation is examined. The digital computer and the simulator studies indicate a considerably faster response with marginally increased overshoot. The tracking optimization technique of minimizing the error between the desired and actual d.c. currents is also examined for improving the system response. This method increases the d.c. current response speed but the current controller output, the firing angles and the d.c. voltages are initially subjected to violent changes. The effect of convertor output voltage harmonics has also been examined. It is noticed that the average d.c. current changes due to a step change in current order are similar when calculated from (i) average d.c. voltage excitations and (ii) actual convertor output excitation including harmonics. The average d.c. excitation can, therefore, be used in dynamic performance studies.

8. REFERENCES

1. Erith, H. A., "H.V.D.C. Transmission", Joint EIC/IEEE Meeting at Montreal, Que., Canada, Feb. 27, 1968.

2. Bateman, L. A., Haywood, R. W. and Brooks, R. F., "Nelson River D.C. Transmission Project", Trans. IEEE, Vol. PAS-88, No.5, May 1969, pp. 888-894.

3. Breuer, G.D., Hunter, E. M., Engström, P. G. and Stevens, R. F., "The Celio Convertor Station of the Pacific HV-DC Intertie", Trans. IEEE, Vol. PAS-85, No.11, Nov. 1966, pp. 1116-1128.

4. Kuwahara, S. and Haglof, L., "Sakuma Frequency Convertor - Early Operational Experience", IEEE Conf. on High Voltate D.C. Transmission at Univ. of Manchester, Part I, Sept. 1966, pp. 34-41.

5. Sachdev, M. S., "Analysis of Composite A-C and D-C Systems", Ph.D. Thesis, 1969, University of Saskatchewan, Saskatoon, Canada.

6. Adamson, C. and Hingorani, H. G., "High Voltage Direct Current Power Transmission", Garraway Limited, London, 1960.

7. Reider, A. M., "Analysis of the Stability of the Control Systems of Kashira-Moscow Direct Current Transmission Line", Direct Current, Vol. 3, No.7, Dec. 1957, pp. 227-240.

8. Kvyatkovskii, V. M. and Melgunov, N. M., "The Steady State Stability of a D.C. Transmission Link When Operating into a Receiving Power Supply System of Comparable Capacity", Direct Current, Vol. 8, No.4, April 1963, pp. 107-115.

9. Hay, J. L., Bhatti, J. S. and Hingorani, N.G., "Simplified Dynamic Simulation of H.V.D.C. System by Digital Computer, Part II - Design of Controller and Test Results", Trans. IEEE, Vol. PAS-90, No.2, March/April 1971, pp. 865-875.

10. Erikson, K. Liss, G. and Persson, E., "Stability of the Control System for H.V.D.C. Transmission Analysis using Theoretically Calculated Nyquist Diagrams", Trans. IEEE, Vol. PAS-89, May/June 1970, pp. 733-740.

11. Clade, J. and Lacoste, H., "Simplified Study of the Stability of Regulation of a D.C. Link", Direct Current, Vol. 12, Feb. 1967, pp. 9-22.

12. Persson, Erik V., "Calculation of Transfer Function in Grid Controlled Convertor Systems with Special Reference to H.V.D.C. Transmission", Proc. IEE, Vol. 117, No.5, May 1970, pp. 989-997.

13. Carroll, D. P. and Krause, P. C., "Stability Analysis of D.C. Power System", Trans. IEEE, Vol. PAS-89, No.6, July/August 1970, pp. 1112 - 1119.

14. Burton, R. S., "State-Space Representation of a H.V.D.C. Tie-line", M.Sc. Thesis, July 1970, Univ. of Saskatchewan, Saskatoon, Canada.

15. Earle, Dennis S., "Frequency Control Studies in A.C.- D.C Systems", M.Sc. Thesis, Dec. 1968, Univ. of Saskatchewan, Saskatoon, Canada.

16. Clifford, J. F. and Schmitt, A. H., "Digital Representation of a D.C. Transmission System and its Controls", Trans. IEEE, Vol. PAS-89, No.1, Jan. 1970, pp. 97-105.

17. Machida, T., "Improving the Transient Stability of A.C. System by Joint Usage of D.C. System", Trans. IEEE, Vol. PAS-85, No. 3, March 1966.

18. Breuer, G. D., Luini, J. F. and Young, C. C., "Studies of Large AC/DC System on Digital Computer", Trans. IEEE, Vol. PAS-85, No.11, Nov. 1966.

19. Krause, P. C. and Carroll, D. P., "A Hybrid Computer Study of a D.C. Power System I", Trans. IEEE, Vol. PAS-87, No.4, April 1968.

20. Peterson, H. A., Krause, P. C., Luini, J. F. and Thomas, C. H., "An Analog Computer Study of a Parallel AC and DC Power System", Trans. IEEE, Vol. PAS-85, No.3, March 1966, pp. 191-209.

21. Peterson, H. A. and Krause, P. C., "A Direct and Quadrature Representation of a Parallel AC and DC Power System", Trans. IEEE, Vol. PAS-85, No.3, March 1966, pp. 220-225.

22. Ainsworth, A. D. and Martin, C. J. B., "Principle of Control for H.V.D.C. Transmission", IEE Conference on H.V.D.C. Transmission at Univ. of Manchester, Part I, Sept. 1966, pp. 158-160.

23. Engström, P. G., "Operation and Control of H.V.D.C. Transmission", Trans. IEEE, Vol. PAS-83, Jan. 1964, pp. 71-77.

24. Hingorani, N. G. and Chadwick, P., "A New Extinction Angle Control for AC/DC/AC Static Convertors", Trans. IEEE, Vol. PAS-87, No.3, March 1968.

25. Forsell, Harry, "The Gotland D.C. Link: The Grid Control and Regulation Equipment", Direct Current, Vol. 2, No.7, June 1955, pp. 109-114 and Vol. 2, No.7, Dec. 1955, pp. 166-170.

26. Machida, T., Yoshida, Y. and Nakamura, H., "A Method of Automatic Frequency Ratio Control by D.C. Systems", Trans. IEEE, Vol. PAS-86, March 1967.

27. Yoshida, Y., Machida, T. and Hingorani, N. G., "Analog Computer Study of Automatic Frequency Ratio Control on an HVDC Transmission System", Trans. IEEE, Vol. PAS-87, No.3, March 1968.

28. Ainsworth, J. D., "The Phase-Locked Oscillator - A New Control System for Controlled Static Convertors", Trans. IEEE, Vol. PAS-87, No.3, March 1968.

29. Ekstrom, A. and Liss, G., "A Refined H.V.D.C. Control System", Trans. IEEE, Vol. PAS-89, May/June 1970.

30. Phadke, A. G., "Generation of Abnornormal Harmonics in High-Voltage AC-DC Power Systems", Trans. IEEE, Vol. PAS-87, No.3, March 1968, pp. 873-883.

31. Ainsworth, J. D., "Harmonic Instability Between Controlled Static Convertors and A.C. Networks", Proc. IEE, Vol. 114, No.7, July 1967, pp. 949-957.

32. Stevenson, W. D., "Elements of Power System Analysis", McGraw Hill Book Company, Inc. 1962, New York, Second Edition.

33. Simoiu, M. P., "Determining the Coefficients of Transfer Function for Automatic Control Elements and Systems", Automatic and Remote Control, Vol. XVIII, No.6, June 1957, pp. 556-571.

34. Chen, C. F. and Haas, I. J., "Elements of Control System Analysis: Classical and Modern Approaches", Prentice-Hall, Inc., Englewood Cliffs, N.J., 1968.

35. Kuo, B. C., "Automatic Control Systems", Prentice-Hall, Inc., Englewood Cliffs, N.J., 1967.

36. Ogata, K., "State Space Analysis of Control Systems", Prentice-Hall, Inc. 1968.

37. Hsu, J. C. and Meyer, A. W., "Modern Control Principles and Applications", McGraw-Hill Book Company, New York, 1968.

38. I.B.M. Application Program, "System/360, Scientific Subroutine Package", 360A-CM-03X, Version III, Programmer's Manual, pp. 167.

39. Athans, M. and Falb, P. L., "Optimal Control", McGraw-Hill Book Company, New York, 1966.

40. Yu, Y. N., Vongsuriya, K. and Wedman L. N., "Application of an Optimal Control Theory to Power Systems", Trans. IEEE, Vol. PAS-89, No.1, Jan. 1970, pp. 55-62.

41. Kanngiesser, K. W. and Lips, H. P., "Control Methods for Improving the Reactive Power Characteristic of HVDC Link", Trans IEEE, Vol. PAS-89, No.6, July/Aug. 1970.

42. Merriam, C. W., "Optimization Theory and the Design of Feedback Control Systems", McGraw-Hill Book Company, N.Y., 1964.

43. Gray, L. D., Remfer, P. S. and Stevenson, L., "Application of Quadratic Optimization to Helicopter Flight Control", J.A.C.C. Conference 1969, pp. 240.

44. Ryder, F. H. and MacLoon, F. C., "The Eel River H.V.D.C. Convertor Station and Development of Electric Utility Interconnections in Eastern Canada and U.S.A." Meeting Power System Planning and Operating section, Canadian Electrical Association, March 1971.

45. Burglund, O. and Liden, I., "Layout Area and Building Volume Requirements for H.V.D.C. Terminals", Trans. IEEE Vol. PAS - 86, No. 10, Oct. 1967, pp. 1161 - 1169.

46. Sachdev, M.S., Chand, J. and Fleming, R.J., "H.V.D.C. Transmission link stability analysis by state space technique", 85th Annual General Meeting, The Engineering Institute of Canada, Sept. 1971.

9. APPENDICES

Appendix I - A 500 mile H.V.D.C. Transmission Scheme.

A 500 mile two terminal h.v.d.c. transmission scheme considered has a nominal d.c. voltage and current ratings of 450 kv and 1.8 kA respectively. It is assumed that individual phase control is used to maintain constant current in the line. Integral constant current controller at rectifier end and constant extinction angle control at inverter terminal are used to control convertor firing angles. The line parameters and convertor ratings are given in Table 9.1.

The system parameters have been converted to 100 volts base voltage and 1 ampere base current and are listed in Table 9.2. The constants of the state space model developed in Chapter 4 are modified and used to determine the system stability and dynamic performance.

The eigenvalues of the characteristic matrix are determined for increasing current controller amplifier gain using an IBM 360/50 digital computer. The system was found unstable and unaffected by the magnitude of amplifier gain. The commutation reactance drop compensation signal at the rectifier terminal provides a positive feedback resulting in system instability in this case. This feedback is not essential for the rectifier operation and the system was modified accordingly. The eigenvalues of the modified characteristic equation have been determined and the root locus plotted for variable current controller amplifier gain is shown in Figure 9.1. An amplifier gain of 4.0 corresponds to near critical damping.

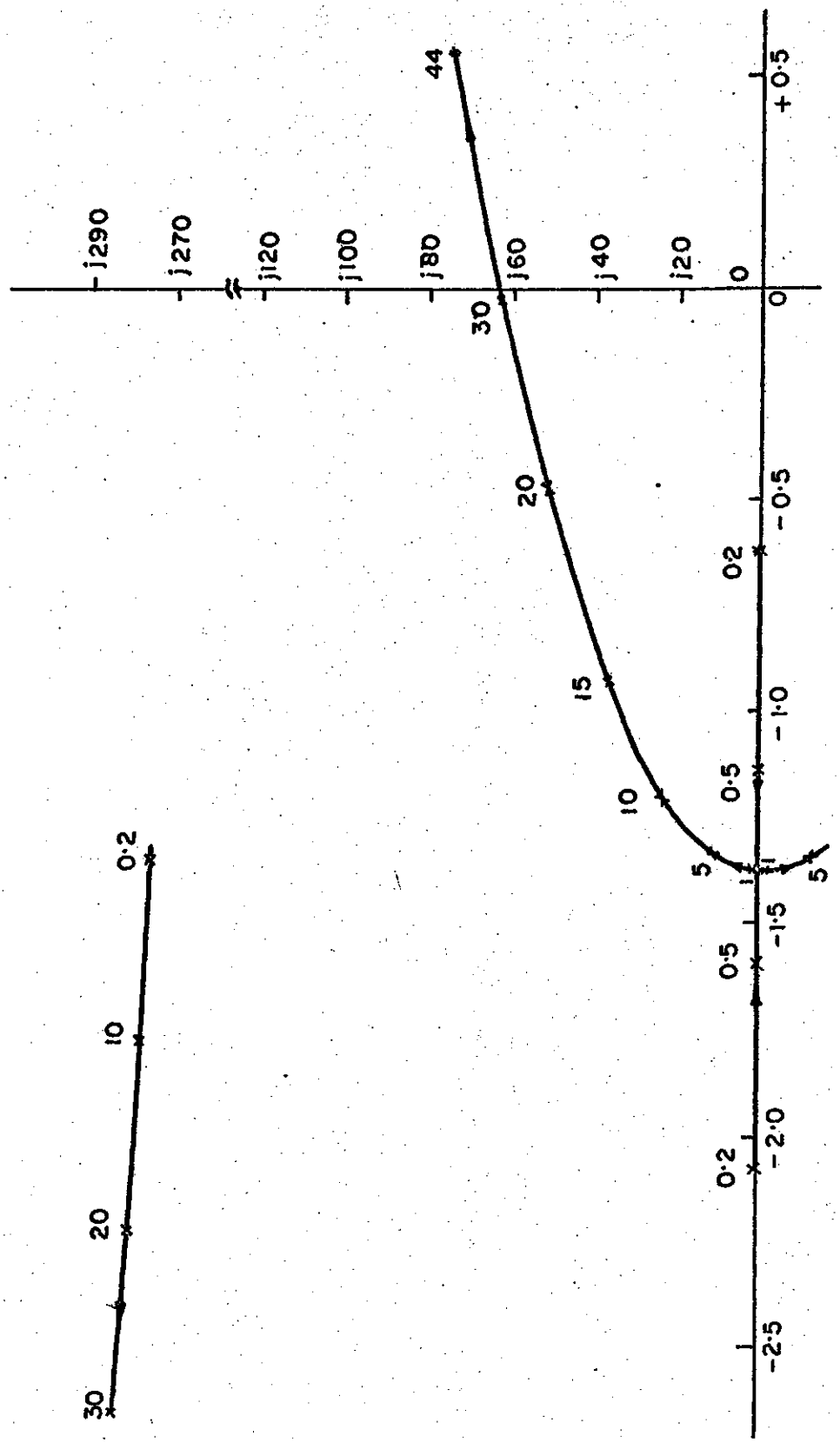

Figure 9.1 Root locus plot for increasing current controller amplifier gain.

The d.c. system was operated such that the line current and d.c. midpoint voltage were 0.924 amperes and 80.0 volts respectively. The rectifier and inverter commutation voltages, inverter firing advance angle, the rectifier firing delay angle and constant current controller output are 76.5 volts, 76.5 volts, 54.5°, 15° and 2.5 volts respectively. With the system operated at this level a step change of +0.04 amps current order was simulated on the digital computer. The calculated line current is shown in Figure 9.2. The d.c. line current settles at the new set value of 0.964 amps. after a transient period of 0.34 secs. The rise time is 0.14 secs and approximately 6 percent overshoot occurs 0.30 secs after the step change is applied. The settling and rise time can be decreased by phase lead compensation or optimization techniques.

Table 9.1 The line parameters and rating of the 500 mile h.v.d.c. scheme.

Direct voltage	450 kv
Direct current	1.8 kA
No of bridges at each terminal	3
D.C. reactor inductance	1.0 henry each
Commutation reactance	11.4 ohms.
Line resistance	7.2 ohms.
Line inductance	0.62 henry
Line capacitance	10.0 μF.

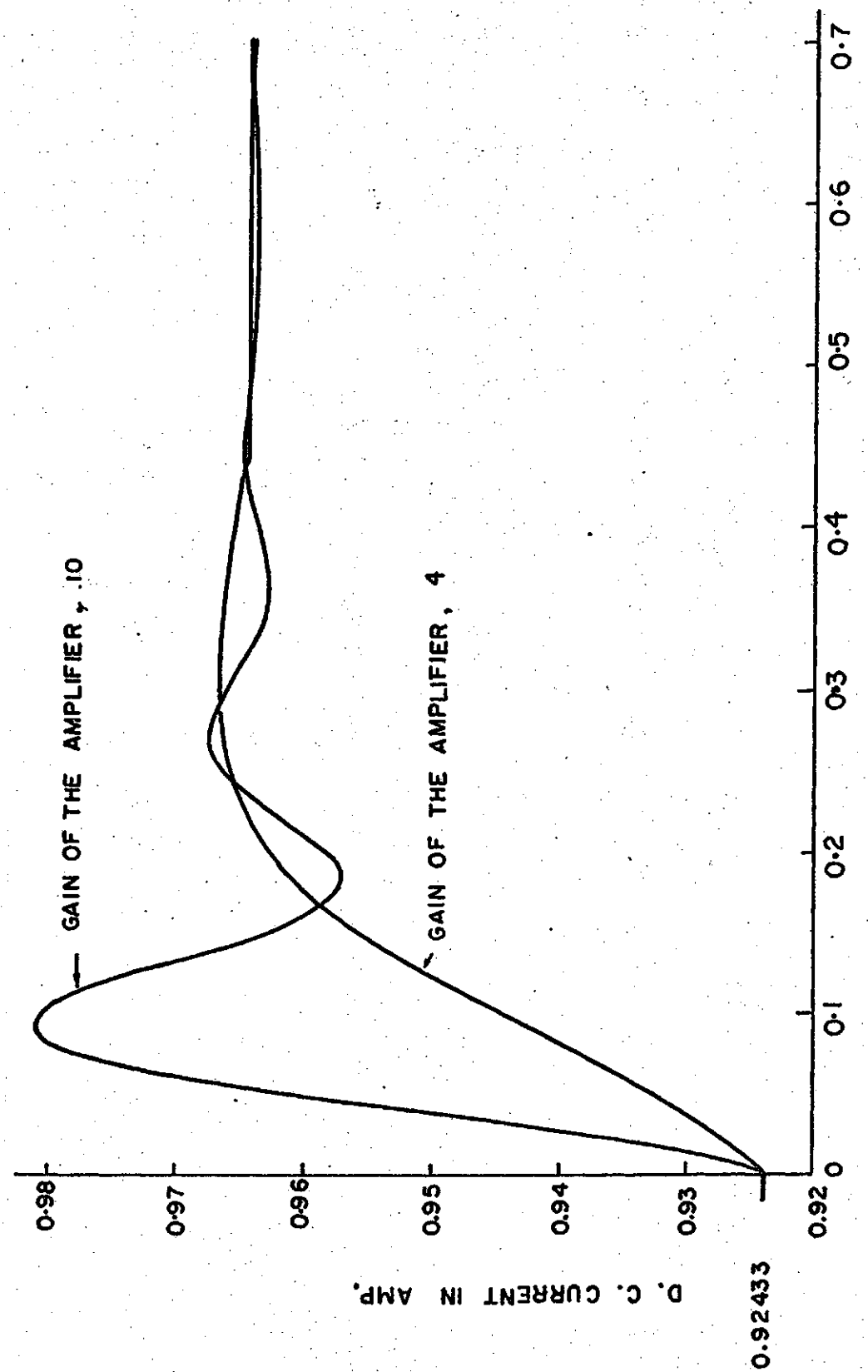

Figure 9.2 The digitally calculated d.c. line current changes for +0.04 ampere current order step change.

Table 9.2 The original and equivalent parameters of the system.

	Original	Equivalent
D.C. reactor inductance in henries (each)	1.0	0.4
Commutation reactance in ohms	11.4	4.56
Line resistance in ohms	7.2	2.88
Line inductance in henries	0.62	0.248
Line capacitance in μF	20.0	50.0

Appendix II - Riccati Equations and Control Vector.

The Hamiltonian for the state-regulator optimization of a system described by

$$\dot{x} = Ax + E\omega \tag{9.1}$$

is

$$H = \frac{1}{2}\left[x^T Q x \right] + \frac{1}{2}\left[\omega^T R \omega\right] + p^T\left[Ax + E\omega\right] \tag{9.2}$$

The canonical equations and the costate vector are given by

$$\frac{\partial H}{\partial p} = \dot{x} \tag{9.3}$$

$$\frac{\partial H}{\partial \omega} = 0 \tag{9.4}$$

$$\frac{\partial H}{\partial x} = -\dot{p} \tag{9.5}$$

$$p = Kx \tag{9.6}$$

The partial differentiation of Hamiltonian H w.r. to costate vector p is

$$\frac{\partial H}{\partial p} = \dot{x} = Ax + E\omega \tag{9.7}$$

Differentiating equation 9.2 w.r. to ω and substituting in equation 9.4, $\frac{\partial H}{\partial \omega}$ is given by

$$\frac{\partial H}{\partial \omega} = R\omega + E^T p = 0 \tag{9.8}$$

Substituting the value of p from equation 9.6 in equation 9.8, the control vector ω is given by

$$\omega = -R^{-1} E^T K x \qquad 9.9$$

The system equation 9.1 is, therefore, given by

$$\dot{x} = (A - E R^{-1} E^T K) x \qquad 9.10$$

Similarly differentiating equation 9.2 w.r. to x and substituting for $\frac{\partial H}{\partial x}$ in equation 9.5, the resulting equation is given by

$$\frac{\partial H}{\partial x} = Qx + A^T p = -\dot{p} \qquad 9.11$$

From equation 9.6, $\dot{p}$ is given by

$$\dot{p} = \dot{K} x + K \dot{x} \qquad 9.12$$

Substituting the value of $\dot{x}$ from equation 9.10, $\dot{p}$ is given by

$$\dot{p} = (\dot{K} + KA - KER^{-1} E^T K)x \qquad 9.13$$

Substituting the values of $\dot{p}$ and p from equations 9.13 and 9.6 into 9.11, $\dot{K}$ is given by

$$\dot{K} = -KA - A^T K + K E R^{-1} E^T K - Q \qquad 9.14$$

The Riccati equation 9.14 and control equation 9.9 corresponds to equations 5.7 and 5.8 respectively.

Appendix III - Effect of penalty factors on the Riccati matrix, control input and dominant eigenvalues.

Five different combinations of state penalty matrix Q and control weighing matrix R were considered. The Riccati matrix, control input and dominant eigenvalues were calculated for these penalty and weighing factors. The combination of matrices Q and R corresponding to critical damping was used in system studies included in Chapter 5. The Riccati matrix K, control input ω_1 and the dominant eigenvalues Z_d for other combinations of the diagonal matrices Q and R are as follows

(i) $Q = (20, 20, 5, 10, 10)$

$R = 0.05$

$$K = \begin{bmatrix} 0.831519 & -0.575999 & 0.009219 & 0.209852 & 2.193560 \\ & 0.777937 & -0.002636 & -0.678671 & -1.081713 \\ & & 0.029775 & -0.501536 & -0.309907 \\ & \text{Symmetric} & & 3190.448486 & 10.634712 \\ & & & & 10.644429 \end{bmatrix}$$

$$\omega_1 = -43.8712\, x_1 + 21.63426\, x_2 + 6.19814\, x_3 - 212.69424\, x_4 - 212.88858\, x_5$$

$$Z_d = -28.99003 \pm j18.34220$$

(ii) $Q = (20, 20, 5, 10, 10)$

$R = 0.01$

$$K = \begin{bmatrix} 0.450415 & -0.292103 & 0.011646 & 0.233255 & 1.169645 \\ & 0.402684 & -0.002741 & -0.681778 & -0.611570 \\ & & 0.014679 & -0.219912 & -0.112387 \\ & \text{Symmetric} & & 1612.379639 & 5.012238 \\ & & & & 5.021511 \end{bmatrix}$$

$$\omega_i = -116.9645\ x_1 + 61.1570\ x_2 + 11.2387\ x_3 - 501.2238\ x_4 - 502.1511\ x_5$$

$$Z_d = -29.05824 \pm j10.84342$$

(iii) $Q = (20, 20, 5, 10, 10)$

$R = 1.0$

$$K = \begin{bmatrix} 2.334960 & -1.828709 & 0.008315 & 0.089890 & 5.893825 \\ & 2.308349 & -0.006138 & -0.521388 & -3.312471 \\ & & 0.093929 & -1.707610 & -1.116225 \\ & \text{Symmetric} & & 7380.949219 & 31.143417 \\ & & & & 31.150955 \end{bmatrix}$$

$$\omega_i = -5.893825\ x_1 + 3.312471\ x_2 + 1.116225\ x_3 - 31.143417\ x_4 - 31.150955\ x_5$$

$$Z_d = -24.89904 \pm j27.52045$$

(iv) $Q = 1, 1, 1, 1, 1$

$R = 1.0$

$$K = \begin{bmatrix} 0.367128 & -0.345457 & 0.001693 & 0.013280 & 1.620099 \\ & 0.365684 & -0.001630 & -0.168497 & -1.407995 \\ & & 0.016170 & -0.622690 & -0.369651 \\ & \text{Symmetric} & & 1259.423096 & 16.582794 \\ & & & & 16.583771 \end{bmatrix}$$

$$\omega_i = -1.620099\ x_1 + 1.407995\ x_2 + 0.369651\ x_3 - 16.582794\ x_4 - 16.583771\ x_5$$

$$Z_d = -10.97055 \pm j29.58500$$

Appendix IV - The Commissioning of the H.V.D.C. Simulator

The initial commissioning of a system is usually performed according to a set procedure provided by the manufacturer. The operation manual supplied by M/S Robinson & Partners Ltd., London, England was used to start the simulator which was found inoperative. The simulator performance was investigated. The commissioning procedure and the remedial measures to rectify the defects noticed are reported in this Appendix.

The h.v.d.c. simulator is designed to operate either in a manual or automatic control mode. The convertor units, d.c. reactors, transmission line units, pulse circuits, d.c. power supply unit and protection units are used in either modes of operation. A synchro unit provides firing signals to the pulse circuits of a convertor for manual operation. The constant extinction angle and constant current control circuits provide firing signals for automatic control operation of the convertors. Before commissioning the simulator the convertors were interconnected using d.c. reactors and transmission line units. The manual, automatic and grid control switches were turned off. The convertor transformers were excited from 230 volts, three phase, 60 cycles per second supply and the d.c. power supply unit was energized from a 120 volt, single phase, 60 cycle per second source. The d.c. supply to manual and automatic control units and protection unit was checked and found satisfactory.

i) Manual control operation

The convertor manual-control operation depends on the performance of the convertor units, transmission line units, synchro units and pulse circuits. The synchro rotors were adjusted to 15^{o} and 160^{o} for rectifier and inverter firing delays respectively. The manual control operation switch was turned on and the outputs of the thyristor pulse circuits were found to be inconsistent and of other than 120 electrical degrees duration. The synchro device and pulse circuits of each convertor unit were checked and adjusted as follows:

Synchro device

The voltage outputs of the synchro units were measured. There was no output from one rectifier synchro phase which was traced to one open synchro brush contact. The brush contacts were cleaned and the system re-energized. A three phase balanced voltage was measured at the synchro output terminals. The synchro outputs are fed to three single phase transformers of the manual control unit and a six phase output is obtained as shown in Figure 3.1. The six phase output was balanced in magnitude and phase by adjusting the R-C circuits provided for this purpose.

Pulse circuits

The six phase balanced voltages of the manual control circuits are applied to the six pulse circuits. The pulse widths were observed to be 120 $\pm$ 10 electrical degrees. The pulse circuits of Figure 3.1 consist of aSchmitt level detector and a bistable circuit. The variable biasing resistors of the Schmitt level detector used in the pulse circuits

were adjusted to eliminate pulse duration errors.

Auxiliary transformers

Three single phase centre tapped auxiliary transformers provide six phase a.c. voltages at a reduced level for valve firing control. The auxiliary transformer primary windings can be connected either in star or in delta configuration by a switch provided for selecting the convertor transformer secondary connections. The commutation voltages lag the convertor transformer secondary phase voltages by 30 electrical degrees. To obtain this phase displacement, the auxiliary transformer primary windings should be delta connected if the convertor transformer secondary is wye connected and vice-versa. It was observed that the auxiliary transformer primary and the convertor transformer secondary windings were similarly connected. The selector switch connections were modified to obtain a six phase a.c. supply which is in phase with the valve commutation voltages. After incorporating the changes and adjustments described above, the simulator was successfully operated at different rectifier and inverter firing angle delays.

ii) Automatic control operation

An attempt to operate the simulator in the automatic control mode was unsuccessful due to unstable outputs of the valve firing pulse circuits. The constant extinction angle control, constant current control and commutation reactance drop compensation ($2\omega LI_d$) circuits were checked to locate the causes of pulse instability. The observations and findings of the investigation are described in the following section.

Constant extinction angle control circuits

A printed circuit board consisting of monostable, clamping, integrating and level detecting elements as shown in Figure 3.2 is provided for constant extinction angle control of each convertor valve. Any sudden changes of a.c. voltages are also detected by this circuitory and the inverter valve firing is advanced to avoid commutation failure. The constant extinction angle control circuits were analyzed and the outputs noticed were compared with the desired forms. The actual and the desired output wave-forms are shown in Figure 9.4. The printed circuit boards and their components were tested. Some transistors were found defective and were, therefore, replaced. The Schmitt level detector 'A' output had an undesirable spike due to stray capacitance effect. A series R-C (22Ω - 100 pF) damping circuit was provided across the output resistor R309 as shown in Figure 9.3. The level detector output was synchronised with the commutation voltage by adjusting the biasing resistor VR301.

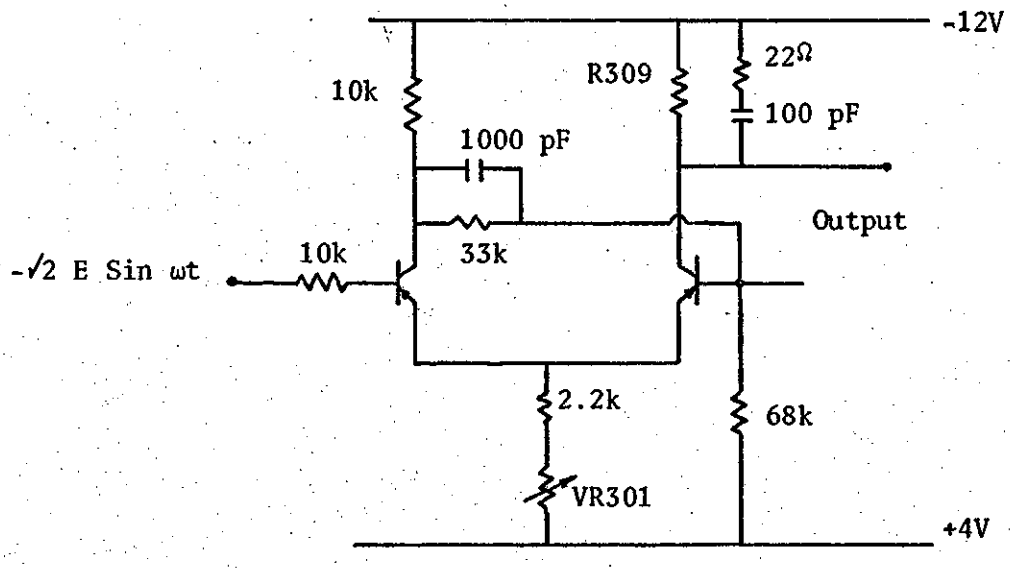

Figure 9.3. Schmitt level detector 'A' for constant extinction angle control.

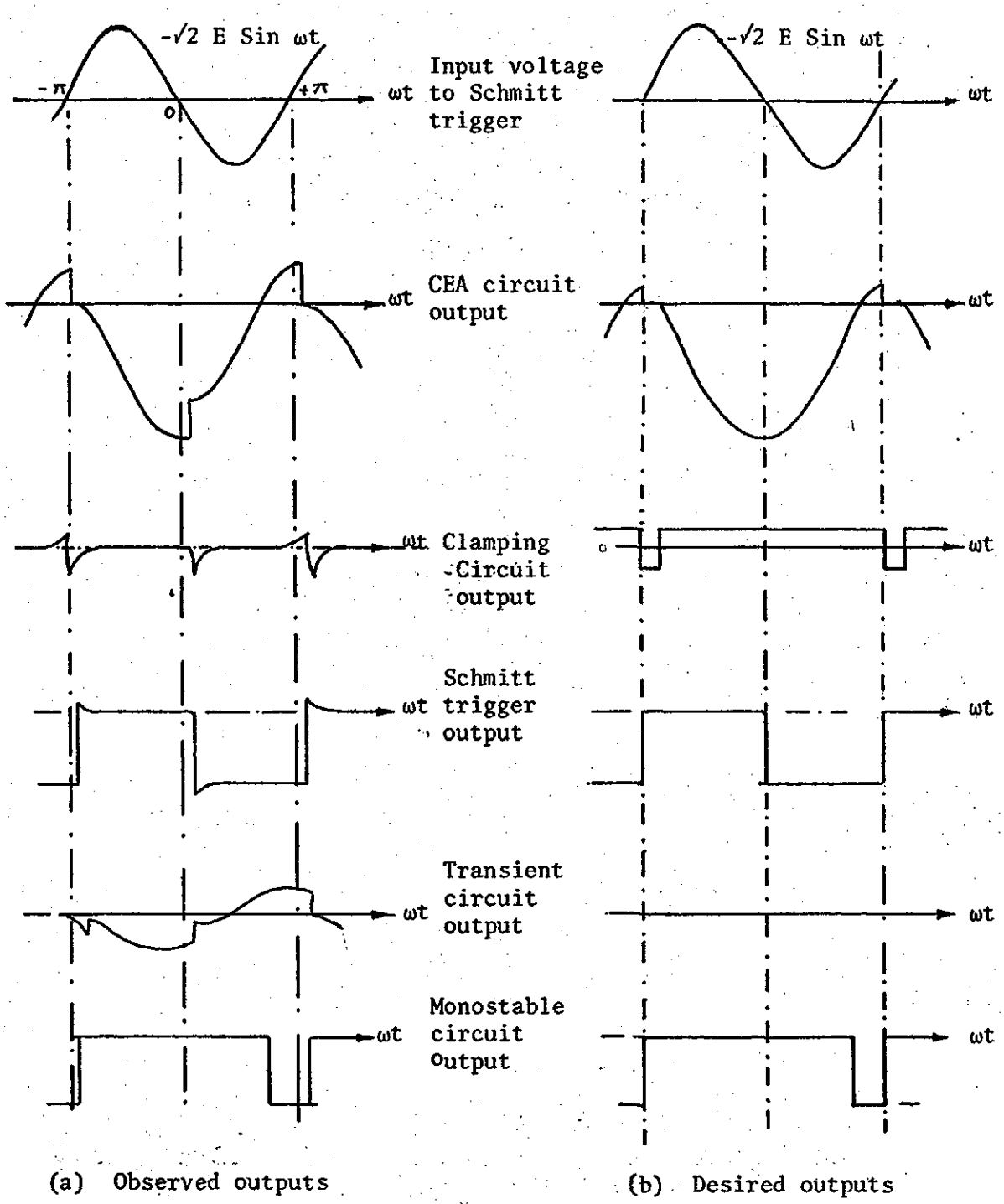

Figure 9.4 Outputs of CEA circuit elements (a) observed (b) desired.

Commutation reactance drop compensation circuit

The d.c. current transformer provides a d.c. voltage output proportional to the current. This voltage is applied to a 500 ohm potentiometer and a voltage proportional to $2\omega LI_d$ signal is tapped. The c.e.a. control circuit output, the constant current controller output, the minimum delay angle pulse and the commutation reactance drop compensation components are applied to a summing junction as shown in Figure 9.5. The commutation reactance ωL and the d.c. current transformer and the summing junction output-input ratios are evaluated to determine the $2\omega LI_d$ potentiometer setting. The input and output wave forms without

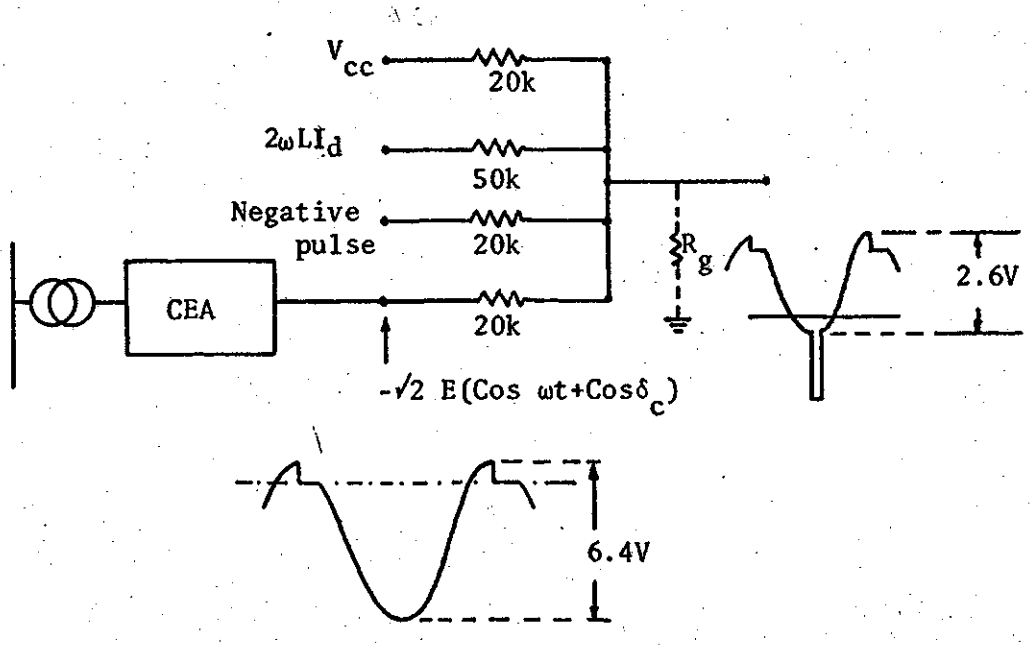

Figure 9.5 Summing junction components and input-output wave forms.

$2\omega LI_d$ and constant current controller inputs are also shown in Figure 9.5. The effective ground resistance R_g at the output of the

summing junction is 13.7 kilohms as given by the equation

$$\frac{Rg}{20+Rg} = \frac{\text{summing junction output peak to peak voltage}}{\text{summing junction input peak to peak voltage}} = \frac{2.6}{6.4}$$

A short circuit test was performed on the convertor transformers applying three phase, 6 volts, 60 cycles/sec. supply to the secondary terminals. The short circuit current and power input at the secondary terminals were 1.1 amperes and 10 watts respectively. The commutation reactance assuming that the convertor transformers are connected to an infinite bus wascalculated to be 1.6 ohms.

The bridge convertor was disconnected from the main transformer and transmission line and the arrangement of Figure 9.6 was used to determine the d.c. current transformer output-input ratio. The d.c. current input

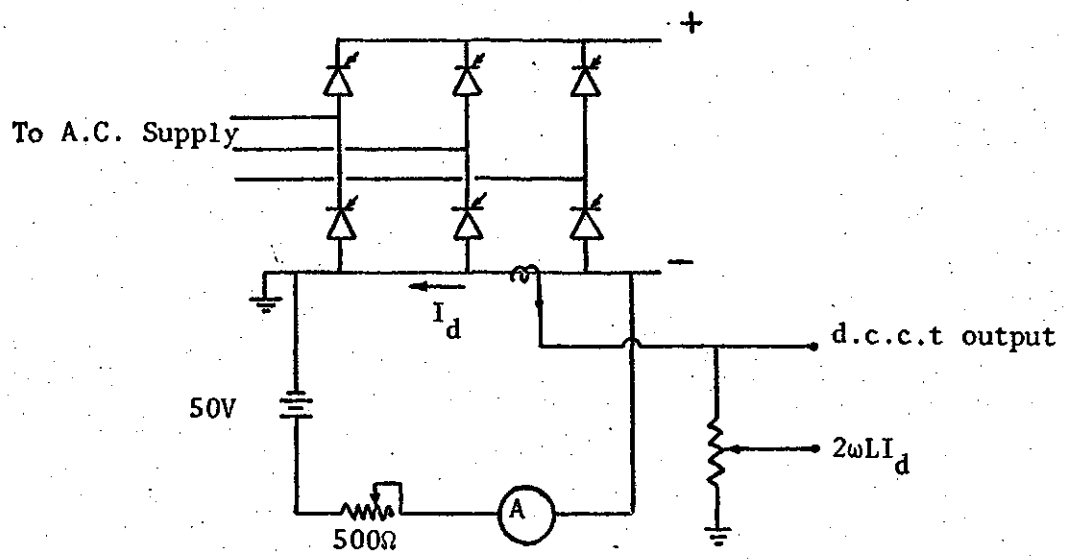

Figure 9.6 Circuit diagram to determine d.c. current transformer output-input ratio.

was varied from 0.0 to 1.0 amperes and the total output voltage was measured. Figure 9.7 shows a 4.4 volts/amp. linear relation between the

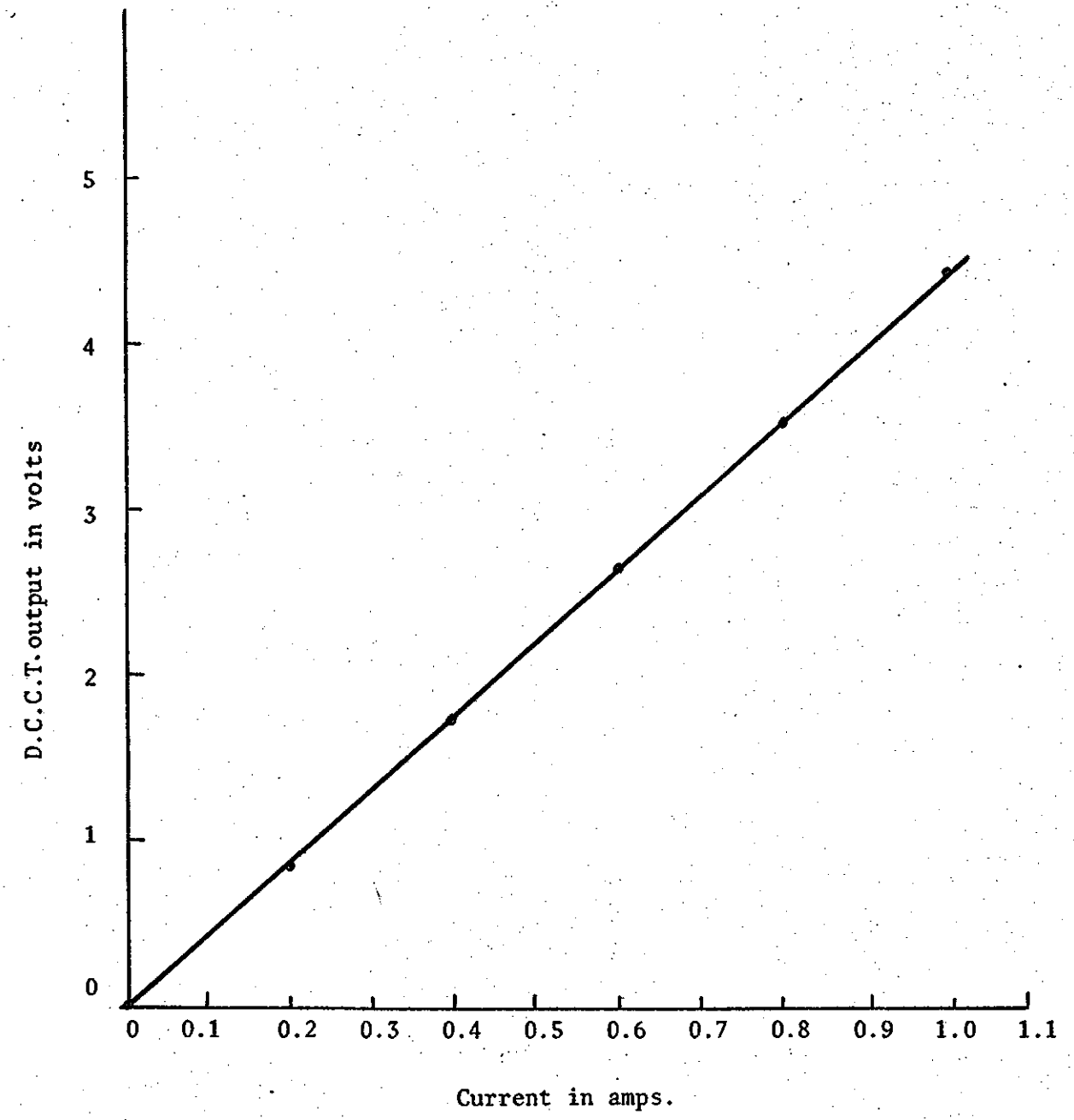

Figure 9.7. D.C.C.T. output vrs. d.c. current plot.

d.c. current transformer output and input.

The summing junction output shown in Figure 9.5 is given by equation 9.15.

$$e = \frac{1}{K_2}(-\sqrt{2}\,E\cos\omega t - \sqrt{2}\,E\cos\delta_c + 2\omega L I_d) + \frac{1}{K_p}V_{cc} \qquad 9.15$$

Where K_2 is the ratio of the commutation voltage to the summing junction output.

K_p is the scale factor for constant current controller output given by $\frac{Rg}{20+Rg}$.

E is the r.m.s. line to line convertor transformer secondary voltage at no load.

The $\sqrt{2}\,E/K_2$ and the commutation voltage E are 1.3 and 76.5 volts respectively. The scale factor K_2 is, therefore, 83.3. The summing junction input for commutation reactance drop compensation of $\frac{2\omega L I_d}{83.3}$ volts is therefore, $\frac{50 + Rg}{Rg}\quad\frac{2\omega L I_d}{83.3} = \frac{2\omega L I_d}{17.9}$ volts. The desired potentiometer setting for commutation reactance drop compensation simulation is given by

$$\frac{(4.4\ I_d)}{500} \cdot R = \frac{2\omega L I_d}{17.9}$$

$$R = 12.75\,\omega L$$

$$= 20.4 \text{ ohms.}$$

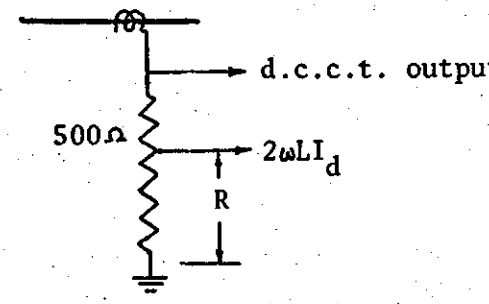

The commutation reactance drop compensation potentiometer was, therefore, adjusted to 20.4 ohms. The convertor transformers and d.c. current transformers of both terminals are similar and therefore the potentiometer for both units were adjusted to 20.4 ohms.

Constant current controller

The constant current controller provides the signal V_{cc} for rectifier firing control. The current controller gain, $\frac{1}{R_a C_a}$ can be varied by changing the size of the feedback capacitor. The simulator started successfully when a 6.7 μF capacitor was used in the feedback loop. The constant current controller amplifier saturated for capacitors of appreciably higher or lower sizes. The amplifier gain is 10 when a 6.7 μF capacitor is used in the feedback loop.